University of Tennessee, Knoxville

TRACE: Tennessee Research and Creative Exchange

Doctoral Dissertations

Graduate School

8-2015

ALTERNATING CURRENT ELECTROKINETICS BASED CAPACITIVE AFFINITY BIOSENSOR: A POINT-OF-CARE DIAGNOSTIC PLATFORM

Haochen Cui
University of Tennessee - Knoxville, hcui2@vols.utk.edu

Follow this and additional works at: https://trace.tennessee.edu/utk_graddiss

Part of the Bioelectrical and Neuroengineering Commons, Biomedical Commons, and the Electronic Devices and Semiconductor Manufacturing Commons

Recommended Citation

Cui, Haochen, "ALTERNATING CURRENT ELECTROKINETICS BASED CAPACITIVE AFFINITY BIOSENSOR: A POINT-OF-CARE DIAGNOSTIC PLATFORM. " PhD diss., University of Tennessee, 2015.
https://trace.tennessee.edu/utk_graddiss/3411

This Dissertation is brought to you for free and open access by the Graduate School at TRACE: Tennessee Research and Creative Exchange. It has been accepted for inclusion in Doctoral Dissertations by an authorized administrator of TRACE: Tennessee Research and Creative Exchange. For more information, please contact trace@utk.edu.

To the Graduate Council:

I am submitting herewith a dissertation written by Haochen Cui entitled "ALTERNATING CURRENT ELECTROKINETICS BASED CAPACITIVE AFFINITY BIOSENSOR: A POINT-OF-CARE DIAGNOSTIC PLATFORM." I have examined the final electronic copy of this dissertation for form and content and recommend that it be accepted in partial fulfillment of the requirements for the degree of Doctor of Philosophy, with a major in Electrical Engineering.

Jie Wu, Major Professor

We have read this dissertation and recommend its acceptance:

Shigetoshi Eda, Gong Gu, Nicole McFarlane

Accepted for the Council:

Carolyn R. Hodges

Vice Provost and Dean of the Graduate School

(Original signatures are on file with official student records.)

ALTERNATING CURRENT ELECTROKINETICS BASED CAPACITIVE AFFINITY BIOSENSOR: A POINT-OF-CARE DIAGNOSTIC PLATFORM

A Dissertation Presented for the
Doctor of Philosophy
Degree
The University of Tennessee, Knoxville

Haochen Cui
August 2015

Copyright © 2015 by Haochen Cui

All rights reserved.

Dedication

I dedicate this to my parents

ACKNOWLEDGEMENT

The work presented in this dissertation would not be possible without the contributions of many individuals, and I can only hope to mention some of the most important here.

I would like to first express my deepest gratitude to Dr. Jie (Jayne) Wu, my Ph.D. mentor, for her professional, meticulous and meritorious guidance. Her excellent mentorship helped me overcome many obstacles one after another throughout my entire graduate study. I firmly believe what I've learnt from her will benefit me in my future life road.

I would like to specially thank Dr.Shigetoshi Eda for providing biological reagents and his generous help in instructing and explaining biological relevant knowledge of my research.

I would like to thank Dr. Gong Gu and Dr. Nicole McFarlane for serving as the committee member. Their unique perspective and meaningful suggestions make my research a more solid and comprehensive work.

I would like to thank my (former) lab mates Kai Yang, Quan Yuan, Cheng Cheng, Shanshan Li, Xiaozhu Liu, Xiaogang Lin and Sakib Hasan for their selfless assistance and cooperation throughout my graduate study. I would also like to thank all my friends and family for their unconditional and continuous support.

Last but not least, I would like to express my special thanks to Meridian Bioscience Inc. for providing me the opportunity for further improvement and perfection of my work. Also thank Center for Nanophase Materials and Science at Oak Ridge National Laboratory for providing cleanroom facilities for microelectrode fabrication.

ABSTRACT

Capacitive bioaffinity detection using microelectrodes is considered as a promising label-free method for point-of-care diagnosis, though with challenges in sensitivity, specificity and the time “from sample to result.” This work presents an alternating current (AC)-electrokinetic based capacitive affinity sensing method that is capable of realizing rapid in-situ detection of specific biomolecular interactions such as probe-analyte binding. The capacitive biosensor presented here employs elevated AC potentials at a fixed frequency for impedimetric interrogation of the microelectrodes. Such an AC signal is capable of inducing dielectrophoresis (DEP) and AC electrothermal (ACET) effects, so as to realize in-situ enrichment of macro and even small molecules at microelectrodes and hence accelerated detection. Experimental study of the DEP/ACET-enhanced capacitive sensing method was conducted, and the results corroborate our hypothesis.

This capacitive sensing method has been shown to work with various types and sizes of biomolecules (such as antibodies, virus and small molecules) to differentiate disease-positive samples from negative samples within or less than two minutes, while conventional assay would require multiple processing steps and take hours to complete. The results showed high accuracy and sensitivity. Overall, this capacitive affinity biosensor may form a basis for the development of a feasible point-of-care diagnostic platform for the detection of infectious diseases in the future.

TABLE OF CONTENTS

Chapter 1 Introduction.. 1

1.1 Biosensor: its future in your health and well-being 1
1.2 Biosensor: its major challenges..3
1.3 Dissertation Outline 5

Chapter 2 Literature review of biosensors...................................... 6

2.1 Various types of biosensors 6
2.1.1 Optical Biosensors...6
2.1.1.1 Fluorescent biosensors 7
2.1.1.2 Surface Plasmon Resonance (SPR) biosensors 8
2.1.1.3 Chemiluminescence (CL) biosensors 9
2.1.2 Electrochemical biosensors..10
2.1.2.1 Amperometric biosensors 10
2.1.2.2 Potentiometric biosensors..11
2.1.2.3 Impedimetric biosensors 12
2.1.3 Piezoelectric biosensors...13
2.1.4 Magnetic biosensors...14
2.2 Comparison of different biosensing techniques....................................16
2.3 Affinity-based biosensing 17
2.3.1 Important metrics..17
2.3.2 Detection: label vs label-free; end-point vs real-time [103]............................18
2.3.3 Affinity biosensors: prospective 19

Chapter 3 Basics of capacitive sensing....................................... 21

3.1 Electrochemical Impedance Spectroscopy (EIS).................................21
3.1.1 EIS introduction 21
3.1.2 Circuit network of electrode-fluid system 21
3.2 Direct capacitive biosensing..24
3.2.1 Electric double layer 24
3.2.2 Interfacial capacitance...26
3.2.3 Capabilities 29

Chapter 4 Basics of AC electrokinetics 30

4.1 The importance of inducing ACEK 30
4.2 ACEK for particle and fluid acceleration 31
4.2.1 Dielectrophoresis (DEP)...31

4.2.2. AC electroosmosis (ACEO) and AC electrothermal (ACET) effect 32
4.2.3 Order of magnitude comparison: ACEK forces vs. natural forces 35

Chapter 5 Sensor Development 37

5.1 Incorporation of direct capacitive sensing and ACEK 37
5.2 Device design 39
5.2.1 Preparation of microelectrode sensor 39
5.2.2 Test fixture and instrument setup 42
5.3 Assay methods 44
5.3.1 Electrode surface cleaning 44
5.3.2 Surface functionalization 47
5.3.2.1 Passive adsorption 47
5.3.2.2 Usage of linker molecules 51
5.3.2.2.1 APTES treatment 52
5.3.2.2.2 Thiol mediation 54
5.3.2.3 Comparison 56
5.3.3 Surface blocking 56
5.3.4 Analyte detection 57
5.3.5 Summary 57
5.4 Sensor Characterization 58
5.4.1 Extracting the values of circuit elements 58
5.4.2 Simplified equivalent circuit 62
5.5. Conclusion 63

Chapter 6 Results of analyte detection 64

6.1 Sample and assay description 64
6.2 Bovine IgG antibody interaction 65
6.2.1 Proof-of-concept 65
6.2.2 Impact of electrode design on detection 68
6.2.3 Impact of electric field strength 70
6.2.4 Determination of LOD 75
6.3 Detection of antibody in serum 75
6.3.1 Sample preparation 76
6.3.1.1 Johne’s disease antigen and serum samples 76
6.3.1.2 Human and Bovine TB specific antigens and serum samples 77
6.3.2 Proof-of-concept 78
6.3.3 Signal optimization 80
6.3.4 Detection results of serum samples 83
6.3.4.1 Johne’s disease 83

6.3.4.2 Human and Bovine tuberculosis 84
6.4 Influenza A virus Detection 86
6.4.1 Sample preparation 87
6.4.2 Specificity 87
6.4.3 Effect of linker molecules 89
6.4.4 Blocking optimization 91
6.4.5 Blind test of clinical swab samples 92
6.5 Small molecule detection 93
6.5.1 Sample preparation 95
6.5.1.1 Bisphenol A 95
6.5.1.2 Progesterone 95
6.5.2 Detection of BPA 96
6.5.2.1 Proof-of-concept 97
6.5.2.2 Study of ACET effect 98
6.5.2.3 Determination of LOD 100
6.5.3 Preliminary detection of PG 100
Chapter 7 Conclusions and Future Work 102
7.1 Summary 102
7.2 Future Work 103
7.2.1 Further improvement of feasibility 103
7.2.2 Multiplexed assay with high specificity 104
7.2.3 Handheld device 104
List of References 105
Vita 125

LIST OF TABLES

Table 1.1 Characteristics of a desired biosensor. 3

Table 2.1 Advantages and disadvantages of different types of biosensors. .. 16

Table 4.1 Parameters involved in ACEK force calculation. 35

Table 5.1 Comparison between passive adsorption and linkers. 56

Table 5.2 Equivalent circuit parameters obtained by curve-fitting the experimental results for SAW electrodes. 59

Table 5.3 Equivalent circuit parameters obtained by curve-fitting the experimental results for gold electrodes. 61

Table 5.4 Measured voltage drop on gold electrodes. 62

Table 6.1 Target analyte description. 64

Table 6.2 Assay description. 65

Table 6.3 dC/dt (%/min) of 1 and 5ng/mL for every 10 seconds. 74

Table 6.4 Repeatability test with bTB samples. Each sample is tested five times on five different chips. 86

Table 6.5 Repeatability test with flu A virus. 1000 ng/mL virus sample is tested five times on five different chips. 90

Table 6.6 Descriptions of various blocking methods and major conclusions. 92

Table 6.7 Blind test results of twenty clinical swab Influenza A samples. 93

Table 6.8 Capacitance change rates within two different time periods. 98

LIST OF FIGURES

Figure 2.1 Fluorescence biosensor developed by previous members of our group (a) Experimental setup. (b) Fluorescence images of immunoassay. 7
Figure 2.2 Schematic view of SPR immunoassay........8
Figure 2.3 Schematic view of CL detection........9
Figure 2.4 Schematic view of a common three electrode system (left) and actual device (right). 11
Figure 2.5 An extended-gate FET biosensor for HAS antibody detection.....12
Figure 2.6 Experimental apparatus of a typical piezoelectric biosensor.........14
Figure 2.7 Schematic of immunocomplex labelling with a magnetic particle..15
Figure 2.8 A GMRS for the detection of the recognition between streptavidin and biotin. 15
Figure 2.9 Basic components of affinity biosensor........17
Figure 2.10 An HRP labeled antibody conjugate. 19
Figure 3.1 Circuit model of the electrode-fluid system. 22
Figure 3.2 Impedance spectrum of an electrode-fluid system........23
Figure 3.3 Nyquist plot of an electrode-fluid system. 24
Figure 3.4 Schematic diagram of EDL together with the variation in potential with distance y from the surface. 25
Figure 3.5 Changes at the electrode surface due to the binding of specific antibody to immobilized antigen........26
Figure 3.6 Two possible topology changes at the solid/fluid interface due to protein binding reaction. (a) The thickness of the interfacial layer increases while its surface area decreases, Cint reduces as a result; and (b) when the increase in the surface area of Cint dominates over the changes in its thickness, Cint increases. (Ab: antibody; Ag: antigen).....28

Figure 4.1 Schematic illustration of DEP force: (a) positive DEP and (b) negative DEP. 32
Figure 4.2 Schematic illustration of ACEO flow. 33
Figure 4.3 Schematic illustration of ACET flow. 34
Figure 5.1 Breaking the diffusion limit by inducing ACEK. 38
Figure 5.2 (a) Commercially available electrode chips, i.e. surface acoustic wave (SAW) resonator chips (PARS 433.92, AVX Corp). The left one is modified for immunosensing. (b) A scanning electron micrograph of the microelectrode array in the SAW chip. 40
Figure 5.3 (a) In-house fabricated gold microelectrodes on silicon wafer with a silicone chamber on top of it; (b) SEM image of the interdigitated array inside. 40
Figure 5.4 Individual sensor after dicing (left: without chamber; right: with chamber). 41
Figure 5.5 Agilent 4294A with 16047E test fixture connected with a data acquisition computer. 43
Figure 5.6 Connection of SAW chip to the test fixture. 43
Figure 5.7 Connection of gold chip to the test fixture. 44
Figure 5.8 Capacitance values with different washing methods. For each condition, five chips are measured. 46
Figure 5.9 (a)-(e) Microscopic images of incubated electrodes. Left column shows the actual image, right column shows the light intensity. 48
Figure 5.10 Different types of linker molecules. (a) APTES and (b) thioctic acid. 52
Figure 5.11 Schematic of APTES treatment of a substrate. 53
Figure 5.12 Comparison of capacitances between washed bare SAW electrodes and APTES-treated SAW electrodes. Five chips are measured and their capacitance values are plotted. 54
Figure 5.13 Schematic of thiol SAM formation and activation with NHS+EDC. 55

Figure 5.14 Comparison of capacitances between washed bare gold electrodes and thiol-mediated gold electrodes. Five chips are measured and their capacitance values are plotted. 55

Figure 5.15 Summary of assay procedure. 57

Figure 5.16 Comparison of measured impedance spectra and curve fitting using the four element equivalent circuit model of SAW electrodes. (Frequency range: 10 kHz-1MHz. Signal applied: 5 mVrms.) 59

Figure 5.17 Comparison of measured impedance spectra and curve fitting using simplified R_f-C_{int} serial connection for SAW electrodes. (Frequency range: 10 kHz-1MHz. Signal applied: 5 mVrms.) 60

Figure 5.18 Comparison of measured impedance spectra and curve fitting of gold electrodes. (a) Using the four element equivalent circuit; (b) Using R_f-C_{int} serial connection. (Frequency range: 100 Hz-1MHz. Signal applied: 5 mVrms.) 61

Figure 6.1 Normalized capacitance change as a function of time within two minutes for three different concentrations of bovine IgG antibody (10, 100 and 1000 ng/mL) in 0.1x PBS and 0.2x PBS respectively. The boxed-in numbers in the figure are the fractional capacitance change rates of different IgG concentrations. 67

Figure 6.2 Antibody binding responses from three different electrodes under similar electric field strength. Each test is repeated three times. Error bar indicates the standard deviation. Control results include both buffer and non-specific binding on un-functionalized electrodes. 69

Figure 6.3 Binding responses of control buffer, non-specific, 10 ng/mL and 100 ng/mL IgG samples under different electric field strengths. Both 2μm and 5μm gold electrodes are tested for comparison. Each test is repeated twice and the error bar indicates standard deviation. 71

Figure 6.4 Normalized capacitance change with time. (a) 2μm electrodes measured at 86 mV/μm; (b) 5μm electrodes measured at 45 mV/μm; (c) 5μm electrodes measured at 86 mV/μm. 73

Figure 6.5 Transient behavior of normalized capacitances of JD serum samples. The samples are various dilutions of JD positive sera (1:20 to 1:200), negative sera (1:20) and 0.1x PBS (control). 80

Figure 6.6 Capacitance change rates of JD positive serum sample and control buffer (0.1X PBS) when they are tested at (a) 100 kHz AC signals of various voltage amplitudes, (b) 100 mVrms AC signals at different frequencies. Each data point shows the average of three tests. Error bar indicates the standard deviation. 82

Figure 6.7 Detection results of Johne's disease serum samples. 83

Figure 6.8 Repeatability test with JD positive sample. Same positive sample is tested five times on five different SAW electrodes. 84

Figure 6.9 Capacitive sensing vs. ELISA of human TB (hTB) positive and negative serum samples. (P: positive samples, N: negative samples; C: control buffer) 85

Figure 6.10 Capacitive sensing vs. ELISA of bovine TB (bTB) positive and negative serum samples from badgers. (P: positive samples, N: negative samples; C: control buffer) 85

Figure 6.11 Specificity test of Influenza A: four different scenarios. 88

Figure 6.12 Capacitance change rates for the four scenarios under 10 and 100 mVrms. Each data point is the average of three repeated tests. Error bar indicates standard deviation. 89

Figure 6.13 Flu A detection results: passive adsorption vs. thiol linker. Each data point is the average of five repeated tests. Error bar indicates standard deviation. 91

Figure 6.14 Characteristic changes of interfacial capacitance with time when different samples arew tested. Binding reactions with 1, 10, 100 and 1000 fM BPA are shown here. Buffer (blank without BPA) and non-specific (1pM BPA sample tested on dummy electrodes) are shown as controls. 98

Figure 6.15 BPA detection results on both electrodes. Buffer tests are 0.1x PBS on functionalized electrodes; non-specific tests are 1-100 fM BPA on dummy electrodes; specific tests use 1-100 fM BPA samples on functionalized electrodes. Each data point is the average of three repeated tests and the error bar indicates standard deviation. 99

Figure 6.16 Detection results of progesterone binding. Different change rates indicate different binding levels. Each test is repeated three times. Error bar represents the standard deviation of three test results. 101

Figure 7.1 Concept of a portable POC device. 104

Chapter 1. Introduction

1.1 Biosensor: its future in your health and well-being

The spread and epidemic of infectious diseases have posed tremendous burden to the whole world [1]. For example, human tuberculosis, caused by Mycobacterium tuberculosis, occurs in more than ten million people worldwide, and is estimated to be responsible for the death of two million people annually [2]. For wildlife and livestock, diseases like Johne’s disease [3] and mastitis [4] causes the reduction of milk production (in dairy cows), weight loss and premature culling clinically affected animals. Particularly, mastitis causes an estimated $1.7-2.0 billion USD annual economic loss to the US dairy industry. Worldwide, it is the most costly disease affecting the dairy industry, incurring economic losses estimated at $50 billion/year.

In the developing world, the situation is even worse [5]. Infectious diseases are responsible for a massive death toll on the populations of developing countries every year. According to World Health Organization (WHO), 21% of childhood death in the Africa region is caused by pneumonia [6]; still in Africa, more than 25% of infants are likely to acquire AIDS in the first year of life if their mothers are infected with HIV [7]; moreover, diarrheal diseases are estimated to cause around 2.5 million deaths among children under 5 years old, of which more than 85% takes place in the world’s poorest places [8, 9].

In the face of such a harsh reality, organizations and nations are putting an increasing number of manpower and material resources towards understanding and negating the proliferation of infectious diseases [10-12]. Among all the efforts, the production of low-cost while practical diagnostic devices is one of the core tasks. Since only with appropriate diagnosis would we be able to perform the necessary therapy. Nevertheless, current diagnostic tools have fallen far behind the needs of the majority, especially in less developed areas.

For instance, most developing countries do not possess even half of the basic medical tools needed for routine health care [13]. In other words, the inabilities to provide practical low-cost devices for point-of-care diagnosis have limited the access to proper test and treatment for those that need them most [14, 15].

Recently, National Academy of Engineering (NAE) has listed healthcare as one of the grand challenges facing our global future. As of now, large percentages of vulnerable population are still seeking improved quality of life, which brings significant opportunity for technology to improve global health. For example, hassle free and comfortable health monitoring systems are always desired [16]; also, there is huge merging market space for disease diagnosis, especially if it can be done in early stage.

As an integral and crucial part of all health services, point-of-care diagnosis tool stands out as a promising future in preventing or minimizing the spread of a virus or disease outbreak. Point-of-care diagnosis refers to the action of conducting simple and quick medical testing or treatment at the site of patient, which is usually accomplished by portable/handheld devices [17, 18]. In this regard, one attractive tool that is capable of providing instant information on a disease outbreak is biosensor [19]. Biosensor is a device designed to detect or quantify a specific biomolecule such as protein or DNA. It is well established that biosensors can be applied in various fields, including medical science [20-22], food and water inspection [23-26], environment surveillance [27] and crop protection [28, 29]. In principle, biosensors offer the possibility of real-time monitoring, and the deployment of these devices in the field would provide a low-cost and rapid detection of diseases. A desired biosensor possesses some general characteristics, as provided by WHO in Table 1.1 [5].

Table 1.1 Characteristics of a desired biosensor.

●	Affordable by those at risk of infection.
●	Sensitive (few false-negative results).
●	Specific (few false-positive results).
●	User-friendly (simple to perform by persons with little training).
●	Rapid treatment at the first visit and robust use without the need for special storage.
●	Equipment-free (that is, no large electricity dependent instruments needed to perform the test.
●	Delivered to those who need it.

In addition, a medically relevant biosensor is highly desired to be able to realize more advanced functions such as multiplex sensing and intelligent data acquisition. As we can imagine, biosensors with aforementioned characteristics will have a giant impact on lifestyle related outcomes of infectious diseases.

1.2 Biosensor: its major challenges

Broadly speaking, there are two major types of biosensors: catalytic biosensor and affinity biosensor [30]. Catalytic biosensors measure the change in the concentration of target sample induced by the catalyzed reaction, they usually require the usage of certain enzyme [31]; while affinity sensors detect the occurrence of specific biomolecular interactions, such as antigen-antibody binding or DNA-DNA hybridization [32] .

Between the two, catalytic biosensors have dominated the biosensor market for decades. For example, one of the most successfully commercialized biosensors is the biocatalytic electrochemical glucose sensor [33, 34], which has benefited millions of diabetic patients. On the other hand, affinity sensors are still largely limited to scientific publications, despite a few commercial products. In general, there are several challenges hindering the development of biosensors, most of which are direct against affinity sensors.

Firstly, the detection with affinity biosensor is a two-step process: (1) immobilization of bioreceptor onto a solid surface and (2) detecting the corresponding change in the surface properties [35]. The stability and activity of immobilized bioreceptor are therefore of vital importance in determining the overall performance of the biosensor. For the moment, despite that various approaches have been studied by different research groups aiming at improving the stability and uniformity of surface coating [36-40], immobilizing the bioreceptor onto selected sites while still retaining its activity remains as one of the top challenges facing the research of affinity sensors.

Secondly, if a biosensor is to be employed for real-time diagnosis with complex reagents like blood or serum, the surface of the sensor must be durable and selective enough for the target analyte. Good selectivity (also known as specificity) [41] enables the detected signal change is caused by specific interactions instead of nonspecific ones. Selectivity is crucial in reality where target amount can sometimes be very limited and much less than interferences [42, 43]. Obtaining adequate selectivity in complex samples such as blood serum or saliva is another major challenge that has to be overcome before any practical use of biosensors.

Thirdly, limit of detection is another challenging issue. Although many publications (biosensors) claim to be able to detect infectious diseases at very low levels [44-46], most of them are determined in the absence of non-target interferences. Since it is rare for such clean samples to be realistic in practical applications, reported limits of detection might be misleading in determining a biosensor’s real-world performance [35]. In real world detection, biosensors should be challenged with mixed target/nontarget analytes to verify its feasibility.

Besides, other issues like usability, robustness and financial cost [47] are all possible limiting factors deterring the practical/commercial application of affinity biosensors.

In this work, we will design, develop and validate a novel affinity biosensor which possesses high potential of becoming a feasible point-of-care diagnosis platform.

1.3 Dissertation Outline

This dissertation is organized as follows.

Chapter 2 introduces and compares various types of biosensors based on different sensing mechanisms. Basic concepts and principles regarding affinity-based biosensing are also mentioned.

Chapter 3 introduces the theory of electrochemical impedance spectroscopy and direct capacitive sensing.

Chapter 4 introduces the basics of AC electrokinetics, including the importance of inducing ACEK to affinity biosensing and the three phenomena of ACEK.

Chapter 5 first describes the concept of incorporating capacitive sensing and ACEK. Afterwards, the whole sensor development process is introduced, including the design and setup of sensing devices, the development of assay methods and the characterization of the capacitive affinity sensor.

Chapter 6 presents the detection results of various types of samples, including antibodies, virus and small molecules. Detailed and in-depth assay development and optimization are also discussed in this chapter.

Finally, the dissertation works are summarized and future works are proposed in Chapter 7.

Chapter 2. Literature review of biosensors

In recent years, biosensors have attracted numerous research effort because of their potential to achieve rapid, inexpensive, and portable on-site diagnosis [48-51]. Yet the design of a feasible biosensor is not an easy task. It requires deep understanding of multidisciplinary topics including biology, material science, chemistry and electrical engineering [52]. This chapter introduces and compares various biosensors such as optical, electrochemical, piezoelectric and magnetic biosensors. In addition, basic concepts and principles of affinity-based biosensing are also mentioned.

2.1 Various types of biosensors

A biosensor is composed of two basic elements: a bioreceptor which enables specific biomolecular interaction and a transducer which converts the biointeraction into a measureable signal, such as a change in color. Based on different types of transducers being involved, biosensors can be classified as optical biosensor (e.g. fluorescence, surface plasmon resonance (SPR) and chemiluminescence), electrochemical biosensor (amperometry or potentiometry, cyclic voltammetry and impedance spectroscopy), piezoelectric biosensor, magnetic biosensor (e.g. giant magnetoresistive sensing) and etc. This section provides a brief overview of various biosensors aforementioned.

2.1.1 Optical Biosensors

Optical biosensors have been long studied, and some of them have already been adopted by the market [53, 54]. As the name implies, optical biosensors transform the biomolecular interaction into an optical signal, such as a change in light intensity. This section introduces several types of common optical biosensors.

2.1.1.1 Fluorescent biosensors

Fluorescence means the emission of visible light from any substance when it absorbs an excitation light of certain wavelength [55]. In fluorescent immunoassay [56], the detection of target biomolecule is done by using a “sandwich assay” [57]. Firstly the primary antibody is immobilized onto the sensor surface, then the secondary antibody which is labelled with fluorophores will be introduced to bind to the primary antibody. After washing away the unbound secondary antibodies, the surface will be excited with a light of certain wavelength so that fluorescence will be emitted and detected. Fluorescence biosensor can realize quantitative determination since the fluorescence signal is directly related to the concentration of bound antibodies. Figure 2.1 [58] demonstrates a fluorescence biosensor developed by some former members in our group, which successfully detected the binding of bovine serum antibody to pathogen specific antigen.

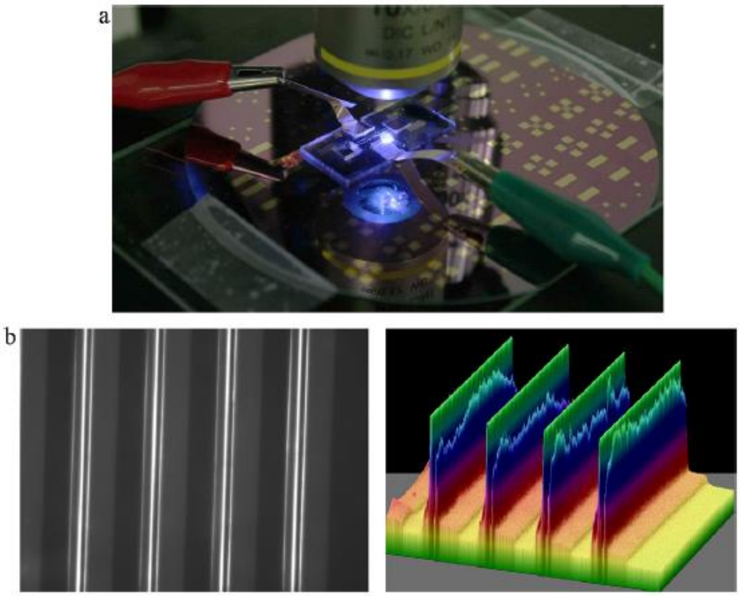

Figure 2.1 Fluorescence biosensor developed by previous members of our group (a) Experimental setup. (b) Fluorescence images of immunoassay.

Fluorescent immunoassay is one of the most widespread approaches in the field of optical biosensor because of its high sensitivity and selectivity. However, it requires multiple steps for antibody incubation and washing, making it too time-consuming, complicated and somewhat unreliable to be used for rapid point of care diagnosis.

2.1.1.2 Surface Plasmon Resonance (SPR) biosensors

SPR technique is an optical method which measures the refractive index of very thin layers of material adsorbed on a metal film [59]. To capitalize on that, SPR biosensor measures the change of refractive index at the fluid/solid interface before and after biointeraction, thus realizing the detection. SPR is very sensitive to binding since even a tiny increase in mass would lead to a proportional change in the refractive index at the fluid/solid interface. In this way, it could monitor the biomolecular interaction information on the substrate. Figure 2.2 [50] demonstrates the principle of a typical experimental configuration for SPR biosensor. A thin gold-film on a glass slide is the transducer, which is optically coupled to a glass prism for the measurement of refractive index. When biointeraction occurs, the refractive index will change accordingly.

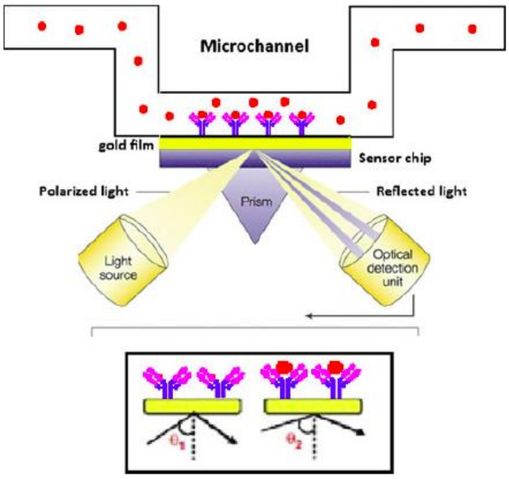

Figure 2.2 Schematic view of SPR immunoassay.

The major advantage of SPR biosensors includes its high sensitivity and the ability to realize real-time detection without any label. However, albeit to the benefits, SPR biosensor often requires sophisticated optical instrumentation and highly trained personnel to operate, making it a costly and complicated method.

2.1.1.3 Chemiluminescence (CL) biosensors

Chemiluminescence is another extensively used optical detection scheme in immunoassays [60]. CL is the light produced by a chemical reaction. CL biosensor detects the appearance and/or concentration of samples based on the intensity of emitted luminescence. As schematically shown in Figure 2.3 [50], samples A and B react with luminol (an intermediate), meanwhile the emitted light can be detected.

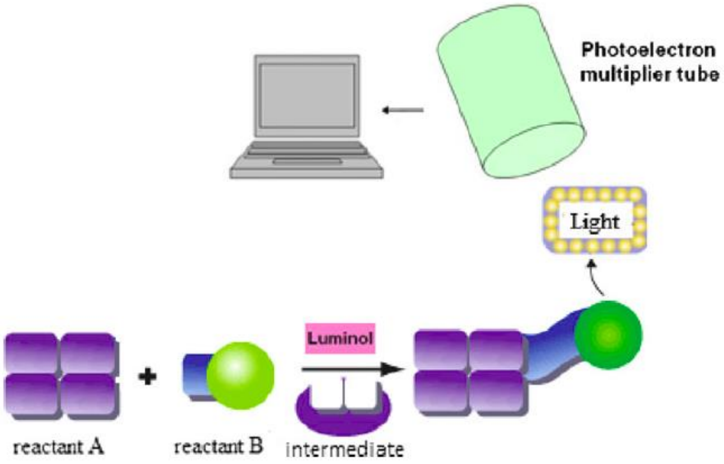

Figure 2.3 Schematic view of CL detection.

CL detection features a very low detection limit [61-63] and wide dynamic. In addition, compared with other optical methods, it does not require an excitation light instrumentation, which brings down the cost while eliminates the background interference. Nevertheless, as it still has a labelling step, CL detection is sometimes too complicated. Besides, the results could be affected by environmental factors such as temperature.

2.1.2 Electrochemical biosensors

Electrochemical biosensors have always been an important part in the field of biosensing [64-69] . Most electrochemical biosensors feature high sensitivity, low cost, low power requirement and seamless integration with standard microfabrication process. Over the past decades, a large amount of publications and demonstrations of innovative detection schemes have been presented [70-73].

Electrochemical biosensors work through the detection of an electric signal resulting from specific biomolecular interactions. Based on the signal generation principles, electrochemical biosensors are mainly categorized into three types: amperometric, potentiometric and impedimetric biosensor. This section provides an overview of these three methods respectively.

2.1.2.1 Amperometric biosensors

Amperometric sensing [49] is one of the most popular approaches among various electrochemical sensing methods. It is realized through the measurement of a current at a fixed (potentiostatic technique) or variable (voltammetric technique) potential [51]. Typical amperometric sensing involves a three-electrode system, as demonstrated in Figure 2.4 [51], which contains a working electrode, a counter electrode and a reference electrode. Current is generated at the working electrode by a redox reaction on the electrode surface. Redox reaction releases electron so that a current would be generated between the working electrode and counter electrode, which is proportional to the amount of the analyte. As the signal is relatively small, enzyme-labeled antibodies are often used for signal amplification purpose.

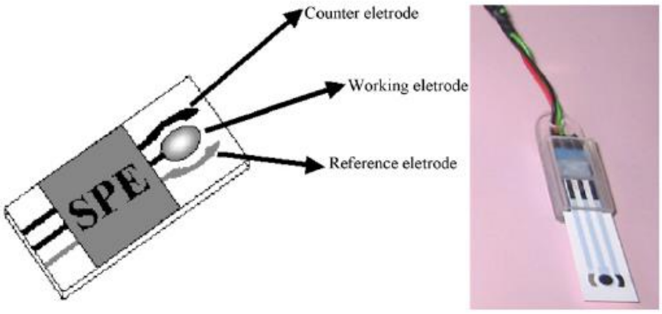

Figure 2.4 Schematic view of a common three electrode system (left) and actual device (right).

As a simple and straightforward sensing method, technology about amperometry has matured comparatively in recent years. In fact, many commercially available point-of-care biosensing systems are based on amperometric detection [74-76]. Among them, electrochemical glucose biosensor based on amperometric sensing is regarded as one of the most successfully commercialized amperometric sensors.

2.1.2.2 Potentiometric biosensors

Potentiometric sensing detects the change on the surface charge or potential charge upon the occurrence of biointeraction at the interface of the sensor [48]. Analytes in aqueous solution possess a net charge polarity, which is related with the isoelectric points [77] of bioparticles and the ionic composition of the sample reagent. The formation of probe-analyte complex will change the net charge density compared with that of probe alone, which can be measured by a potentiometer. A reference electrode in the same solution is set at a constant potential as a reference.

Aside from the change of net charge, the potentiometric signal can also be generated by changes in the pH or redox state. Broadly speaking, there are ion-selective electrodes (ISE) [78], field effect transistor (FET) [79, 80] , and light addressable potentiometric sensors [81]. As an example, Figure 2.5 [49] demonstrates a FET potentiometric biosensor for the detection of human serum albumin (HAS) antibodies.

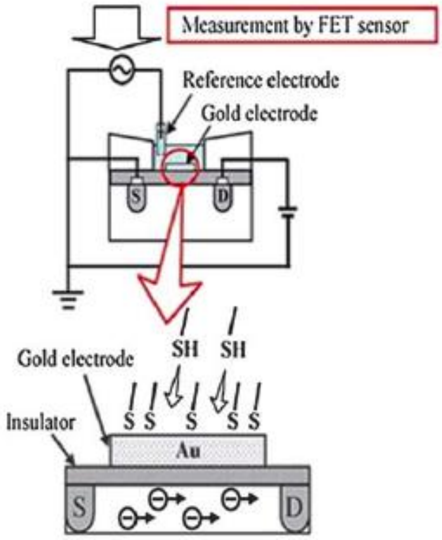

Figure 2.5 An extended-gate FET biosensor for HAS antibody detection.

2.1.2.3 Impedimetric biosensors

Impedimetric biosensors are based on impedance measurements of the biosensing system [35, 82]. It can characterize the electrical properties of the system without destroying it. An alternating current (AC) signal is applied between a pair of working electrodes, in this way the electrolysis of the electrodes [83] can be eliminated, providing a more accurate and authentic readout. In a microfluidic immunoassay, the variation of the impedance caused by the biomolecular interaction can be measured by an impedance analyzer [84]. One of the greatest advantages of impedimetric sensor is that label-free detection could be easily realized.

Recently, the research on impedimetric biosensors is directed in several directions [85], such as improving immobilization methods of receptors [86-89], exploring nanostructured electrode to amplify detection signal [39], and investigating equivalent circuit or data processing algorithm to effectively correlate analyte concentration with impedance change [90, 91] .

To sum up, compared with optical biosensor which normally requires specific and complicated equipment, most electrochemical biosensors can be readily fabricated from various conducting substrates using standard chip manufacturing methodologies. The relative low cost of electrochemical biosensor is one of the main reason that it is attracting extensive attention from both academia and industry.

2.1.3 Piezoelectric biosensors

When electric field is applied on the quartz crystal, mechanical deformation will be produced. On the contrary, when mechanical stress is applied, electric field will be generated [50]. This phenomenon is known as piezoelectric effect and the material with this characteristic is called a piezoelectric material [92].

The basic equations describing the relationship between the resonant frequency of an oscillating piezoelectric crystal and the mass deposited on the crystal surface is known as the Sauerbrey equation [93]:

$$\Delta \mathrm{F} = -2.3 * 10^{6} f^{2} \frac{\Delta m}{A} \qquad (2.1),$$

where ΔF is the frequency change in oscillating crystal in Hz, f is the frequency of piezoelectric quartz crystal, Δm is the mass of deposited analyte, and A is the area of electrode surface. According to this equation, if biointeractions take place at the surface, the resonance frequency of the piezoelectric crystal would change based on the concentration of the analyte, thus quantitative analysis can be achieved. Figure 2.6 [94] demonstrated the schematic of piezoelectric biosensing system.

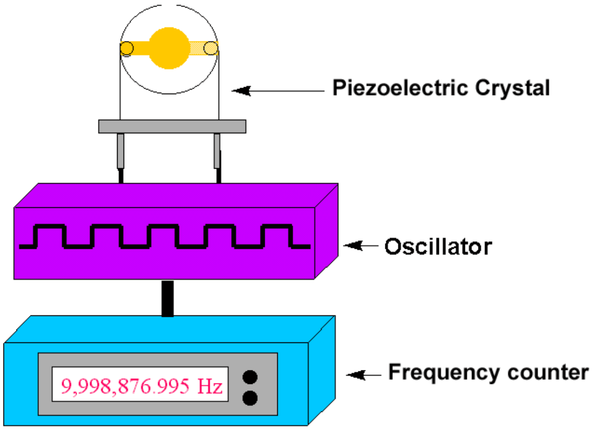

Figure 2.6 Experimental apparatus of a typical piezoelectric biosensor.

The most widely applied piezoelectric biosensor is quartz crystal microbalance (QCM), which is also known as “micro weighing instrument” [50, 95]. It works based on the piezoelectric effect to measure the mass of change on the sensor surface without the usage of label. For a classic QCM, a thin quartz crystal is placed between two electrodes, which serve to generate an AC electric field across the crystal. Under the generated field, crystal will vibrate at its resonance frequency (usually around 10-50 MHz). The vibrational displacement of the crystal changes with mass loading, thus enabling the measurement of the change in the resonant frequency of the crystal. QCM is highly sensitive to mass. For instance, Su et.al [96] reported a QCM sensor for the detection of *E.Coli* O157: H7 with a detection limit of 10^3 CFU/mL.

Compared with optical biosensors, piezoelectric biosensor does not require a labelling step, which is its biggest advantage. In addition, it features high sensitivity, real-time readout, and low cost. Nevertheless, the greatest limitation facing piezoelectric biosensor is its accuracy and repeatability, since it is extremely hard to achieve a uniform surface coating with piezoelectric materials.

2.1.4 Magnetic biosensors

Magnetic biosensing introduces magnetic beads as label particles (see Figure 2.7 [97]). After the occurrence of biointeractions, the formation of the biocomplex is measured by detecting the appearance of the magnetic particles, which can be performed in several ways. A simple method to detect magnetic particles is to measure optically the fraction of the surface that has been covered, yet it does not exploit the magnetic features of the particle. To capitalize on that, a more general way is to detect the changes in the magnetic field caused by the presence of the magnetic particles, which is performed by using giant magnetoresistance sensor (GMRS) [98]. When magnetic particle gets close to a GMRS, the resistance of the magnetoresistor will decrease because the magnetic field is influenced by the magnetic particles. Figure 2.8 [99] demonstrates a GMRS detecting the binding of streptavidin to biotin. It should be noted that magnetic particles need to be aligned, otherwise the magnetic field will cancel each other.

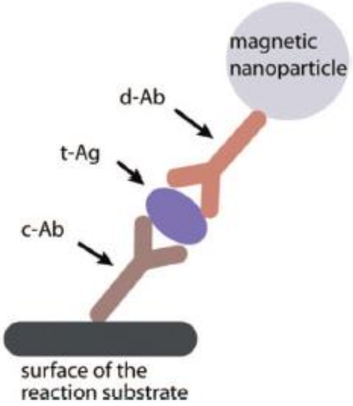
magnetic nanoparticle
d-Ab
t-Ag
c-Ab
surface of the reaction substrate

Figure 2.7 Schematic of immunocomplex labelling with a magnetic particle.

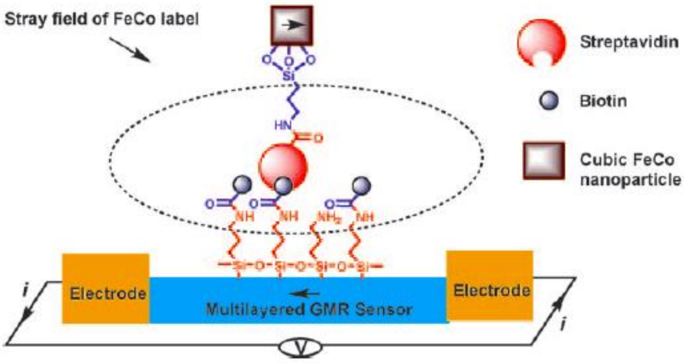
Stray field of FeCo label
Streptavidin
Biotin
Cubic FeCo nanoparticle
HN
O
NH
NH_2
Si
Electrode
Multilayered GMR Sensor
Electrode
i
i
V

Figure 2.8 A GMRS for the detection of the recognition between streptavidin and biotin.

In addition, magnetic biosensors have been demonstrated in the detection of many other biological samples such as the antigen of Y.pestis [100], polycyclic aromatic hydrocarbons [101] and colorectal circulating cancer cells [102] with very low limit of detection. It is regarded as a good competitor for point-of-care applications but requires further developments with respect to fluidic delivery and usage with clinical samples. Another drawback of magnetic biosensors is the requirement of label, which further complicates the procedure.

2.2 Comparison of different biosensing techniques

Based on different sensing mechanisms aforementioned, here we listed the advantages and disadvantages regarding each type of biosensors in Table 2.1.

Table 2.1 Advantages and disadvantages of different types of biosensors.

Sensor Types		Advantages	Disadvantages
Optical biosensors	Fluorescence	High sensitivity; good stability; real-time detection	Complicated steps; time consuming; costly equipment
	SPR	High sensitivity; non-invasive; label-free; real-time detection	sophisticated optical instrumentation ;highly trained personnel required
	CL	Low detection limit; wide dynamic; relative low cost	Complex procedure; label required; can be affected by environmental factors.
Electrochemical biosensors	Amperometric	Simple, straightforward; easy to integrate;	Low sensitivity; poor stability.
	Potentiometric	High specificity; label-free	Low sensitivity; too-complicated.
	Impedimetric	Label-free; low cost; easy to perform	Lack of specificity
Piezoelectric biosensors		Ultra high sensitivity (pictogram level); label-free	Poor repeatability; poor stability
Magnetic biosensors		Low detection limit; high sensitivity	Label required; hard to be integrated into a platform.

Compared with other sensing techniques, microelectrode impedimetric biosensing is rather advantageous due to its simplicity in operation and its low cost in fabrication. Moreover, the ability to achieve in-situ detection without the requirement of labelling makes it even more promising towards the building of a reliable and feasible biosensor for real world diagnosis.

2.3 Affinity-based biosensing

Affinity biosensors detect biological particles based on specific binding between analyte and probe molecules, as schematically shown in Figure 2.9. Probe molecules, also known as bioreceptors, are first immobilized onto a solid surface prior to adding the analyte sample solution. The analytes of interest are then introduced and form probe-analyte complexes at the surface [103]. A transducer is involved to transform the biological interaction into a measureable signal (either optical, electrical or etc.), which can thus be measured by the appropriate instrument.

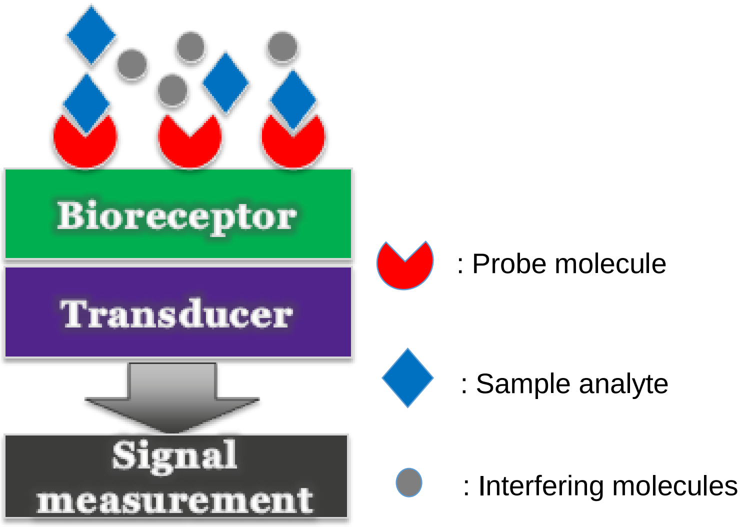

Figure 2.9 Basic components of affinity biosensor.

2.3.1 Important metrics

Several important metrics used to judge the performance of a biosensor are sensitivity, specificity, reproducibility, reliability and etc. Sensitivity may refer to two different concepts: one is the lowest detectable analyte concentration, which is more commonly known as the limit of detection (LOD) [104]; the other is how detection signal changes when the analyte concentration changes, i.e. the slope of the calibration curve [105]. In this work, sensitivity refers to the latter definition and it's differentiated with LOD. Specificity, also known as selectivity, means the ability of the sensor to detect the analyte of interest while other interfering molecules are present, which is often the case of real biological samples. In addition, reproducibility represents the sensor's ability to reproduce the same study by either the same person or a different researcher independently. Reliability, as a whole, depends on both the sensor's specificity and reproducibility [65]. All of these aforementioned metrics would together determine the feasibility of a biosensor to be applied for real world diagnosis.

2.3.2 Detection: label vs label-free; end-point vs real-time [103]

Biosensors are able to provide a quantitative detection of analytes of interest, as the measurable signal is directly related to the concentration of the analyte. Depending on whether a label molecule is needed to generate a readable signal, analyte detection can be classified as labeled or label-free detection. Label molecules are molecules with unique properties such as fluorescent particles [106, 107], chemiluminescent particles [108, 109] or redox markers [70, 110]. Figure 2.10 shows an example of a horseradish peroxidase (HRP) labeled antibody, which is commonly used in immunoassay to as a signal amplifier [111, 112]. Prior to labeled detection, label molecules are attached to the analyte of interest, thus the detection of sample analyte can be achieved through the detection of label molecules. The usage of labeled detection usually enables much higher sensitivity, as the signal is enhanced by the unique properties of the labels [48].

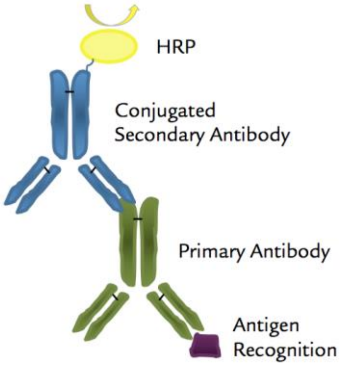

Figure 2.10 An HRP labeled antibody conjugate.
(Source: http://www.rockland-inc.com/custom-antibody-conjugation.aspx)

Compared with labeled detection, label-free detection, which enables direct detection of analyte of interest, is attracting more attention in recent years [35, 113, 114]. Labeling can sometimes be problematic. For example, it is difficult to label irregular or tiny molecules. Besides, labeling complicates the procedure and brings more uncertainty to the detection [115].

Another way of classifying detection methods is based on the time point where actual detection occurs. End-point detection occurs after the biointeraction is stopped, it is a single point measurement of the probe-analyte complex. As a result, it causes more inaccuracy and only limited reaction information can be obtained. Real-time detection [116-118], on the other hand, measures the reaction continuously while the biointeraction is taking place, thus allowing instantaneous and more precise information.

As we could tell, a label-free and real-time detection system [119, 120] would be more favorable towards the development of biosensors for practical applications.

2.3.3 Affinity biosensors: prospective

As mentioned in the Chapter 1.2, the majority of affinity biosensors are still under the level of academic researches either due to the lack of reliability or the excessive costs. However, compared with catalytic biosensors, affinity biosensors are more versatile and flexible in terms of diagnosis applications. Catalytic biosensors require the usage of catalyst to trigger certain chemical reaction, which limits their application field and complicates their readout. On the other hand, affinity biosensors can detect any biointeractions happened at the sensor surface through various methodologies, thus enables a much broader application range.

Despite current challenges, current researches regarding affinity biosensors have demonstrated their potential to become feasible and effective tools for real world disease diagnosis in the near future.

Chapter 3. Basics of capacitive sensing

3.1 Electrochemical Impedance Spectroscopy (EIS)

Among various affinity-based sensing methods, impedimetric sensing is promising due to its reasonable cost, ease of operation and the ability to realize label-free and real-time detection. In this chapter, we start with the introduction of Electrochemical Impedance Spectroscopy (EIS), which stands as the fundamental of impedimetric sensing techniques.

3.1.1 EIS introduction

Electrochemical impedance spectrum [121-123] analysis is a well-established method for characterizing an electrolytic cell. Usually a small signal perturbation is applied to the electrode across a wide frequency range, the corresponding magnitude and phase responses are measured and plotted as the impedance spectrum [103]. In EIS, a network of electronic components can be developed to represent an electrochemical cell. A change in the EIS spectra can be correlated with a change in the (di) electric properties near the electrode/electrolyte interface due to biomolecular interactions. The ability of realizing label-free detection with relatively easy configuration has made EIS a popular biosensing method for decades [124].

3.1.2 Circuit network of electrode-fluid system

The impedance of an electrode immersed in liquid can be approximated as a network of capacitive and resistive components, as conceptually shown in Figure 3.1. It consists of fluid resistance (R_f) and capacitance (C_f), which represents the resistance and capacitance from the bulk fluid; and charge transfer resistance (R_{ct}) and interfacial capacitance (C_{int}), which origins from the electrode/fluid interface. EDL refers to the electric double layer [125, 126], which usually forms at the electrode/fluid interface. EDL will be discussed in detail in the next section. The charge transfer resistance [127] is attributed to the interactions of ions in the solution with the electrons in the electrodes which produce a current.

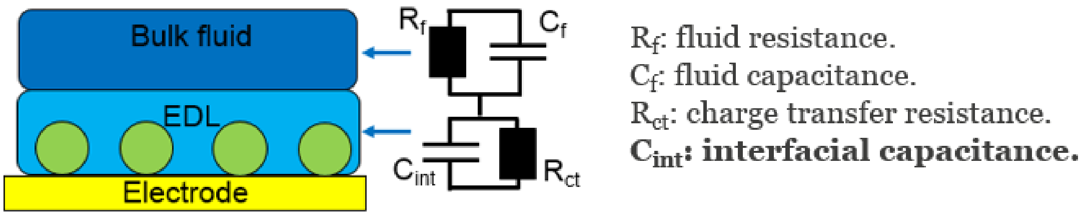
Bulk fluid
EDL
Electrode
R_f
C_f
C_{int}
R_{ct}
R_f: fluid resistance.
C_f: fluid capacitance.
R_{ct}: charge transfer resistance.
C_{int}: interfacial capacitance.

Figure 3.1 Circuit model of the electrode-fluid system.

There are two types of electrochemical reactions: Faradaic reaction and non-Faradaic reaction. If charge transfer across the interface is cause by the flow of a DC current, it is regarded as a Faradaic reaction. For Faradaic reaction, charge transfer resistance is the dominating factor of the impedance response. On the other hand, if no DC current flows across the interface and the charges are associated with the movement of ions, the reorientation of dipoles [126] and etc., it is regarded as a non-Faradaic reaction. This work focuses on affinity sensing based on non-Faradaic reactions, in such cases, interfacial capacitance will dominate the impedance response of the system [103].

Figure 3.2 shows an impedance spectrum of an electrode-fluid system, which is also known as the Bode plot [128]. Bode plot provides frequency related information, which can be related to the equivalent circuit model of the system: at low frequency range (usually <100 Hz), R_{ct} dominates the impedance, therefore it favors the sensors base on Faradaic reaction; while at high frequency range (usually >1 MHz), the impedance will be dominated by R_f and C_f, which have almost zero impact to interface impedance. For affinity-based biosensing, most biointeractions happen at the interface, therefore such high frequency range becomes inappropriate. Only at intermediate frequency range (from several kHz upto several hundred kHz) will the impedance be dominated by interfacial capacitance, which serves as the proper frequency range for this work.

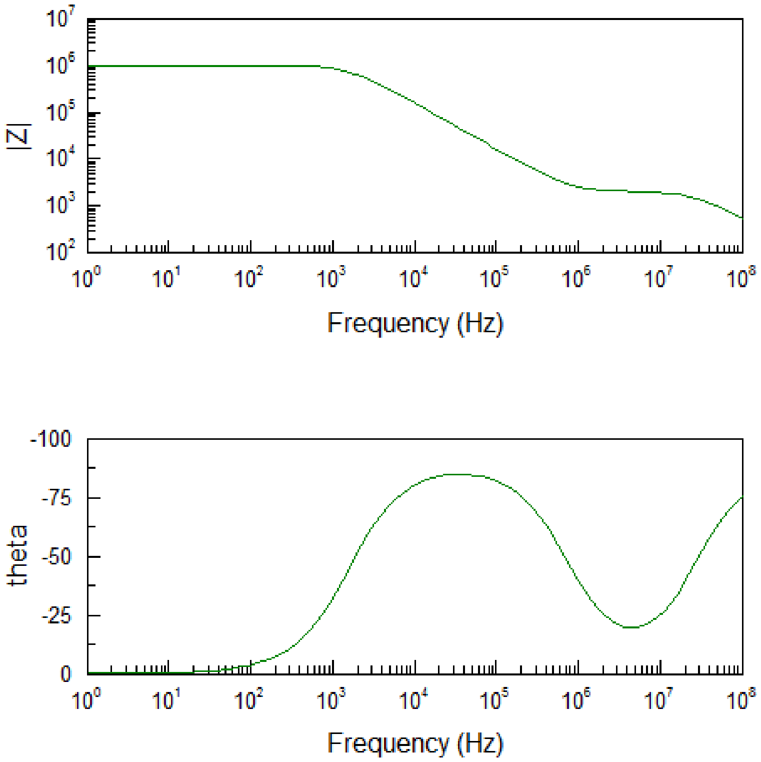

Figure 3.2 Impedance spectrum of an electrode-fluid system.

Another popular method for impedance presentation is Nyquist plot, where the real part of the impedance is plotted on the X-axis and the imaginary part is plotted on the Y-axis [129]. Figure 3.3 shows a Nyquist plot obtained using the proposed circuit model. Nyquist plot is mostly applied to sensors based on Faradaic reaction, as R_f and R_{ct} can be easily determined from it [130]. As shown in Figure 3.3, the diameters of the two semicircles would be the value of R_f (the smaller one on the left) and R_{ct} (the larger one the right), respectively.

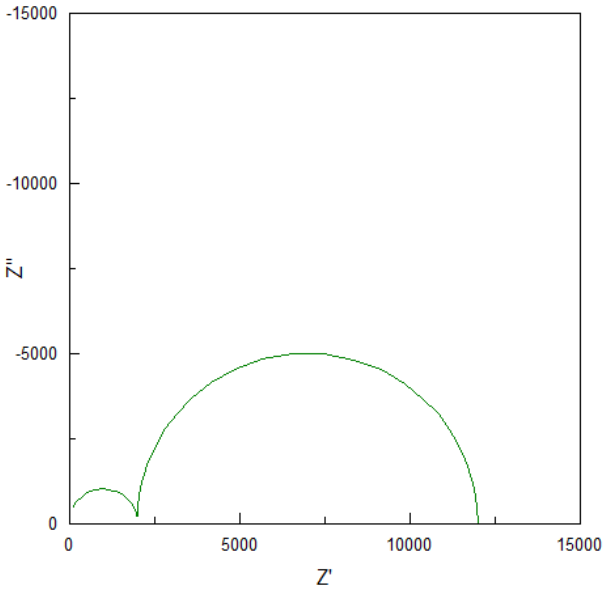

Figure 3.3 Nyquist plot of an electrode-fluid system.

3.2 Direct capacitive biosensing

Albeit its usefulness, regular EIS requires complex data analysis to extract the relevant biological information. In recent years, direct capacitive biosensing has become an active embranchment of impedimetric sensing [131-133], as its ability to convert a signal of biomolecular interaction straight to a change in capacitance.

3.2.1 Electric double layer

When a solid material is immersed into an electrolytic solution, the solid surface will acquire surface charges. To maintain charge neutrality, a thin layer of counter ions is formed at the solid/liquid interface to neutralize the surface charges at the solid surface, which is commonly known as the electric double layer (EDL), as schematically shown in Figure 3.4 [126]. Electrically, EDL can be modeled as a capacitor. The layers of counter ions and surface charges are equivalent to the two plates in a capacitor, and the plate separation distance is the EDL thickness, which is characterized by Debye length (κ^{-1}) [134]. Debye length defines the distance where potential decays exponentially from $\emptyset_0$ (y=0) to $\emptyset_0/e$ (y=κ^{-1}), which is approximately the range that the applied potential can change the charge distribution in the bulk solution. This represents the range that the changes of charge distribution, due to biointeractions, can lead to the changes in interfacial capacitance [103].

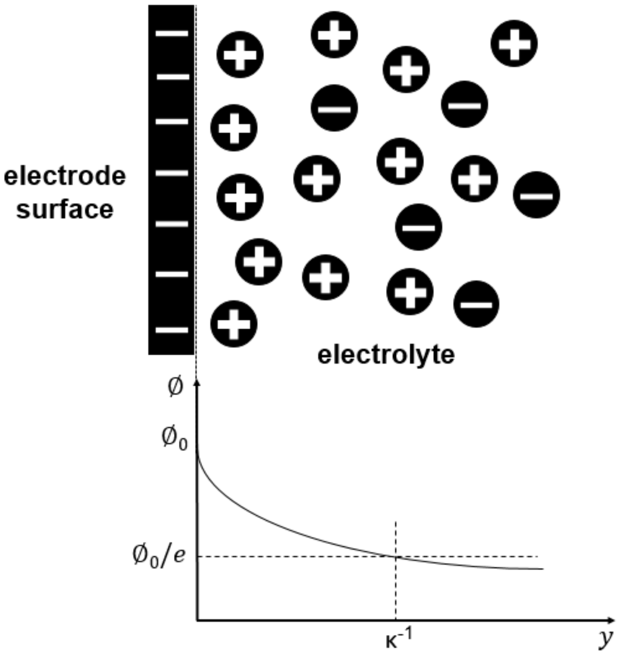

Figure 3.4 Schematic diagram of EDL together with the variation in potential with distance y from the surface.

The value of Debye length is given by Eqn (3.1) [126]:

$$\kappa^{-1} = \sqrt{\frac{\varepsilon k_B T}{2z^2q^2n_0}}, \qquad (3.1)$$

where ε is the permittivity of the electrolyte, k_B is the Boltzmann constant, T is the temperature, z is the valence, q is the charge on a single electron and n_0 is the number density of charge. Debye length is inversely proportional to the electrical conductivity of the fluid. For most biological reagents, it is a few nms thick [126, 134].

3.2.2 Interfacial capacitance

Capacitive biosensors exploit the change in thickness or dielectric properties of the dielectric layer at the electrolyte–dielectric interface, which will lead to a change in the interfacial capacitance of the device upon the occurrence of biointeractions.

The interfacial capacitor consists of a series connection of equivalent capacitors caused by EDL and biomolecule deposition. When biomolecules are adsorbed onto the electrode surface, the interfacial capacitance (C_{int}) will change due to the change in the thickness and surface area of C_{int}, which can then be used to indicate the deposition of biomolecules or particles on the electrode as well as to be correlated with the biomolecule or particle concentration in the fluid. The whole process is schematically shown in Figure 3.5 (using antigen-antibody binding as an example).

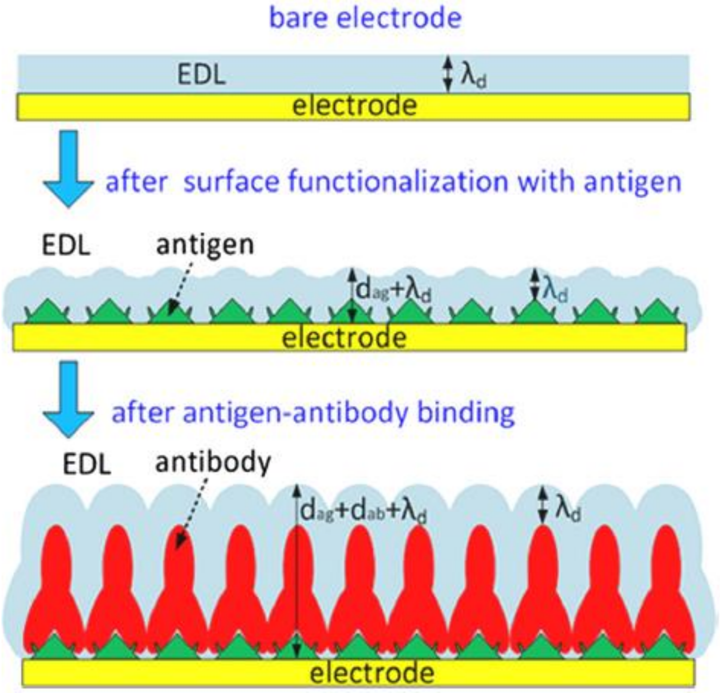
bare electrode
EDL
λ_d
electrode
after surface functionalization with antigen
EDL
antigen
$d_{ag}+\lambda_d$
λ_d
electrode
after antigen-antibody binding
EDL
antibody
$d_{ag}+d_{ab}+\lambda_d$
λ_d
electrode

Figure 3.5 Changes at the electrode surface due to the binding of specific antibody to immobilized antigen.

As schematically shown in Figure 3.5, at first the interfacial capacitance of bare electrode is given as:

$$\mathrm{C_{int,0}} = \varepsilon_s \mathrm{A_{int}} / \lambda_d \,, \tag{3.2}$$

where ε_s is the permittivity of the solution, $\mathrm{A_{int}}$ is the surface area of the interfacial capacitor of the electrode, and λ_d is the thickness of the double layer. Then, after the electrode surface is deposited with antigens, the capacitance changes to:

$$\mathrm{C_{int,ag}} = \mathrm{A_a} / (\left({}^{1}/_{\varepsilon_p} \right) d_{ag} + \left({}^{1}/_{\varepsilon_s} \right) \lambda_d) \,, \tag{3.3}$$

where ε_p is the permittivity of the antigen probes. The relative permittivity of probe is around 2-3 [135] , while that for water solution is around 80. $\mathrm{A_a}$ is the surface area after antigen deposition, and d_{ag} is the antigen thickness. At last, after the antibody binding reaction, the dielectric layer becomes the sum of the EDL (λ_d), the antigen probe (d_{ag}), and the bounded antibodies (d_{ab}). As a result, the interfacial capacitance changes to:

$$\mathrm{C_{int,ab}} = \mathrm{A_b} / [\left({}^{1}/_{\varepsilon_p} \right) (d_{ag} + d_{ab}) + \left({}^{1}/_{\varepsilon_s} \right) \lambda_d] \,, \tag{3.4}$$

where $\mathrm{A_b}$ is the surface area of the interfacial capacitor after binding, d_{ab} is the antibody thickness. Subtracting $\mathrm{C_{int,ag}}$ by $\mathrm{C_{int,ab}}$, we could get the relative change of interfacial capacitance caused by antibody binding (assuming that $\mathrm{A_a} \approx \mathrm{A_b}$):

$$\Delta \mathrm{C} / \mathrm{C_{int,ag}} = \frac{\mathrm{C_{int,ab}} - \mathrm{C_{int,ag}}}{\mathrm{C_{int,ag}}} = -d_{ab} / [\left(d_{ag} + d_{ab} \right) + \left({}^{\varepsilon_p}/_{\varepsilon_s} \right) \lambda_d], \tag{3.5}$$

Consequently, the surface binding, i.e. the addition of d_{ab}, can be detected through $\Delta \mathrm{C} / \mathrm{C_{int,ag}}$.

Furthermore, since $\Delta \mathrm{C} / \mathrm{C_{int,ag}}$ can be directly correlated with the amount of bounded biomolecules on the electrode surface, capacitive sensing is a quantitative detection method to a certain extend. In reality, when measuring the impedance of an electrode/electrolyte cell, there always exist inconsistencies from sensor to sensor, mostly due to the variations in electric properties of real life samples and the bottom-up nature of surface functionalization. As a result, the baseline and initial capacitances will have a range instead of a well-defined value. Using the capacitance change rate, the uncertainty in test results can be reduced, since the aforementioned test variations will largely be factored out.

The aforementioned change of interfacial capacitance can be either positive or negative, as conceptually shown in Figure 3.6. Antibodies are deposited onto the surface because of binding. The thickness of the dielectric layer increases, which could cause a decrease in the interfacial capacitance (Figure 3.6a). On the other hand, randomly deposited antibodies could cause an increase in the interfacial capacitor's surface area due to extra topology introduced by the antibody, especially when the probe (antigens) are spaced apart, leading to a higher interfacial capacitance (Figure 3.6b). Both changes could occur during the binding. Oftentimes, one type of change dominates over the other, then the detection of binding is possible.

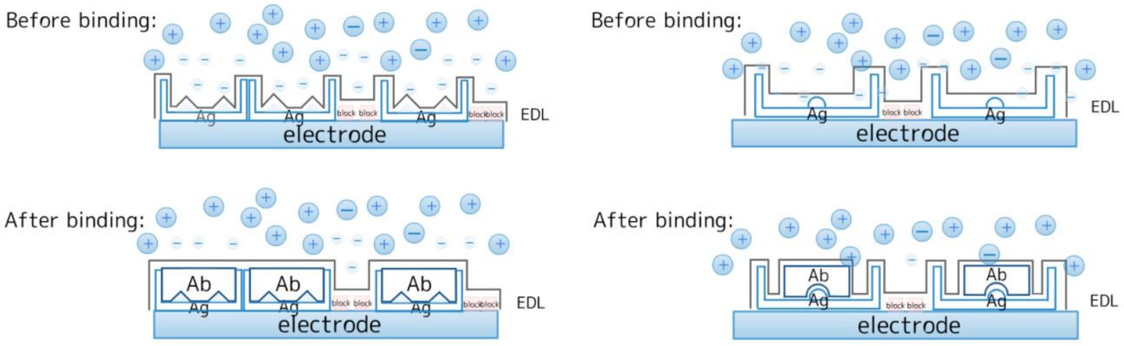

(a) (b)

Figure 3.6 Two possible topology changes at the solid/fluid interface due to protein binding reaction. (a) The thickness of the interfacial layer increases while its surface area decreases, Cint reduces as a result; and (b) when the increase in the surface area of Cint dominates over the changes in its thickness, Cint increases. (Ab: antibody; Ag: antigen)

The situation in Figure 3.6a, i.e. a decrease in C_{int} due to antigen-antibody binding, is more commonly observed [84]. In a diluted buffer, the EDL is relatively thick. As EDL envelops the antibodies on the electrodes, fine features on the scale of EDL thickness (d_{edl}) will be lost, and the C_{int} change will be dominated by an increase in its thickness, i.e. C_{int} reduces. When EDL thickness is comparable to that of antibody topology, a positive change of C_{int}

is possible, especially in a buffer of high ionic strength [136].

In this work, after a great amount of experiments, we found that both an increase and a decrease in C_{int} could possibly arise from probe-analyte binding, depending on the type of sample being tested. Preliminary experiments are conducted to support the above hypothesis about the interfacial capacitance change. Buffer of two different ionic strengths, 1 mM and 2 mM phosphate buffer saline (PBS), are used. The results corroborate that the EDL thickness (~nm) relative to the characteristic length of deposited macromolecules will determine whether a decrease or an increase in interfacial capacitance would result from binding reactions. The detailed results will be discussed in Chapter 6.

3.2.3 Capabilities

In general, capacitive affinity sensing technique has two major functions: realizing the study of nanoscale surface structure and deposition; and carrying out the detection of specific surface biomolecular interactions. In this work, the first function is used for the monitoring surface quality of sensor electrodes, while the second function is applied to detect specific biomolecular interaction, such as antigen-antibody binding.

Chapter 4. Basics of AC electrokinetics

4.1 The importance of inducing ACEK

Affinity-based biosensors typically rely on passive diffusion of analytes for binding reaction, which in many cases lead to long detection time and lack of sensitivity. It could take hours or even days for the amount of bound molecules to reach a detectable level [137, 138]. To achieve a useful sensitivity within practical time scales beyond what is dictated by the limitation of molecular diffusion, active guidance of biomolecules is needed to direct them to sensors. A number of strategies have been investigated to provide sample concentration in liquids, such as magnetic particles [139, 140] and optical tweezers [141, 142]. However, those methods are somewhat too complicated for POC testing [5]. In contrast, electrokinetic in-situ concentration of analytes can be seamlessly incorporated into capacitive detection to break the diffusion limit.

Alternating current electrokinetics (ACEK), as a particle and fluid manipulation mechanism, has minimal requirements on the device fabrication and operation to be incorporated into a detection system, -- only microelectrodes and their AC signal source need to be added. This chapter introduces the three fundamental phenomena of ACEK [143]: dielectrophoresis (DEP), AC electroosmosis (ACEO), and AC electrothermal effect (ACET). Among them, DEP induces directional particle movement, while ACEO and ACET manipulate particles through fluid viscosity and gradients in local conductivity. An order of magnitude estimation of ACEK forces is also provided and compared with some other natural forces.

4.2 ACEK for particle and fluid acceleration

AC electrokinetic microfluidics [126] emerged in the 1990s and has been intensively studied as a means to manipulate particles or macromolecules. It has been demonstrated by several groups [144-147] that ACEK working with microelectrodes can induce *in situ* concentration of particles for improved detection sensitivity and throughput. Initial studies in our group have investigated ACEK concentration of biomolecules by both numerical study [148] and experiments [149, 150]. ACEK effects exploit AC electric field to induce particle and fluid movement, so that biomolecules can be in-situ concentrated onto microsensors [151]. When an inhomogeneous AC electric field is applied to an aqueous solution, both particle movement and fluid microflows can be induced to transport particles.

4.2.1 Dielectrophoresis (DEP)

The manipulation of particles by DEP is based on the difference between the particle polarizability and that of the medium solution at a certain frequency [147]. When a particle is placed in a non-uniform electric field, electric field density on one side of the particle will be larger than that on the other side, which would lead to a net force on the particle. This force is called a DEP force. As shown in Figure 4.1 [152] , DEP force can either be positive (when the particle is more polarizable than its surroundings) or negative (when medium is polarizable than the particle). Positive DEP leads the particle to move towards the high electric filed region, while negative DEP does the opposite.

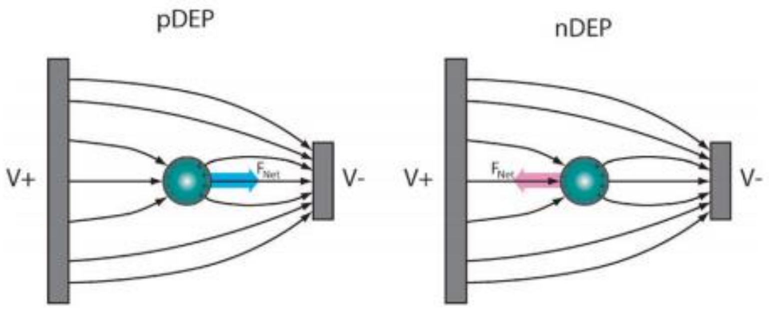

(a) (b)

Figure 4.1 Schematic illustration of DEP force: (a) positive DEP and (b) negative DEP.

Theoretically, DEP force on a spherical particle can be expressed as follows:

$$\mathrm{F_{DEP}} = \pi a^3 \varepsilon_m \mathrm{Re}\left[\frac{\varepsilon_p^* - \varepsilon_m^*}{\varepsilon_p^* + 2\varepsilon_m^*}\right]\nabla|E|^2 \approx \pi a^3 \varepsilon_m \mathrm{Re}\left[\frac{\varepsilon_p^* - \varepsilon_m^*}{\varepsilon_p^* + 2\varepsilon_m^*}\right]\frac{|E|^2}{r}, \qquad (4.1)$$

where $\varepsilon^* = \varepsilon - j\sigma/\omega$ is the complex permittivity with ε, σ and ω being permittivity, electrical conductivity and angular frequency; subscript p and m denote particle and medium, respectively. Re is the real part of a number, and $\left[\frac{\varepsilon_p^* - \varepsilon_m^*}{\varepsilon_p^* + 2\varepsilon_m^*}\right]$ is known as Clausius–Mossotti factor (f_{CM}) and is frequency dependent with a value between -0.5 and 1. a is the particle radius; E is the electric field strength, and r is the distance to the center of the electrode gap. f_{CM} determines the polarity of DEP force: when it is positive, the particle will experience positive DEP force, moving towards high electric field regions, such as electrode edges; when it is negative, the particles will experience negative DEP force, being repelled from electrodes. Positive DEP is employed for particle concentration in this work.

4.2.2. AC electroosmosis (ACEO) and AC electrothermal (ACET) effect

Based on Eqn (4.1), the magnitude of DEP force depends largely on the particle volume. In case of nanoscale biomolecules such as antibodies (small radius), DEP is effective only with high $\nabla|E|^2$, i.e. high electric field gradient, which means that molecules need to be within a very short distance from the electrodes to experience sufficient DEP attraction, which can be difficult for some circumstances. Fortunately, ACEO and ACET could work as a perfect complementation, inducing fluid movements which will carry molecules towards the electrode surface even from a long range.

"AC electroosmosis refers to the microfluidic motions generated at electrode surfaces when AC signals are applied. It relies on the induction and movement of mobile charges in the double layer at electrode surfaces and typically happens at low frequencies when the interfacial impedance dominates.[143]" The schematic of ACEO flow is shown in Figure 4.2. Moreover, ACEO typically dominates at low ionic strength. The flow velocity of ACEO has been observed to decrease significantly with increasing conductivity and eventually drop to zero above 0.085 S/m [153]. For biological applications, the ionic strength of suspending medium must maintain a certain level so that biomolecules can stay alive. In this study, phosphate buffered saline (PBS) containing 15 mM Na+ is used as the medium, with a conductivity of 0.18 S/m, thus ACEO flow will be negligible.

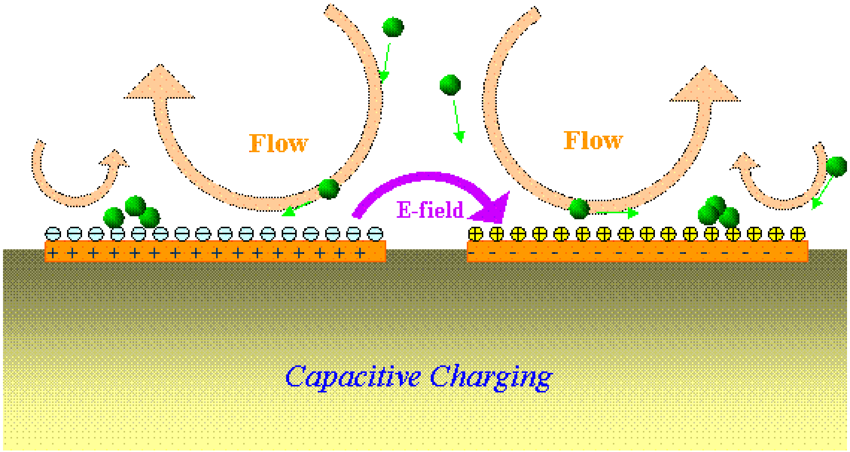

Figure 4.2 Schematic illustration of ACEO flow.

To actuate fluid at such high conductivities, a feasible option is to use AC electrothermal effect. ACET has been demonstrated as a promising technique to manipulate conductive fluids [154-157]. The AC electrothermal effect results from the interactions of AC electric fields and temperature gradients in the fluid.

Therefore it favors higher fluid conductivity, since higher temperature gradient could be generated, leading to stronger ACET flows.

ACET effect could exert volume force on fluid to generate microflows as: [153, 158]

$$< F_{ET} >= -M(\omega, t)\ (\frac{\varepsilon_m \sigma_m V_{RMS}^4}{2k\pi^3 r^3 T}) \approx 0.011\,\frac{\varepsilon_m \sigma_m}{k}\pi r E^4, \qquad (4.2)$$

where M is a dimensionless factor which predicts the variation of force with frequency: for frequencies lower than 1 MHz, i.e. ${}^{\omega\varepsilon_m}/_{\delta_m} \ll 1$, $M = +6.6$, where ω is angular frequency. ε_m and $\sigma_m$are the permittivity and conductivity of the fluid, respectively. V_{RMS} is the RMS (root mean square) value of the applied voltage. k is the fluid thermal conductivity; r is the distance to the center of the electrode gap and T is the temperature in Kelvin.

The schematic of ACET flow is shown in Figure 4.3 [159]. At the frequency range of this work, ACET flow can be regarded as frequency-independent, and scales with the electric conductivity of fluid. With planar electrodes, ACET effect will induce vortices above each electrode, and the microflows will convect the embedded particles towards the electrode surface [160]. Because fluidic forces have no dependence on particle size (from Eqn (4.2)), ACET microflows will be well suited for transporting biomolecules to the electrodes. Furthermore, previous work by our group member Liu [58] have shown that ACET effect is playing an important role in increasing detection sensitivity.

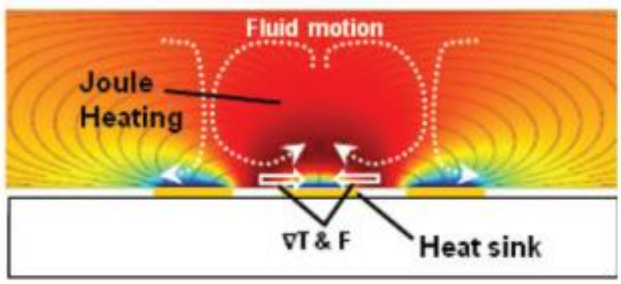

Figure 4.3 Schematic illustration of ACET flow.

Combining DEP and ACET effect, nanoscale particles are collected over a large range to the electrodes, so as to realize accelerated and sensitive detection of biomolecular binding reaction.

4.2.3 Order of magnitude comparison: ACEK forces vs. natural forces

For the purpose of showing the effectiveness of ACEK in flow acceleration and particle concentration, this section compares the relative magnitudes of different forces (i.e. ACEK forces and natural forces) and their induced flow velocities.

First, an order of magnitude estimation of DEP and ACET forces is provided using Eqns (4.1) and (4.2), with parameters assumed to be close to the application purpose of this work. Table 4.1 lists the parameters involved in calculation.

Table 4.1 Parameters involved in ACEK force calculation.

●	$\mathbf{E} = {}^{\boldsymbol{V}}/_{\boldsymbol{\pi r}}$, r= 0.5 um.
●	Applied voltage: V= 1 Vrms.
●	Particle mass and size: molecular weight: 150 kDa, which is equal to 2.5e-22 kg. Particle is assumed as spherical with radius of 10nm (a=10 nm)
●	$\mathbf{Re}[\boldsymbol{f_{CM}}]$=1, f= 100 kHz.
●	Permittivity of medium: $\boldsymbol{\varepsilon_m} = \boldsymbol{\varepsilon_r \varepsilon_0} =$ 80*8.85e-12 F/m.
●	Electrical conductivity of medium: $\boldsymbol{\sigma_m}$= 0.18 S/m
●	Thermal conductivity of medium: k= 0.6 W/ (m*K).
●	Temperature: T=300 K.
●	Viscosity of medium: $\boldsymbol{\eta}$= 1e-4 kg/ (m*s).

According to Eqn (4.1), the time-averaged DEP force is calculated to be:

$$F_{DEP} = \pi a^3 \varepsilon_m Re[f_{CM}] \nabla |\mathrm{E}|^2 \approx 4.4 * 10^{-16} N \tag{4.3}$$

Then, according to Stokes' law [161], DEP velocity is calculated to be:

$$v_{DEP} = {}^{F_{DEP}}/_{6\pi\eta a} \approx 20\ \mu m/s \tag{4.4}$$

As shown in Eqn (4.1), $F_{DEP} \propto |\mathrm{E}|^2$, so if the applied voltage drops to 100 mVrms, DEP velocity will drop to $0.2\ \mu m/s$.

Based on Eqn (4.2), time-averaged volume ACET force on fluid is calculated to be:

$$F_{ET} = -M(\omega, t)\left(\frac{\varepsilon\sigma V_{RMS}^4}{2k\pi^3 r^3 T}\right) \approx 610\,\frac{\mathrm{N}}{m^3} \quad (4.5)$$

Again, applying Stokes' law gives us an estimation of the fluid velocity [153]:

$$v_{ACET} \approx \frac{5*10^4}{1}\,\frac{\varepsilon\sigma V_{RMS}^4}{k\eta r}\left|\frac{1}{\sigma}\frac{\partial\sigma}{\partial T}\right| = 42\,\mu\mathrm{m/s} \quad (4.6)$$

Since $F_{ACET} \propto |\mathrm{E}|^4$, ACET velocity will drop to 4.2 nm/s if the voltage drops to 100 mVrms.

Next, let's consider the effect of natural forces. Gravity is the main external influence on a particle suspended in a fluid, which is given as:

$$F_g = V(\rho_p - \rho_m)g \approx 0.2\, m_p g = 5 * 10^{-22} N, \quad (4.7)$$

where ρ_p and ρ_m are mass densities of particle and fluid, respectively. m_p is the mass of the particle. In practical cases, the factor 0.2 might be even smaller since many particles have densities close to water [153]. It is clear that $F_g \ll F_{DEP}$, which means gravitational force is negligible compared to electrical forces. In addition, the effect of natural convection can also be neglected compared to electrical forces [158].

Other than the aforementioned forces, diffusion driven by Brownian motion can also move particles [162]. Diffusion is non-deterministic, which means it could disrupt the directional movement of particles induced by ACEK. However, many literatures [144, 146, 159, 160] have shown that randomized diffusion is not strong enough to affect ACEK acceleration and concentration of sub-micro particles [158].

To sum up, order of magnitude comparison of different forces proves the effectiveness of ACEK in flow acceleration and particle concentration, which opens up the opportunity of developing rapid affinity biosensing techniques.

Chapter 5. Sensor Development

Having introduced the basic theories of capacitive sensing and AC electrokinetics movement, this chapter will move on to discuss the advantages of incorporating the two theories together for affinity biosensing. Furthermore, we will go into the details of device design and experimental considerations as we describe the development of the ACEK-based capacitive affinity biosensor.

5.1 Incorporation of direct capacitive sensing and ACEK

For the majority of the state-of-the-art impedimetric affinity biosensors, there are still some obstacles to be overcome for them to be used for POC detection. First, many impedimetric tests would require sophisticated and oftentimes time-consuming data processing to extract binding related information. Expensive benchtop impedance analyzers are usually needed if high test frequencies (>1 MHz) are used. Second, most of the reported impedance assays were conducted with highly processed samples. To be viable as a POC diagnostic system, sample preparation must be simple enough to be performed on site. Third, as mentioned in Chapter 4, most of the currently-tested systems still require at least 30 minutes to perform a single incubation step with abundant molecules or even longer time for more diluted analyte. While this is an improvement over standard enzyme-linked immunosorbent assay (ELISA) method [163], an incubation time of half an hour or more may still be too long under some field testing circumstances. For example, testing multiple wild animals in field would be much more feasible if a more rapid test becomes available.

In this work, a novel affinity biosensor is developed by incorporating ACEK effect seamlessly with the signal interrogation process for *in situ* biomolecule enrichment and real-time biointeraction process monitoring through direct capacitance measurement. Unlike conventional impedimetric sensing, which uses a low AC voltage of 5-10 mV before and after the occurrence of biointeraction, the ACEK-based capacitive sensor reads the electrode impedance continuously with a fixed AC signal at a specific frequency, which is predetermined based on the biological reagents and sample types being tested. Such an AC signal would be able to break the diffusion limit by inducing ACEK effects to convect/attract biomolecules to the electrode surface, as shown in Figure 5.1. Meanwhile, the applied signal would stay in the “safe” range, i.e. minimum electrochemical reactions or other impedimetric artifacts will be involved as interferences.

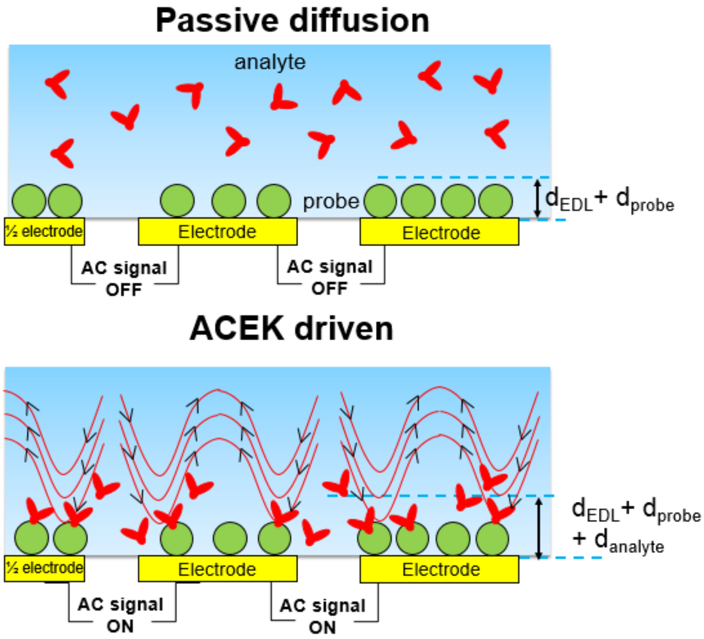
Passive diffusion
analyte
probe
$d_{EDL} + d_{probe}$
½ electrode
Electrode
Electrode
AC signal OFF
AC signal OFF
ACEK driven
$d_{EDL} + d_{probe} + d_{analyte}$
½ electrode
Electrode
Electrode
AC signal ON
AC signal ON

Figure 5.1 Breaking the diffusion limit by inducing ACEK.

Furthermore, it should be noted that the same AC signal is used to measure the capacitance (and its change) between microelectrodes, which directly indicates the activity and level of biointeractions occurring on the microelectrodes. So in the ACEK-based capacitive assay, analyte enrichment and capacitive detection are conducted simultaneously. Incorporation of ACEK with sensors has been investigated for various types of sensors, such as microcantilevers [164], fluorescent labeled affinity sensing [58], quartz crystal microbalance [165], and most commonly seen, impedimetric sensing [166-168]. For all the aforementioned reports, the ACEK concentration step is separate from the detection step, which is more complicated to operate than the capacitive assay developed in this work.

Incorporating direct capacitive sensing with ACEK effect, the ACEK-based capacitive affinity biosensor can be very effective in enriching biomolecules concentration over a large range and thus realizing accelerated detection at real-time.

5.2 Device design

This section covers the details about sensor design and instrument setup, which includes elaborate information about the electrodes and the measurement devices.

5.2.1 Preparation of microelectrode sensor

The ACEK-based capacitive affinity biosensor utilizes arrays of coplanar interdigitated microelectrodes, which are obtained in two ways: 1) By modifying commercially available electrode chips, i.e. surface acoustic wave (SAW) resonator chips (PARS 433.92, AVX Corp). 2) By in-house fabricating gold (Au) coplanar microelectrodes on silicon wafer. Images of original and modified SAW chips are shown in Figure 5.2a, and the scanning electron micrograph (SEM) of the interdigitated electrode array in the SAW chip is shown in Figure 5.2b. Meanwhile, images of in-house fabricated gold electrodes are shown in Figure 5.3 (a) and (b).

The reason we choose such type of electrode design is that similar interdigitated microelectrodes have been used by both our previous group members [148] and other groups [169, 170] to study ACEK effects, and it is proved to be very effective at generating DEP effect for particle enrichment as well as ACET effect for fluid streaming.

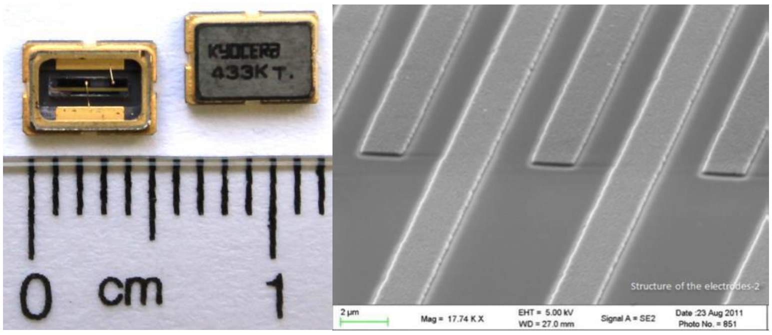
KYOCERA
433K T.
0 cm 1
Structure of the electrodes-2
2 µm
Mag = 17.74 K X
EHT = 5.00 kV
WD = 27.0 mm
Signal A = SE2
Date :23 Aug 2011
Photo No. = 851

(a) (b)

Figure 5.2 (a) Commercially available electrode chips, i.e. surface acoustic wave (SAW) resonator chips (PARS 433.92, AVX Corp). The left one is modified for immunosensing. (b) A scanning electron micrograph of the microelectrode array in the SAW chip.

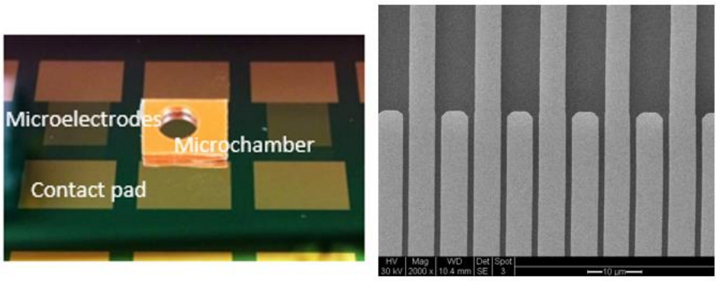
Microelectrodes
Microchamber
Contact pad
HV 30 kV
Mag 2000 x
WD 10.4 mm
Det SE
Spot 3
10 µm

(a) (b)

Figure 5.3 (a) In-house fabricated gold microelectrodes on silicon wafer with a silicone chamber on top of it; (b) SEM image of the interdigitated array inside.

The preparation of sensors involves chip modification (if needed) and electrode cleaning. Let's first focus on the preparation of SAW electrode chips

The first task is to remove the metal cover of the device to expose the working electrode array for use. This is done by using an X-Acto knife to first pierce the top cover near the edge of the chip. After piercing, the next step is to pry up on the lid to break the edge loose, then cover will be able to be sliced down. The metal casing around the electrode chip is about 4mm (L) x 2.5mm (W) x 1mm (H) = 10 µL, serving as a microchamber for sample solutions. The interdigitated electrodes are made of aluminum deposited on quartz substrate. Each microelectrode is 1.4 µm wide, 170 µm long, 200 nm thick, and separated by a 1.1 μm gap from one another, as shown in Figure 5.2b. The interdigitated electrodes are electrically connected to two contact pads on the chip bottom, which will be connected to an impedance analyzer for measurement.

Next, the SAW electrode chips are cleaned with the following procedure:

1. Soak the chips in acetone for 20 minutes.
2. Rinse the chips with isopropyl alcohol (IPA) for 30 seconds.
3. Rinse the chips with purified water for another 30 seconds.
4. Blow-dry the devices with clean air for 10 seconds to remove excess liquid. Use lab air to blow dry chips.
5. Put the chips into UV Ozone cleaner (BioForce®) for 15 minutes.

The modified SAW resonator will be denoted as SAW electrodes in later sections.

For gold electrodes on silicon wafer, the fabrication process is described briefly as follows: 50 nm of gold is deposited on top of silicon substrate which has 100 nm of SiO_2 as insulating layer and 10 nm of chromium (Cr) as adhesive layer. The fabricated microelectrode arrays have interdigitated configuration with two different dimensions, symmetric electrodes with a characteristic length of 2μm (with widths of 2μm separated by 2μm gaps), denoted as 2μm gold electrodes, and asymmetric electrodes with a characteristic length of 5μm (with widths of 5μm and 25μm separated by 5μm and 25μm gaps), denoted as 5μm gold electrodes. The size of the contact pad of each chip is 3 mm* 4mm. After fabrication, the whole wafer will be diced and each gold chip will be taken down as an individual sensor, as could be seen in Figure 5.4.

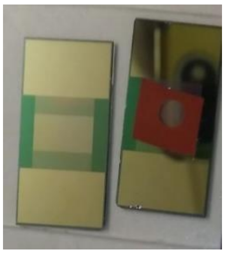

Figure 5.4 Individual sensor after dicing (left: without chamber; right: with chamber).

The preparation of gold chip electrodes on silicon is easier, as the working electrodes are already exposed. The cleaning procedure for gold chip electrodes is described as follows:

1. Sprinkle acetone on top the chip, wipe the surface with a clean non-woven wiper for several times.
2. Sprinkle isopropyl alcohol on top the chip, wipe the surface with a clean non-woven wiper for several times.
3. Sprinkle purified water on top the chip, wipe the surface with a clean non-woven wiper for several times.
4. Blow-dry the devices with clean air for 10 seconds to remove excess liquid. Use lab air to blow dry chips.

After electrode cleaning, a silicone microchamber (2.5mm in diameter and 0.9mm in depth, JTR24R, GraceTM Bio-labs) is sealed onto the wafer with electrodes inside for sample loading, as shown in Figure 5.3a and 5.4. The liquid amount within the chamber is also around 10 µL, similar to that of SAW electrodes. In addition, the microchamber is sufficiently high, so that electric fields and ACEK effects can fully develop, as shown by numerical simulation [148].

The cleaned SAW electrodes/gold electrodes on wafer will then be saved for surface functionalization, which is going to be discussed in later sections.

5.2.2 Test fixture and instrument setup

In this work, impedance data is acquired using a high precision impedance analyzer (Agilent® 4294A) with its 16047E test fixture, and the data is recorded through its LAN port onto a computer using software Data Transfer V3.0 (SEKONIC®), as shown in Figure 5.5.

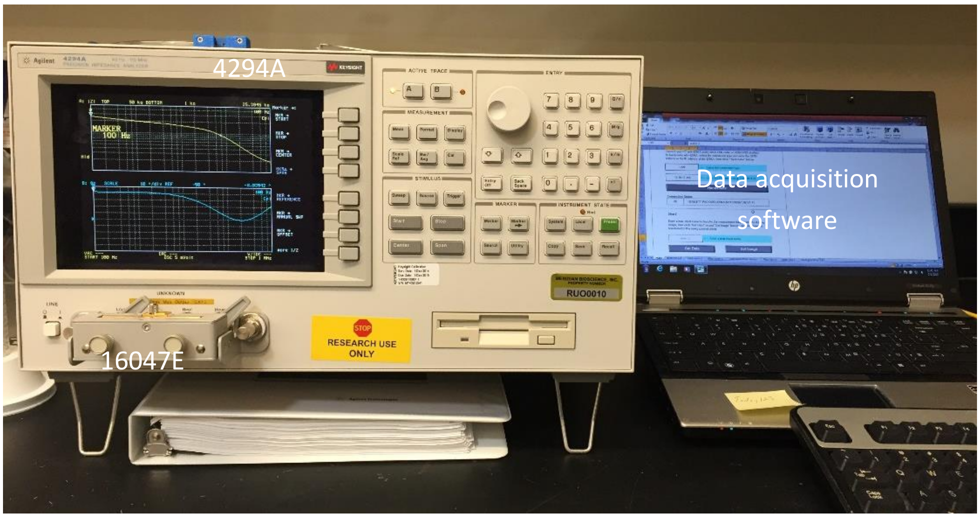
4294A
Data acquisition software
16047E
RESEARCH USE ONLY
RUO0010

Figure 5.5 Agilent 4294A with 16047E test fixture connected with a data acquisition computer.

For SAW electrode chips, in order to connect the sensor electrodes to the 16047E fixture, two connection wires are soldered to pins on the back of each chip, as shown in Figure 5.6. The soldered chips will then be connected to the test fixture of the impedance analyzer.

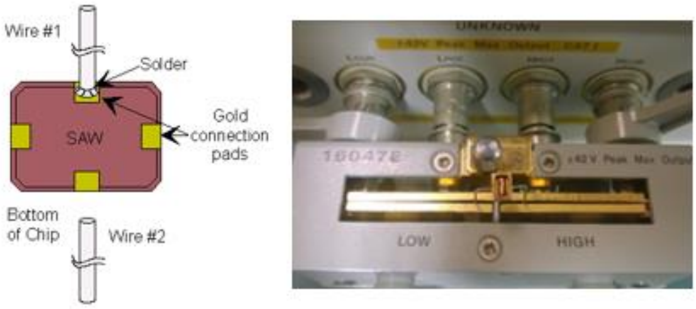
Wire #1
Solder
SAW
Gold connection pads
Bottom of Chip
Wire #2
UNKNOWN
16047E
LOW
HIGH

Figure 5.6 Connection of SAW chip to the test fixture.

In terms of making connection of gold electrode chips, a custom build fixture is designed for the chips to be mounted, as shown in Figure 5.7. Then the custom build fixture will be connected to the impedance analyzer.

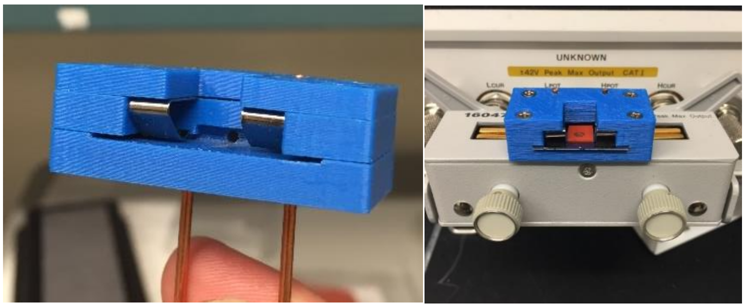

Figure 5.7 Connection of gold chip to the test fixture.

5.3 Assay methods

With sensors and measurement instruments being introduced, this section moves on to the discussion of assay methods step by step, including electrode surface cleaning, surface functionalization with probes, surface blocking and analyte detection method.

5.3.1 Electrode surface cleaning

The quality/cleanness of electrode surface plays an essential part in determining whether a sensor is usable for biomolecular detection or not. Any residue or interference remained on the surface might lead to a failure in detection. Different electrode surface qualities (levels of cleanness) may quite likely be manifested through the interfacial capacitances, due to variations in the composition of dielectric layer, surface topologies or the ability to acquire surface charges. In this work, various electrode cleaning methods are conducted and their effectiveness are manifested through reading the interfacial capacitance values, demonstrating the capability of capacitive sensing described in 3.2.3.

Before moving on to further discussion, it is worth mentioning that two types of surfaces may exist:

1. Fresh surface, which means the surface has not been treated with any chemicals or biological stuffs. In this case, the major purpose of cleaning

is to remove any dirt or impurities that might come from fabrication or environment. Normally a mild wash is enough. SAW electrode has more concerns to obtain a clean fresh surface since it involves lots of modifications. For gold electrodes on wafer, the cleaning for fresh surface is a largely standardized procedure.

2. Used surface, which means the surface has been treated with chemicals or biological stuffs. In this case, the goal is to recover the surface to its fresh state.

Surface cleaning in this section refers to the cleaning of fresh surfaces with the focus on SAW electrodes.

As listed in the explanatory text of Figure 5.8, three different cleaning methods have been tried to clean SAW electrodes. After each trial, interfacial capacitances of bare electrodes are measured with an excitation signal of 5 mVrms. 0.1x phosphate-buffered saline (PBS), which refers to 1 mM phosphate buffer (pH 7.0) containing 15 mM NaCl, is used as measuring buffer for capacitance measurement. PBS is a buffer commonly used in biological studies, which is isotonic and non-toxic to bioparticles.

For SAW electrodes, since reactance at 100 kHz represents closely that of the interfacial capacitor, capacitance values at 100 kHz are adopted as the indicator of the interface conditions. Strong correlation between the interfacial capacitance values and the cleaning methods has been found, as shown in Figure 5.8.

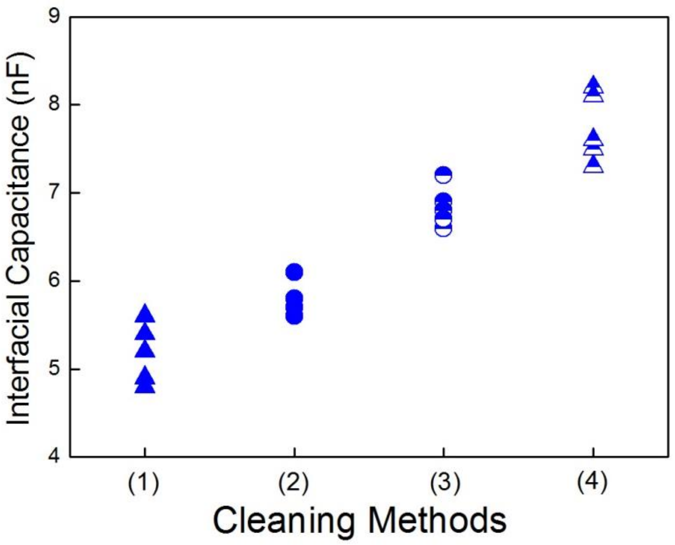

Figure 5.8 Capacitance values with different washing methods. For each condition, five chips are measured.
(1): no wash
(2): wash with DI water only
(3): wash with acetone-IPA-DI water
(4): wash with acetone-IPA-DI water-Ozone cleaner

Lowest capacitance values are found when no wash is applied. Capacitance values gradually increase with the addition of cleaning steps, particularly noticeable between methods (2) and (3), (3) and (4). This could be explained by the hypothesis that before cleaning, the electrode surface is covered by a thin film of dielectrics (possibly from unintended growth or deposition of contaminants or other materials), while with added/more aggressive cleaning, the thickness of the film is reduced or the area covered by the film is getting less. According to $C=\varepsilon S/d$ (d is the thickness of surface film), with d decreasing, C would certainly increase. As a result, we choose method (4) for cleaning the electrodes, as has already been mentioned in 5.2.1.

The cleaning of gold electrode surface mentioned in 5.2.1 is the widely accepted effective procedure for wafer cleaning, hence it will not be discussed here.

5.3.2 Surface functionalization

For affinity-based biosensors, prior to analyte detection, a layer of probe molecule needs to be immobilized onto the electrode surface to realize biospecificity. This step is known as surface functionalization. The quality of surface functionalization is crucial to the successful detection of analyte, as it determines the number of available binding sties. Generally speaking, there are two types of surface functionalization methods: passive adsorption and the usage of linker molecules. In this work, both of these methods are adopted and their effects are compared.

5.3.2.1 Passive adsorption

Biomolecules can be directly attached to metal surface due to the hydrophobic and electrostatic interactions between each other [103, 136]. Passive adsorption of probe molecules, also known as direct attachment, is the simplest way of functionalizing a surface, which involves only the incubation of electrodes with a solution containing the probe molecules for a certain period of time (usually several hours to overnight).

For passive adsorption, the major concern is functionalization time. Incubation time could largely influence the quality of the probe layer. Therefore, in order to seek the optimal incubation time, a commonly used protein molecule (bovine IgG whole molecule) labelled with fluorescent dyes (concentration: 100 ng/mL, diluted in 0.1x PBS) are immobilized on 5μm gold electrodes for different amount of times (6hrs, 12hrs and 24hrs). After washing away any unbound molecules, the electrodes are observed under a confocal microscope (Nikon® LV-100D FLUOR Microscope) for functionalization quality check, as shown in Figure 5.9.

Figure 5.9 (a)-(e) Microscopic images of incubated electrodes. Left column shows the actual image, right column shows the light intensity.

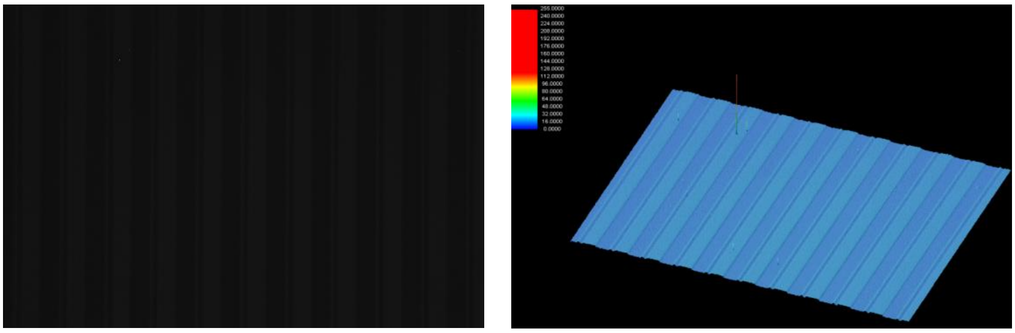

(a) Control- blank electrode

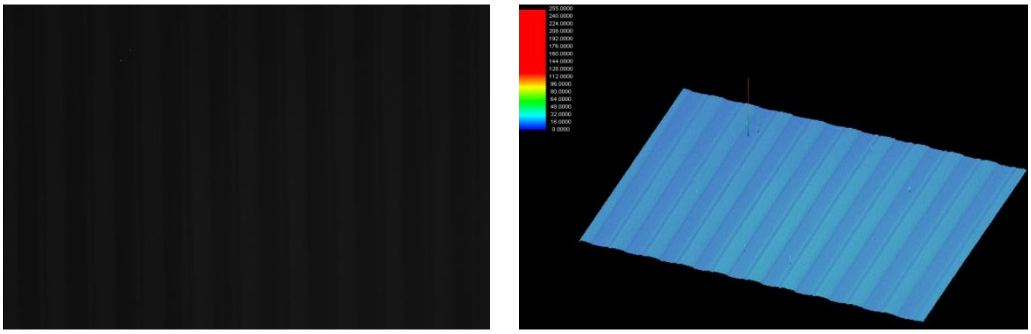

(b) Control- electrode incubated with 0.1xPBS solution

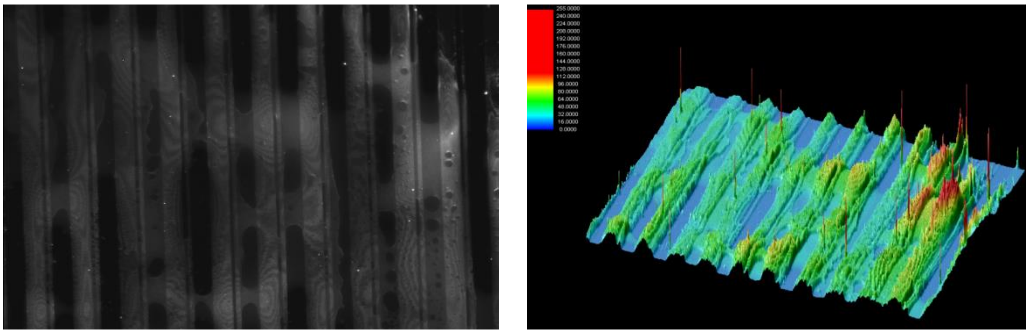

(c) After 6 hours of incubation with IgG

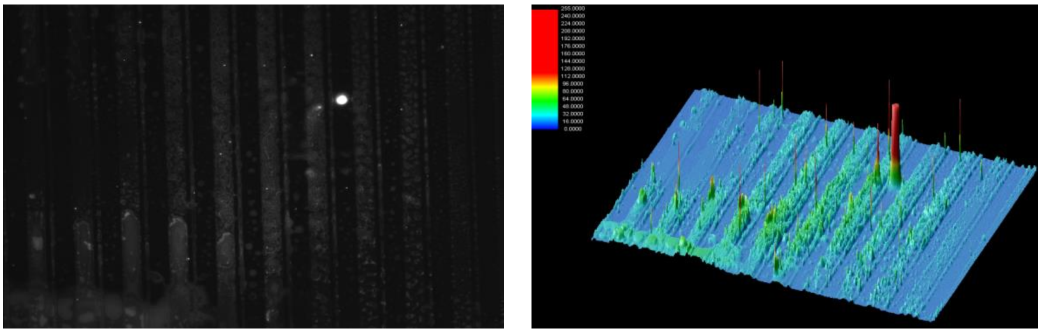

(d) After 12 hours of incubation with IgG

Figure 5.9 continued.

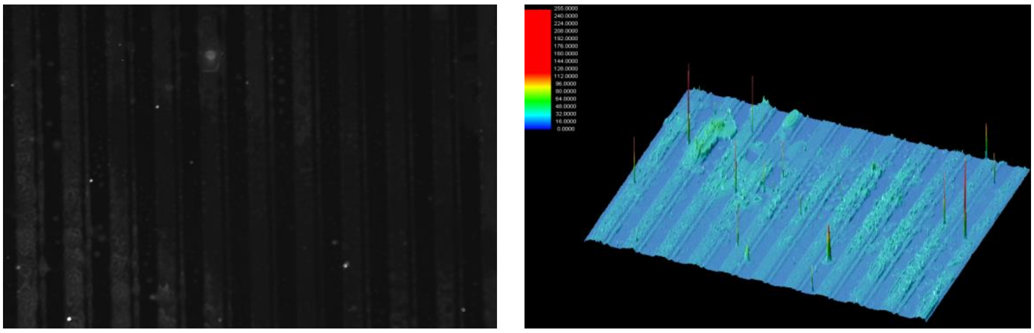
255.0000
240.0000
224.0000
208.0000
192.0000
176.0000
160.0000
144.0000
128.0000
112.0000
96.0000
80.0000
64.0000
48.0000
32.0000
16.0000
0.0000

(e) After 24 hours of incubation with IgG

Figure 5.9 continued.

For PBS diluted protein molecules, it is clear that six hours incubation produces a relatively stronger and more uniform surface functionalization. Thus six hours is adopted as the functionalization time for passive adsorption for PBS diluted molecules. While for ethanol diluted probe molecules, since it is not able to process a fluorescent label, we choose the most widely applied immobilization time in a traditional ELISA test [171], which is overnight (~16 hrs).

Although biomolecules can be immobilized to the electrode surface through passive adsorption, it has several limitations [103]:

1. Hydrophobic and electrostatic bonds are weak bonds. As a result, biomolecules can be easily removed from the surface using certain solvents or detergents.
2. The surface coverage by passive adsorption might be low especially for biomolecules with different shapes, sizes and orientations [82].
3. It is hard to realize uniform coating by passive adsorption.

5.3.2.2 Usage of linker molecules

Compared to passive adsorption, the usage of linker molecules serves as a better surface functionalization method, as it is able to form strong covalent bond between biomolecules and electrode surface. Moreover, linker molecules tend to form self-assembled monolayers (SAM) on the electrode surface, which possess well-defined composition, structure and thickness [172-174]. Therefore a uniform coating is more likely to be realized by applying linker molecules.

Thiols and polysiloxanes have been widely applied as effective linkers for probe immobilization [175, 176]. Functional thiol groups are commonly used on gold surfaces because they have thiol compounds (S-H groups) which possess very strong affinity to gold surfaces [172]. On the other hand, polysiloxanes are more frequently used on metal oxide surfaces, as they could form SAMs on metal oxide surface by silanol (-Si-O-) and siloxane (-Si-O-Si-) [177].

In this work, SAW electrodes are made of aluminum, which is easily oxidized under its neutral state. As a result, 3-aminopropyltroethoxysilane (APTES) [178], as one of the most extensively used polysiloxanes, is applied as the linker molecule for SAW electrodes. While for gold electrodes, functional thiol groups are applied as the linker molecules. Figure 5.10 shows the chemical structures of APTES (a) and thioctic acid (b), which is a commonly used functional thiol linkers [103].

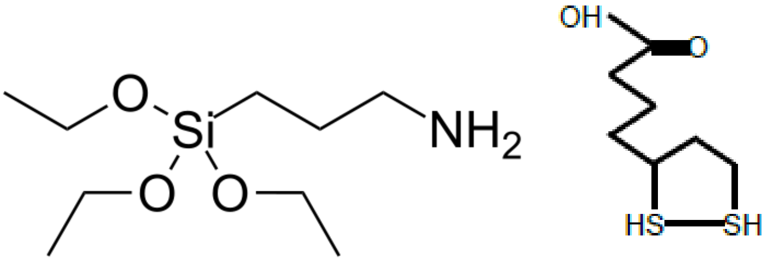

(a) (b)

Figure 5.10 Different types of linker molecules. (a) APTES and (b) thioctic acid.

(Source: 3-Aminopropyltriethoxysilane | 919-30-2". Chemicalbook.com. Retrieved 2012-08-01.)

5.3.2.2.1 APTES treatment

As schematically shown in Figure 5.11, on one end, APTES has non-hydrolysable hydroxyl groups which can bond strongly to metal oxides; on the other end, it has amine groups that can form strong interaction with amino group in biomolecules [179]. Therefore, biomolecules would form a much more stable and stronger bond with the electrode surface.

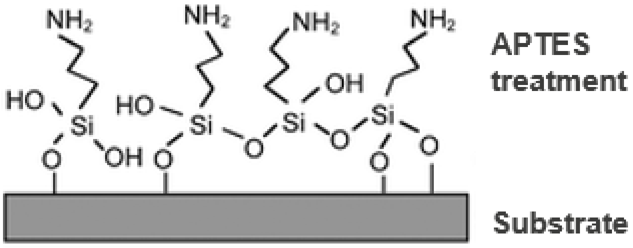

Figure 5.11 Schematic of APTES treatment of a substrate.

After a fair amount of trial, the procedure for APTES treatment for SAW electrodes is set as follows:

1. Cleaned SAW electrodes are exposed to 10v/v% APTES in absolute ethanol for 15 minutes under room temperature.
2. The electrodes are rinsed with 96% ethanol three times, dried with air gun and then baked at 125°C for 30 min.
3. The electrodes are incubated with 2.5v/v% glutaraldehyde for 1 hour at room temperature. Glutaraldehyde is used to modify the chemical reactivity of the formed SAMs [175].
4. The electrodes are washed with DI water for three times.
5. The electrodes are incubated with solution containing probe molecules (protein in this work) for five hours in a humidor at room temperature.
6. The electrodes are washed with 0.1x PBST, which is 0.1x PBS containing 0.05 v/v% Tween 20 (Fisher Scientific, Pittsburgh, PA), for three times to remove any unbound probe molecules

Similar to that of electrode surface cleaning, the effectiveness of APTES treatment is checked through reading the capacitance values, as shown in Figure 5.12. As could be seen, APTES-treated chips showed much smaller capacitance, since most part of the electrode surface is covered by non-hydrolysable hydroxyl groups and amino groups, causing the loss in its dielectric properties.

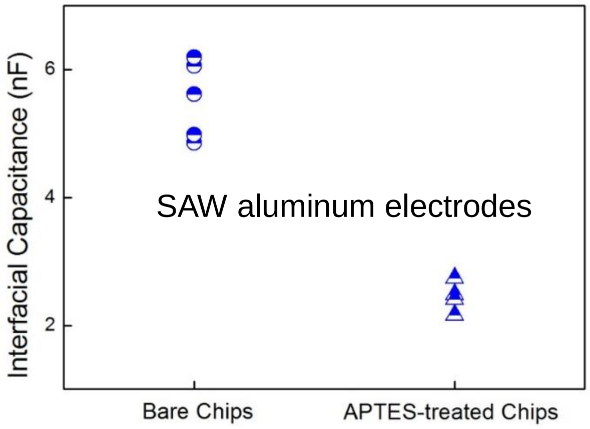

Figure 5.12 Comparison of capacitances between washed bare SAW electrodes and APTES-treated SAW electrodes. Five chips are measured and their capacitance values are plotted.

5.3.2.2.2 Thiol mediation

As aforementioned, thiol linker has S-H groups at their terminal ends which could form strong bond with the gold surface. Meanwhile, the head group of thiol linker is carboxylate group, which could be further activated for biomolecule binding.

In this work, the formation of functional thiol groups is described using 3-MPA (3-mercatopropionic acid), which is a commonly used thiol linker: (Figure 5.13 gives a schematic of the thiol formation and activation.)

1. Cleaned gold electrodes are modified by immersion of 1mM 3MPA and 50 mM PBS buffer (pH =10) for 17 hours to form a self-assembled monolayer with carboxylate termination. Alkaline pH is employed to increase the solubility of 3-MPA in PBS buffer.
2. After 17 hours, the electrodes are cleaned with distilled water.
3. The terminal carboxylate groups are then activated for 1 hour in 75mM EDC and 15 mM NHS [180] in 50 mM PBS buffer (pH=7.3). After EDC+NHS activation, ester groups in NHS will be able to form strong covalent bond with the amino group in biomolecules.
4. The electrodes are then cleaned with 0.1x PBST for three times.

5. The electrodes are then immersed for two hours into a solution containing probe molecules and 50 mm PBS at pH 7.3, forming amide bonds to the protein surface.
6. The electrodes are then cleaned with 0.1x PBST for three times to remove any unbound probe molecules.

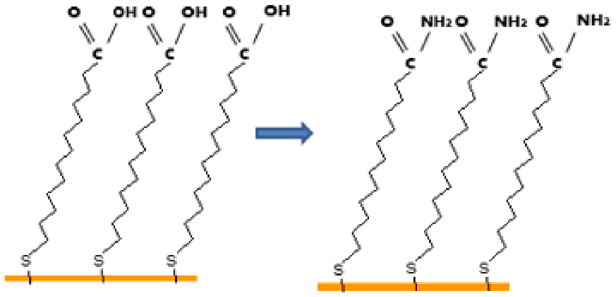

After formation of thiol SAM. **Activation of SAM with NHS+EDC.**

Figure 5.13 Schematic of thiol SAM formation and activation with NHS+EDC.

Again, the effectiveness of thiol mediation is also checked by reading their capacitance values, as shown in Figure 5.14. Compared with bare gold electrodes, thiol-mediated electrodes showed smaller capacitance values, which proves that the thiol groups are functional.

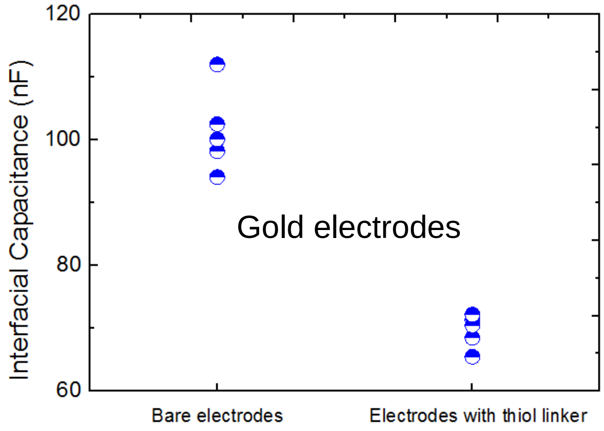

Figure 5.14 Comparison of capacitances between washed bare gold electrodes and thiol-mediated gold electrodes. Five chips are measured and their capacitance values are plotted.

5.3.2.3 Comparison

Here we summarizes and compares the pros and cons of passive adsorption and the usage of linker molecules, as shown in Table 5.1.

Table 5.1 Comparison between passive adsorption and linkers.

Passive Adsorption	**Linker molecules**
Simple to operate, easy to be removed	More complex to operate; harder to be removed
Weak bond: hydrophobic and electrostatic interactions. Can easily be reversed.	Strong bond: covalent bond between molecules and surface. Irreversible.
Low surface coverage, especially for proteins and antibodies.	Well-defined composition, structure and thickness. Enables more stable and uniform coating.

Effects of different functionalization methods will be compared in Chapter 6 when related analyte detection results are mentioned.

5.3.3 Surface blocking

After surface functionalization, surface blocking will be performed to cover any unoccupied space on the electrode surface to minimize non-specific binding. In this work, blocking buffer used is buffer B, which is PBS-T containing 10 v/v% SuperBlock (PIERCE Biotechnology, Rockford, IL). Different blocking times and concentrations of blocking reagent (0.1x, 0.2x or 1x) might cause different impacts towards analyte detection. The impact of blocking will also be discussed in Chapter 6.

5.3.4 Analyte detection

After surface functionalization and blocking, the probe-coated electrodes will be washed with 0.1x PBST to remove any unbound molecules. Then the electrode chips will be connected to the impedance analyzer and analyte samples will be introduced to the surface for detection.

When sample analyte is introduced, the interfacial capacitance of the electrode is continuously measured at a predetermined frequency for a certain period of time (from 15 seconds to 2 minutes, depending on the binding activity). ACEK-based capacitive affinity sensing method adopts a dimensionless quantity – the percentage change in the measured capacitance to indicate analyte deposition onto the electrode, which is the slope of normalized capacitance change versus time (%/minute) and found by least square linear fitting method [181]. Normalized capacitance is calculated as
Norm (Cint, t) = Cint, t/ Cint, 0, where Cint, t and Cint, 0 are the measured interfacial capacitances at time t and time zero, respectively. Doing so circumvents the need for a reference sensor, minimizes size difference from sensor to senor, further simplifying the detection procedure and instrumentation.

5.3.5 Summary

Overall, the basic steps of the capacitive affinity biosensing is summarized in Figure 5.15.

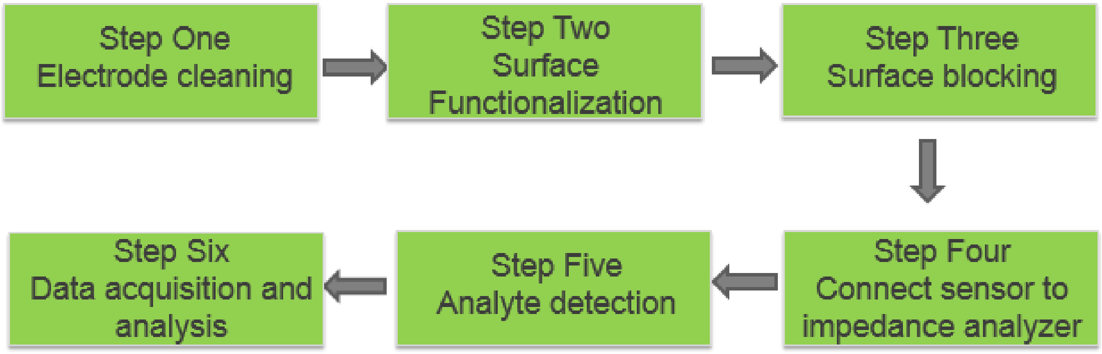
Step One
Electrode cleaning
Step Two
Surface
Functionalization
Step Three
Surface blocking
Step Four
Connect sensor to
impedance analyzer
Step Five
Analyte detection
Step Six
Data acquisition and
analysis

Figure 5.15 Summary of assay procedure.

5.4 Sensor Characterization

In the development of the capacitive affinity biosensor, impedance spectra analysis of the electrode-fluid system is conducted to determine which circuit elements would predominately account for the biomolecular interaction. As mentioned in Chapter 3, EIS analysis is a well-known characterization method for impedimetric based affinity sensor to relate the biomolecular interaction with corresponding changes in electric signals.

5.4.1 Extracting the values of circuit elements

Upon the occurrence of biomolecular interaction, impedance spectra of the electrode-fluid system would change accordingly. By fitting the impedance spectra with the proposed equivalent circuit model, biomolecular interaction would be corresponded to changes of resistance and/or capacitance values of the model.

Since SAW electrodes and gold electrodes have different materials and designs, values of circuit elements would be different between the two types of sensor.

SAW electrodes are first examined. 0.1x PBS is adopted as measuring buffer. 10 ng/mL goat anti-bovine IgG antibody (analyte) binding with immobilized bovine IgG (probe) is used to represent biomolecular interaction. Before and after the analyte binding step, impedance spectra of the electrode-fluid system are recorded at 5 mVrms from 10 kHz to 1 MHz, a range of the most interest to our detection. The proposed equivalent circuit model is employed for curve fitting and extracting component values. The measured impedance spectra together with fitted curves are shown in Figure 5.16, with extracted circuit parameters given in Table 5.2.

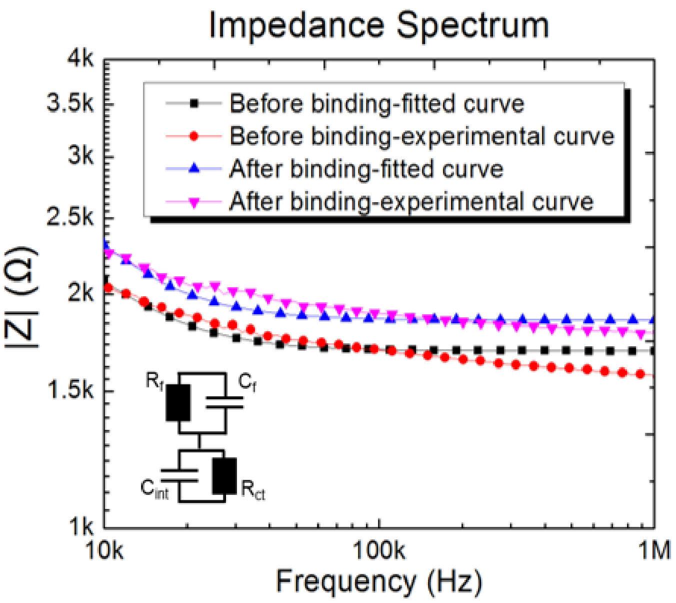

Figure 5.16 Comparison of measured impedance spectra and curve fitting using the four element equivalent circuit model of SAW electrodes. (Frequency range: 10 kHz-1MHz. Signal applied: 5 mVrms.)

Table 5.2 Equivalent circuit parameters obtained by curve-fitting the experimental results for SAW electrodes.

Steps	**R_{ct}(Ω)**	**C_{int} (nF)**	**R_f(Ω)**	**C_f (pF)**
Before binding	750	30	1750	3
After binding	800	24	1850	3

Of the four circuit elements listed in Table 5.2, R_{ct} and C_{int} describe the electrical properties at the electrode-fluid interface, while R_f and C_f describe the properties of the bulk fluid. Since the enrichment effect by ACEK is the most pronounced at 100 kHz, it is adopted as the testing frequency in our ACEK impedance sensing. At 100 kHz, the reactances for C_{int} and C_f are calculated to be ~53 Ω (<<R_{ct}) and 530 kΩ (>>R_f), respectively. It can be seen that C_{int} and R_f dominate the impedance response for the frequency of interest to this work (100 kHz). Consequently, the equivalent circuit in the inset of Figure 5.16 can be simplified to a series connection of R_f-C_{int} as shown in the inset of Figure 5.17. In Figure 5.17, the impedance responses from the R_f-C_{int} serial connection are plotted along with the measured impedance spectra, and good agreements between them can be seen over the frequency range of 10 kHz-1MHz.

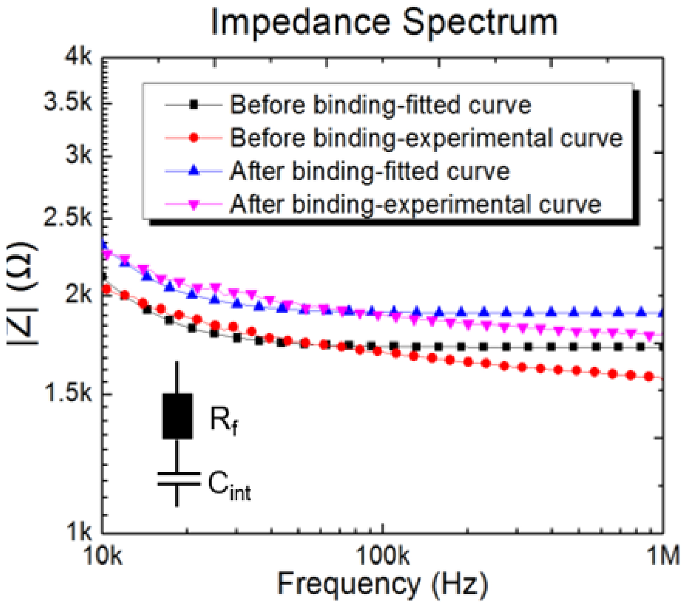

Figure 5.17 Comparison of measured impedance spectra and curve fitting using simplified R_f-C_{int} serial connection for SAW electrodes. (Frequency range: 10 kHz-1MHz. Signal applied: 5 mVrms.)

For gold electrodes, impedance spectra of the electrode-fluid system are recorded from 100 Hz to 1 MHz at 5 mVrms with 0.1x PBS as measuring solution. The measured impedance spectra together with fitted curves are shown in Figure 5.18, with extracted circuit parameters given in Table 5.3.

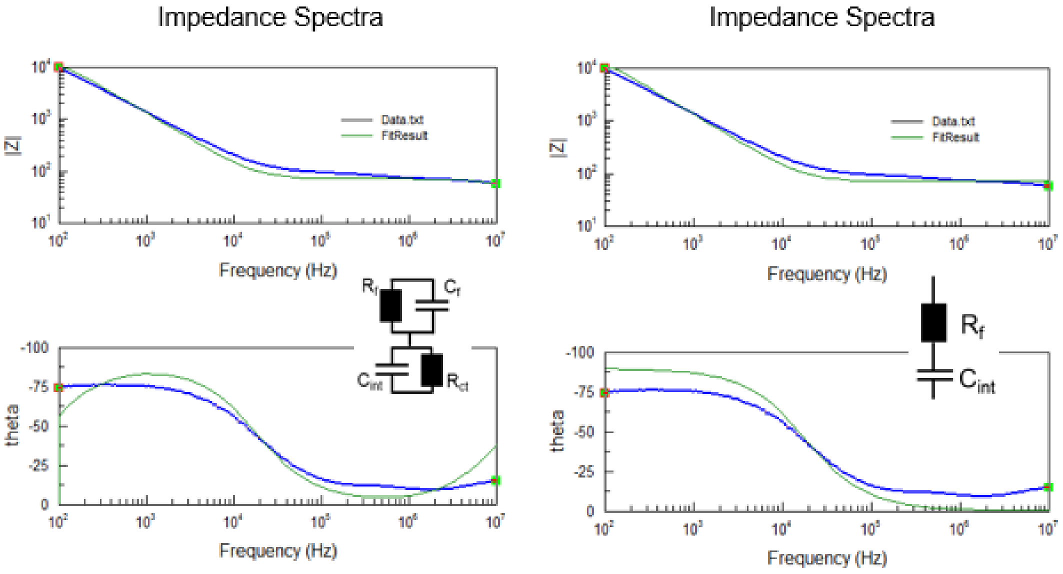

(a) (b)

Figure 5.18 Comparison of measured impedance spectra and curve fitting of gold electrodes. (a) Using the four element equivalent circuit; (b) Using R_f-C_{int} serial connection. (Frequency range: 100 Hz-1MHz. Signal applied: 5 mVrms.)

Table 5.3 Equivalent circuit parameters obtained by curve-fitting the experimental results for gold electrodes.

	Value	Impedance (reactance) at 100 kHz
R_{ct}	20 kΩ	20 kΩ
C_{int}	120 nF	13 Ω
R_f	80 Ω	80 Ω
C_f	0.2 nF	94 kΩ

As shown in Table 5.3, at 100 kHz, the reactances for C_{int} and C_f are calculated to be ~13 Ω (<<R_{ct}) and 94 kΩ (>>R_f), respectively. Therefore, it is also true that C_{int} and R_f dominate the impedance response of gold electrodes at the frequency range of our interest.

Besides, it is worth mentioning that the impedance of the gold electrodes after loading sample is measured to be in the range of 80-100 Ω at 100 kHz, and the impedance analyzer used for capacitance measurement has an internal resistance of 25 Ω. Thus, loading effect cannot be neglected for gold electrodes, i.e. the output voltage from the impedance analyzer is divided between the sensor and analyzer, and the actual voltage applied onto the sensor is lower than the nominal voltage set for the impedance analyzer. To obtain the actual voltage drop, an oscilloscope (Agilent DSO3062A) is connected to the sensor during measurement. The measured voltages show around 30% decrease from the nominal measuring voltage for gold electrodes. Table 5.4 gives the actual voltage drops corresponding to the displayed voltages on the impedance analyzer. On the other hand, the impedance of SAW electrodes is over 1 kΩ, so the loading effect is negligible (<2% drop).

Table 5.4 Measured voltage drop on gold electrodes.

(Unit: mVrms, rms: root mean square)

Nominal voltage	50	100	200	400	500	1000
Actual voltage	43	81	142	275	338	655

5.4.2 Simplified equivalent circuit

The above analysis shows that for the frequency range of interest to this work (around 100 kHz), a serial connection of R_f and C_{int} could adequately account for the impedance presented by the microelectrode/electrolyte system, with C_{int} predominantly responsible for the biointeraction process. Correspondingly, impedance value measured by the impedance analyzer is in the form of $Z_{meas} = R\text{-}jX = R + {}^{1}\!/_{j\omega C_{meas}}$, where R and X are the real part and imaginary part of the measured impedance, respectively. From the imaginary part, a capacitance value of $C_{meas} = {}^{1}\!/_{\omega X}$ can be found for a preset angular frequency. Based on the above discussion of the electrode impedance spectra, C_{meas} corresponds approximately to C_{int}. Therefore, the change in C_{meas} can be directly used to indicate the biomolecule deposition on the electrode surface, which greatly simplifies the process of interpreting experimental data.

5.5. Conclusion

In this chapter, we discussed the theoretical advantages of incorporating direct capacitive sensing with AC electrokinetics induced fluid and particle movement, which is the capability to realize rapid real-time and label-free detection of biomolecular interactions. We also described the two types of sensor electrodes: SAW aluminum electrodes and gold electrodes on silicon wafer. Furthermore, we discussed the assay procedure step by step, including different methods of electrode surface cleaning and various options for surface functionalization. Quality check of surface cleaning and functionalization by reading capacitance values proves their effects. Finally, EIS characterization showed that an R_f-C_{int} serial connection is able to represent the electrode-fluid system, which further simplifies our data interpretation.

Chapter 6. Results of analyte detection

6.1 Sample and assay description

In this chapter, detections of different types of analytes using the ACEK-based capacitive affinity sensor are presented and discussed. As listed in Table 6.1, three types of analytes are briefly described, each of which has its own research or realistic significances. More specifically, antibody includes anti-bovine IgG, Johne's disease (JD) serum and Human& Bovine tuberculosis (hTB and bTB) serum; virus refers to Influenza A virus; and small molecule includes Bisphenol A (BPA) and Progesterone (PG). More of their research or realistic significances will be mentioned when the specific assay is discussed.

Table 6.1 Target analyte description.

Types		Description
Antibody	Anti-bovine IgG antibody	Simple and straight binding, highly specific and sensitive [182].
	Johne's disease (JD) serum sample	One of the most economically important diseases of livestock [183].
	Human & Bovine Tuberculosis(TB) serum sample	A chronic infectious disease affects a broad range of mammalian hosts including human and cattle [2].
Virus	Influenza A (Flu A) virus sample	One of most common causes of flu pandemics [184].
Small molecule	Bisphenol A (BPA)	Exposure of BPA could probably cause adverse health issues to humans[185].
	Progesterone(PG)	Progesterone level can be an indicator towards pregnancy [186].

Moreover, Table 6.2 provides an overview of each assay by briefly describing the probes and target analytes, the types of sensor used, surface functionalization method and the sample diluent of each assay. Again, more detailed description will be provided when the specific assay is discussed.

Table 6.2 Assay description.

Probes	Target analyte	Sensor used	Surface functionalization	Sample diluent
Bovine IgG whole molecules	Anti-bovine IgG antibody	SAW and gold	Passive adsorption (6hrs)	0.1x PBS
JD specific antigen	Antibody in serum	SAW	Passive adsorption Overnight (16hrs)	100 % ethanol
Human/bovine TB specific antigen	Antibody in serum	SAW	Passive adsorption Overnight (16hrs)	0.1x PBS
Influenza A antibody	Spiked and nasal swap virus	Gold	Passive adsorption (6 hrs) and thiol mediation (2 hrs)	0.1xPBS
Specific aptamer against BPA	Spiked BPA sample	SAW and gold	Thiol mediation (2 hrs)	0.1x PBS
Anti-progesterone polyclonal antibody	Spiked progesterone sample	SAW	Passive adsorption (6 hrs) and APTES treatment (5 hrs)	0.1x PBS

We start this chapter by discussing anti-bovine IgG antibody detection. Afterwards, the detection of two types of serum antibodies (JD and TB) is presented. Influenza A virus detection is then discussed with focus on the usage of linker molecules. Finally, small molecule detection is discussed.

6.2 Bovine IgG antibody interaction

6.2.1 Proof-of-concept

Immunoglobulin G (IgG) is the most common type of antibody found in blood and extracellular fluid [187], it has a well-defined “Y” structure with two available antigen binding sites. As a proof-of-concept experiment, we study the specific binding of goat anti-bovine IgG (H+L) antibody (unlabeled) to bovine IgG whole molecules using our SAW electrodes. Both the bovine IgG whole molecule and anti-bovine IgG antibody are purchased from Jackson ImmunoResearch, West Grove, PA:

- CromPure bovine IgG whole molecule, Jackson ImmunoResearch, cat#001-000-003, stock 10 mg/mL.

- AffiPure Goat anti-bovine IgG (H+L), Jackson ImmunoResearch, cat#101-005-003, stock 2 mg/mL.

The experimental procedure is described as follows: 10 μL of bovine IgG whole molecules at concentration of 10 μg/mL (diluted in 0.1x PBS) is first added on cleaned SAW electrodes as probe molecule, and the SAW electrodes are then kept in a humidor for six hours for surface functionalization under room temperature. After surface functionalization, the electrodes are washed with 0.1x PBST for three times and then blocked with 0.1x buffer B for 30 minutes. The electrodes are then connected to the impedance analyzer and anti-bovine IgG antibody samples will be introduced to the surface. Anti-bovine IgG antibodies are tested at concentrations from 10 ng/mL to 1000 ng/mL (diluted in 0.1x PBS). An AC signal of 100 mVrms at 100 kHz is then continuously applied for two minutes and the corresponding capacitance change versus time is recorded. In addition, the same experiment is repeated with doubled PBS concentration, i.e. 0.2x PBS, which means 1 mM phosphate buffer (pH 7.0) containing 30 mM NaCl.

Figure 6.1 presents the curves of normalized capacitance changes versus time for three IgG concentrations in both 0.1x and 0.2x PBS. During the tests, the interfacial capacitances changed linearly with time. No saturation or depletion of the antibodies can be observed from these curves within the 2-minute detection period. The slopes of these capacitance curves, i.e. the fractional capacitance change rates (‰/min), are calculated as a quantitative indication of antibodies bounded to the electrode surface. It can be seen that the fractional capacitance change rate shows strong correlation with the concentration of antibody. 0.1x and 0.2x PBS are test as the negative control, which gives a change rate of 2.14 ‰/min for 0.2x PBS and -1.17 ‰/min for 0.1x PBS. The magnitude of capacitance change consistently increases with increasing concentration of IgG antibody. With 10 ng/mL IgG antibody, the change rates are 12.36 ‰/min for 0.2x PBS and -6.01 ‰/min for 0.1x PBS. At

1000 ng/mL IgG antibody, the change rates increase to 49.10 ‰/min for 0.2x PBS and -30.72 ‰/min for 0.1x PBS.

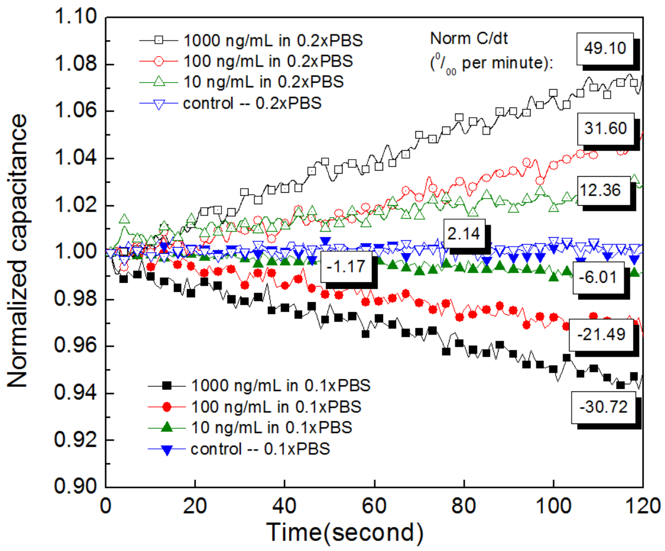

Figure 6.1 Normalized capacitance change as a function of time within two minutes for three different concentrations of bovine IgG antibody (10, 100 and 1000 ng/mL) in 0.1x PBS and 0.2x PBS respectively. The boxed-in numbers in the figure are the fractional capacitance change rates of different IgG concentrations.

It should be noted that the change of capacitance with antibody binding can either be positive or negative. As has been theoretically discussed in Chapter 3, we hypothesize the reason to be the difference in separation among different probes, with the difference in their length scale comparable to EDL thickness. Theoretically, due to the stronger ionic strength, 0.2x PBS has a thinner EDL than 0.1x PBS. So by varying the ionic strength of buffer, it effectively changes the relative gap between the bounded antibodies. The results shown in Figure 6.1 support our hypothesis regarding the causes of change in interfacial capacitance, as antibodies diluted in 0.1x PBS consistently yields a decrease in capacitance, while antibodies diluted in 0.2x PBS yields an increase in capacitance.

6.2.2 Impact of electrode design on detection

In Chapter 4, we discussed ACEK and its possible effects towards binding detection. In theory, ACEK induced fluid flow and particle movement are related with the electrode design as well as the electric field strength being applied. In this section, we discuss the impact of different electrode designs. The impact of electric field strength will be discussed in the next section. Still, we use the binding of goat anti-bovine IgG antibody (analyte) to bovine IgG (probe) to represent the biomolecular interaction. Both of them are diluted in 0.1x PBS.

To demonstrate the impact of electrode designs on biomolecule enrichment and detection, sensor responses from three types of electrodes are obtained under similar electric field strength for a range of antibody concentrations. Three sensing electrodes used are SAW electrodes (i.e. 1μm electrodes), 2μm gold electrodes and 5μm gold electrodes on silicon wafers. The experimental procedure is the same as described in 6.2.1. The characteristic electric field strength for a sensor is estimated as the applied voltage divided by the half circle over narrow electrode gap ($\mathrm{E} = {}^{V}\!/_{\pi r}$, r is the distance to the center of the electrode gap). The electric field strengths are 50 mV/μm for SAW electrodes and 46 mV/μm for gold electrodes.

Figure 6.2 shows the responses of the three different electrodes to various concentrations of IgG antibody samples. To account for possible artifacts from applying electric signal to biological samples, buffer without analytes is tested on functionalized electrodes as negative control experiments. In addition, to demonstrate specificity, non-specific binding tests with sample solution containing 10 ng/mL antibody are performed on un-functionalized electrodes. Measurement at each data point is repeated three times.

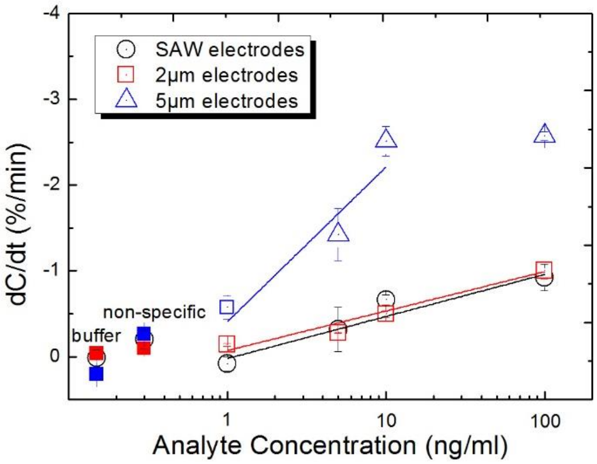

Figure 6.2 Antibody binding responses from three different electrodes under similar electric field strength. Each test is repeated three times. Error bar indicates the standard deviation. Control results include both buffer and non-specific binding on un-functionalized electrodes.

As shown in Figure 6.2, the capacitance change rates are very similar between SAW electrodes and 2μm gold electrodes for all the concentrations tested (1, 5, 10 and 100 ng/mL), while 5μm gold electrodes exhibited much larger responses. The SAW and 2μm gold electrodes have a logarithmic dependence on IgG concentration ranging from 1 to 100 ng/mL. Their sensitivities are found by linear curve fitting to be -0.59 ± 0.12 and -0.49 ± 0.07 %/log (ng/mL) with a Pearson correlation coefficient R^2 [188] of 0.88 and 0.94 for SAW and 2μm gold electrodes, respectively. In comparison, 5μm gold electrodes yield a sensitivity of -1.80 ± 0.69 %/log (ng/mL), more than three times that of SAW and 2μm gold electrodes. The 5μm gold electrodes exhibit logarithmic dependence on IgG concentration from 1 to 10 ng/mL, however, there is no increase in sensor response when the IgG level becomes higher than 10 ng/mL, probably due to saturation of binding sites by strong ACEK enrichment. As the electric field strengths are similar between the electrodes, so the differences between their output magnitudes can only be attributed to the electrode geometric differences. According to Eqns (4.1) and (4.2), DEP is more pronounced with smaller electrodes, while ACET effect favors larger microelectrodes. Since SAW and 2μm gold electrodes have similar output, it may be concluded that DEP and ACET effect are comparable for electrodes with a characteristic size of 2μm and less. While for larger electrodes, ACET force will dominate, which is demonstrated by the significant improvement in the sensitivity of 5μm gold electrodes over 2μm electrodes.

Relatively speaking, the negative control experiments using blank buffer exhibit very little responses. SAW electrodes, 2μm gold electrodes and 5μm gold electrodes show capacitance change rates of $0.01 \pm 0.09\ \%/\mathrm{min}$, $-0.03 \pm 0.03\ \%/\mathrm{min}$ and $0.21 \pm 0.05\ \%/\mathrm{min}$, respectively. The outputs of non-specific binding tests on un-functionalized electrodes are a little larger, but still show little capacitance changes, $-0.19 \pm 0.10\ \%/\mathrm{min}$ for SAW electrodes, $-0.09 \pm 0.03\ \%/\mathrm{min}$ for 2μm gold electrodes and $-0.26 \pm 0.01\ \%/\mathrm{min}$ for 5μm gold electrodes, which attests to the specificity of our tests. Also, based on Figure 6.2, sensor output more positive than $-0.30\%/\mathrm{min}$ is defined as being non-reactive, i.e. negative response.

6.2.3 Impact of electric field strength

The impact of the applied electric field strength on IgG antibody binding detection is studied in this section using gold electrodes, with AC electric field strength ranging from 13 mV/μm to 86 mV/μm. This helps to establish a range of electric field strength for effective improvement by ACEK effects. Binding detection results of 10 and 100 ng/mL IgG antibodies on both 2μm and 5μm gold electrodes are shown Figure 6.3.

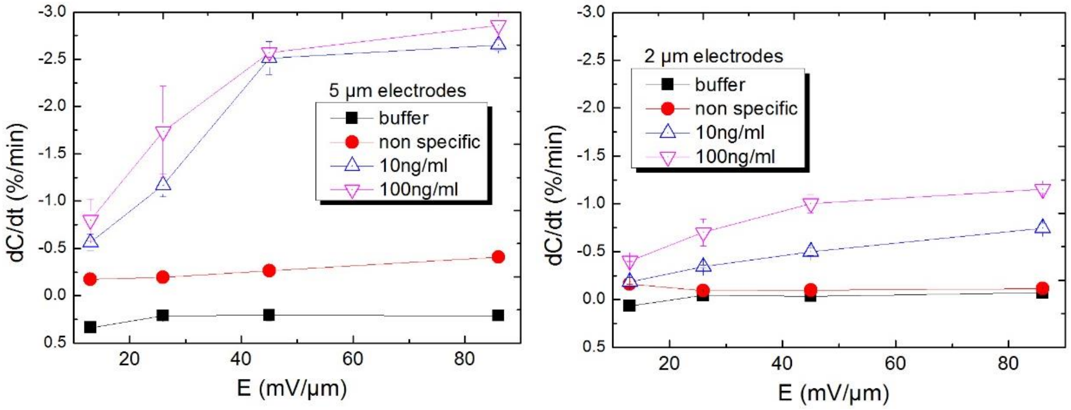

Figure 6.3 Binding responses of control buffer, non-specific, 10 ng/mL and 100 ng/mL IgG samples under different electric field strengths. Both 2μm and 5μm gold electrodes are tested for comparison. Each test is repeated twice and the error bar indicates standard deviation.

From Figure 6.3, it is first noted that at 13 mV/μm, the sensor responses are small for all cases, even for 100 ng/mL sample on 5μm gold electrodes. This indicates that this electric field strength is too low to induce sufficient ACEK effects to effectively enhance binding reactions. For 5μm gold electrodes, the change rates are slightly more negative than $-0.30\%/\mathrm{min}$, the cut-off point for a detection. Second, it is evident that the capacitance change rate increases steadily with electric field strength, indicating that binding is aided by AC electric field, which strongly supports that AC electric field can induce usable DEP and ACET effects. Third, the difference in the responses between 2μm and 5μm gold electrodes widens quickly at higher electric field strength, which is consistent with Eqn (4.2) of ACET force $F_{ACET} \propto r|E|^4$, especially for responses to 10 ng/mL antibody samples. So it is clear that enrichment by ACET effect is more dominant in larger electrodes. Last, the rate of increase in sensor response becomes less when the electric field strength goes above 45 mV/μm, especially for 5μm gold electrodes. So the range of AC electric field strength can be estimated to be between 13 and 45 mV/μm for effective induction of ACEK enhancement in affinity sensing.

Furthermore, it should be noted that if the electric field strength is higher than 45 mV/μm, ACEK effects become so strong that sufficient analyte molecules are transported close to the electrodes, and the surface binding shifts from transport-limited domain to reaction-limited domain. The outputs from 5µm electrodes are strongly indicative of saturation of binding sites. There is little difference between its response to 10 and 100 ng/mL IgG samples, and there is no increase in sensor response at electric field higher than 45 mV/µm.

A comparison of the output transients between 2µm and 5µm gold electrodes shows that ACET flows are the cause of binding saturation, as shown in Figure 6.4. For 2µm gold electrodes at 86 mV/µm, as shown in Figure 6.4a, the decrease in capacitance consistently becomes larger with more concentrated IgG samples. The interfacial capacitance decreases linearly with time with little indication of saturation. However, for 5µm gold electrodes, saturation begins to show for IgG above 10 ng/mL even at 45 mV/µm. The change rate in normalized capacitance becomes larger as IgG concentration increased from 1 ng/mL to 5 ng/mL and 10 ng/mL. For 100 ng/mL, the capacitance initially dropped quickly then became more gradual after 10 seconds, which is indicative of slowdown in binding reaction. At 86 mV/µm, the indication of saturation kinetics became much more pronounced. The capacitance curves for 10 ng/mL and 100 ng/mL overlap each other and asymptotically approach a maximum of capacitance change, which is characteristic of specific binding.

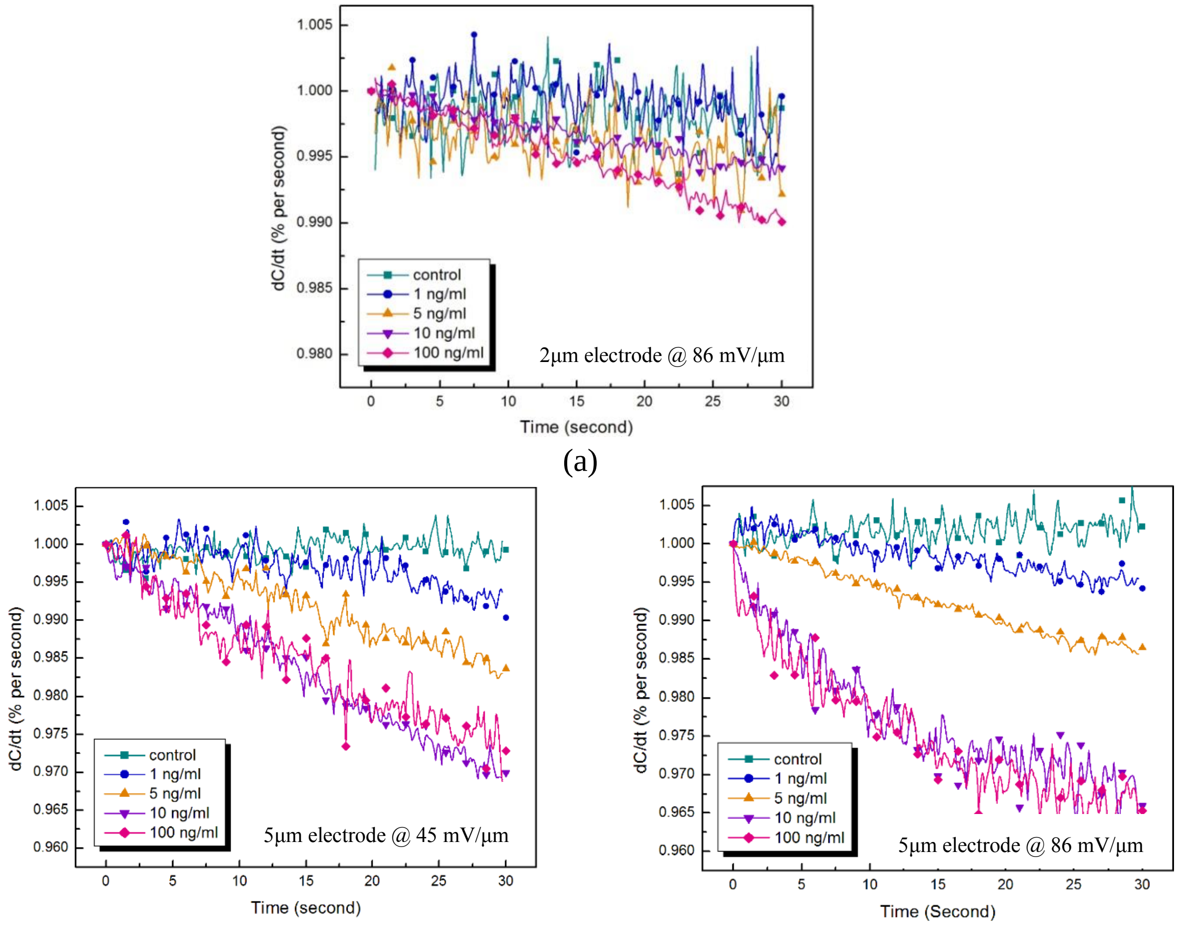

(a)

(b) (c)

Figure 6.4 Normalized capacitance change with time. (a) 2µm electrodes measured at 86 mV/µm; (b) 5µm electrodes measured at 45 mV/µm; (c) 5µm electrodes measured at 86 mV/µm.

ACET effect is expected to be more obvious for detecting diluted analyte since longer range of enrichment is involved. In fact, sample enrichment is more highly desired for diluted samples. Table 6.3 shows the capacitance change rate of 1 and 5 ng/mL IgG sample at 10-second time periods. It can be seen clearly that binding events change from transport-limited for 2µm gold electrodes or at lower electric field to reaction-limited at higher electric field for 5µm gold electrodes. In the first 10 seconds, 2µm gold electrodes show a capacitance change rate of $0.40\ \%/\mathrm{min}$. As time goes by, the change rate becomes more negative from $-0.29\ \%/\mathrm{min}$ in 10-20 seconds to $-0.82\ \%/\mathrm{min}$ in 20-30 seconds, which indicates increasing binding rate as a result of biomolecules being gradually transported to the vicinity of electrode surface. Similar situation is shown for 5μm gold electrodes at 45 mV/μm. In comparison, it is a different scenario for 5μm gold electrodes at 86 mV/μm. At 1 ng/mL, its change rate is $-1.13\,\%/\mathrm{min}$ in the first 10 seconds and slows down in subsequent time periods, indicating a faster transport of analytes at 86mV/μm than at 45 mV/μm. At 5 ng/mL, the C_{int} change rate is fairly constant, probably because there are plenty of analytes for binding. It is clear from Table 6.3 that larger electrodes are better at enriching analytes and the enrichment effect is caused by AC electric field. Both the much larger response and its transient behavior of 5μm gold electrodes indicate that 5μm gold electrodes can induce much stronger ACEK effect, mostly ACET effect, to enhance detection of more diluted analytes.

Table 6.3 dC/dt (%/min) of 1 and 5ng/mL for every 10 seconds.

Conditions	**0-10 sec.**	**10-20 sec.**	**20-30 sec.**
2μm@86 mV/μm (1 ng/mL)	0.40	-0.29	-0.82
5μm@45 mV/μm (1 ng/mL)	-0.04	-0.67	-1.53
5μm@86 mV/μm (1 ng/mL)	-1.13	-0.56	-0.66
5μm@86 mV/μm (5 ng/mL)	-0.90	-1.42	-1.37

From a physics viewpoint, electric field of 2μm or smaller electrodes is concentrated around the electrode corners and between the electrodes, while electric field of 5μm electrodes could reach further into the fluids. ACET effect, as a body force, need some distance away from solid phase to effectively generate convection [189]. Otherwise, the friction from the solid surface will be overwhelming (no slip boundary condition). Consequently, 5μm electrodes is able to generate much stronger ACET convections than 2μm electrodes, which in turn provides a much larger signal.

6.2.4 Determination of LOD

With the limit of detection (LOD) being defined as more than three standard deviations from that of control tests, the LODs of SAW and 2μm gold electrodes are found to be 10 ng/mL (their capacitance change rates at 10 ng/mL are $-0.50 \pm 0.04\ \%/\mathrm{min}$ and$-0.50 \pm 0.04\ \%/\mathrm{min}$. In contrast, 5μm gold electrodes showed a change rate of $-0.60 \pm 0.13\ \%/\mathrm{min}$ for 1 ng/mL IgG sample. So the LOD for 5μm gold electrodes is 1 ng/mL, increasing by approximately one order of magnitude from SAW and 2μm gold electrodes.

6.3 Detection of antibody in serum

In this section, we will move on to the detection of more complex serum samples. Serum is a blood component collected after blood has coagulated. It contains various types of proteins, including antibodies [190]. In this work, three types of serum samples with realistic significances are tested: Johne's disease (JD) serum sample, human tuberculosis (hTB) serum sample and bovine tuberculosis (bTB) serum sample.

Johne's disease is a chronic disease of mainly ruminants leading to granulomatous enteritis, persistent diarrhea, progressive wasting and finally death [191, 192]. The disease is distributed globally among domestic ruminants and wildlife species [193, 194].

Tuberculosis (TB) is also a chronic infectious disease that affects a broad range of mammalian hosts including humans and cattle. Human TB is estimated to cause more than two million deaths every year. Although bovine TB, caused by Mycobacterium bovis, has been mostly eradicated in the livestock industry of developed countries, the disease in wildlife still poses a risk to livestock, tourism economy, and wildlife conservation. Global economic losses from bovine TB total US$ 3 billion annually. In developing countries, bovine TB still causes serious concerns not only for wildlife, but also for public health, food safety and the economy of livestock industries.

Conventional methods of chronic diseases diagnosis are labor-intensive, time-consuming and/or expensive. For example, medical evaluation of human TB includes a medical history, physical examination, radiographic imaging (conventional chest X-ray), microbiological smears, and bacterial cultures. It may also include a tuberculin skin test or other measurements of cellular immunity, such as interferon-gamma release assays (IGRA). For human TB, the Cepheid Xpert MTB/RIF assay has recently been used for on-site diagnosis but the assay is costly [195, 196]. Bovine TB in animals is commonly confirmed by post mortem examination of gross lesions and bacterial culture. Global control and prevention of TB has partly been hampered by the lack of effective diagnostic methods, so there is an urgent need for more simple, rapid and sensitive on-site diagnosis of TB [5].

It should be noted that both JD and TB serum samples are composed of mixtures of complex fluids, hence the exact antibody concentrations of these complex serum samples are unknown.

6.3.1 Sample preparation

6.3.1.1 Johne’s disease antigen and serum samples

The preparation of Johne’s disease specific antigen and serum samples is described as follows:

- *Johne’s disease (JD) specific antigen:* A bacterial pathogen Mycobacterium avium subsp. paratuberculosis (MAP), which is the causative agent of JD, is used to extract antigen as described previously elsewhere [197]. MAP is obtained from Dr. John P. Bannantine in the USDA/NADC (Ames, IA) and is cultured in Middlebrook 7H9 medium (Becton Dickinson Microbiology Systems, Franklin Lakes, NJ) with 10% OADC (oleic acid-albumin-dextrose-NaCl) (Becton Dickinson Microbiology Systems, Franklin Lakes, NJ). The medium is supplemented with 2 µg/mL of Mycobactin J (Allied Monitor, Fayette, MO). The cultures are maintained at 37°C without shaking until they reach an optical density of approximately 0.7 at 600 nm. MAP is harvested from the liquid culture at stationary phase and centrifuged at 2,600 × g for 10 minutes; the pellet is resuspended in 80 % ethanol, agitated by vortex at room temperature for 2 minutes, and centrifuged at 10,621× g for 10 minutes. The supernatant is then collected, diluted in 100 % ethanol (1:80 v/v) and used as antigen for this assay.

- *Johne's disease serum sample:* Ten JD-positive serum samples are obtained from 10 different dairy cows (breed: Holstein; average age: 2.8 years old; gender: female) tested positive for JD by bacterial culture and ELISA [171]. Ten JD-negative serum samples are obtained from 10 different cows (breed: Holstein; average age: 2.4 years old; gender: female) tested negative for JD by the procedures mentioned above. The bovine serum samples used in this work are kindly provided by National Animal Disease Center, USDA, Ames, IA. For testing, the serum samples are diluted with 0.1x PBS before use.

6.3.1.2 Human and Bovine tuberculosis specific antigens and serum samples

The preparation of human and bovine tuberculosis specific antigens and serum samples is described as follows:

- *Human tuberculosis (hTB) specific antigen:* Purified protein derivative (PPD) of *Mycobacterium tuberculosis* (Accurate Chemicals, NY) is adopted as the probe molecule and immobilized at a concentration of 10 µg/mL (diluted in 0.1x PBS).
- *hTB serum samples:* A total of 11 human serum samples are obtained from the WHO (World Health Organization/Tropical Diseases, Special Programme for Research and Training) and tested for hTB. Six of these samples are obtained from patients tested positive for hTB based on prior TB history and bacterial culture results. Five of these samples are obtained

from patients tested negative for hTB based on the above mentioned tests. Serum samples are diluted in 0.1x PBS before testing.

- *Bovine tuberculosis (bTB) specific antigen:* A virulent strain of *Mycobacterium bovis* (HC2005T), which is originally isolated from an *M. bovis* infected dairy cow, is cultured in Middlebrook's 7H9 medium with addition of 0.05% Tween 80, 10% oleic acid-albumin-dextrose-NaCl at 37℃. For antigen preparation, *M. bovis* bacilli is harvested from stationary phase cultures, suspended in 80% ethanol (80 mg wet weight of bacteria/mL) and agitated by vortex to dislodge surface antigens. The dislodged *M. bovis* antigen is diluted (1:80) in the ethanol solution and used as antigen in this assay.
- *bTB serum samples:* A total of 10 badger serum samples are provided by Animal Health and Veterinary laboratories Agency (AHVLA), UK. The bovine TB positive samples (n=5) are obtained from badgers which had previously tested positive for *M. bovis* by bacterial culture from clinical samples collected *ante mortem* and by ELISA for interferon-gamma. The negative serum samples (n=5) are obtained from animals from a region of the UK considered free from *M. bovis* infection in badgers and which are confirmed to be negative for bTB through repeat testing by the procedures mentioned above. Serum samples are diluted in 0.1x PBS before testing.

6.3.2 Proof-of-concept

For proof-of-concept, one of each of the JD positive and negative samples are tested using SAW electrodes to demonstrate the capability of distinguish serum positive/negative samples. The experimental procedure is described as follows: 10 μL of JD specific antigen is coated on cleaned SAW electrodes for overnight (16hrs) under room temperature, then the functionalized electrodes are washed with 0.1xPBST for three times and blocked with 0.1x buffer B for 30 minutes. JD negative serum sample is diluted in 0.1x PBS with a volume ratio of 1:20, while JD positive serum sample is diluted with 0.1x PBS with a volume ratio from 1:20 to 1:200 dilution for proofing quantitative detection as well. An AC signal of 100 mVrms at 100 kHz is continuously applied as the measuring signal for 200 seconds.

Theoretically, disease positive serum samples contain higher concentrations of antibodies that will specifically bind to the antigens from the causative agent of the disease. Therefore, disease positive serum samples should exhibit larger change of C_{int} than disease negative samples.

The normalized capacitance change rates for various dilutions of JD positive sera are plotted in Figure 6.5, negative serum sample and buffer are tested as control groups. The slopes of these capacitance curves, i.e. capacitance change rates, are also shown in the plot. As shown in Figure 6.5, the capacitances of JD negative serum sample and PBS stay rather constant during the test, while that of JD positive serum sample decreases monotonically with time due to specific recognition of serum antibodies. For the positive sample diluted at 1:20, the capacitance change rate reaches $-54.6\ ‰/\mathrm{min}$. While for negative sample and PBS, the related numbers are only $-1.6\ ‰/\mathrm{min}$ and $-2.6\ ‰/\mathrm{min}$, respectively. The low capacitance change rate of the negative sample indicates that signal interferences from non-specific interactions are at a very low level.

Furthermore, as expected, when the sample becomes more diluted, the capacitance change rate decreased from $-54.6\ ‰/\mathrm{min}$ at 1:20 dilution to $-1.1\ ‰/\mathrm{min}$ at 1:200 dilution. Highly diluted sera (e.g. 1:160 dilution and 1:200 dilution) cannot be differentiated from the control tests. For JD positive serum samples with dilution from 1:120 to 1:40, the normalized capacitance change rate shows a logarithmic dependence on serum dilution. The dependence could be expressed as:

$$\mathrm{y}\ \left({‰}/{min}\right) \approx -73.7\ \mathrm{log\ (serum\ dilution)} - 157.5, \qquad (6.1)$$

with Pearson correlation coefficient R^2=0.912. The results demonstrate that the

ACEK-based capacitive affinity biosensor is a quantitative method within a range of antibody concentrations.

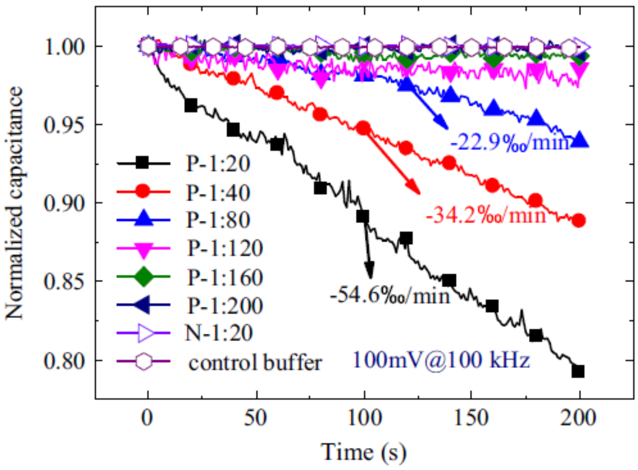

Figure 6.5 Transient behavior of normalized capacitances of JD serum samples. The samples are various dilutions of JD positive sera (1:20 to 1:200), negative sera (1:20) and 0.1x PBS (control).

6.3.3 Signal optimization

Furthermore, as discussed in the detection of bovine IgG antibody, if the short “sample to results” time is a result of AC electrokinetics enrichment, then the capacitance change rate should exhibit a certain dependence on the applied AC signal. Therefore, as a reinforcement to the proof-of-concept experiments, binding of JD positive serum samples are tested under different AC signals using SAW electrodes, following the same experimental procedure described before.

Firstly, the frequency of the signal is fixed at 100 kHz while the amplitude is varied from 5 mVrms to 500 mVrms. The capacitance change rates are obtained and plotted in Figure 6.6a as a function of voltage amplitude. As could be seen, with JD positive serum, the capacitance change rate increases monotonically with the magnitude of AC signals. The change rates from the positive sample are significantly higher than those from the control samples except for the results at 5 mVrms, while the change rate remained consistently low ($< \pm 3.7$ ‰/min) for the control experiments (0.1x PBS) during the same voltage range. It indicates that 5 mVrms is too low to induce any ACEK effects to enhance specific biointeractions between antigens and antibodies. With 5 mVrms applied, the capacitance change rate is merely -5.2 ± 0.8 ‰/min, only slightly higher than that of the control samples, which is -3.7 ± 2.1 ‰/min. Such a small difference between JD positive serum sample and the control sample would not warrant an accurate detection of specific binding. Meanwhile, the capacitance change rate increases rapidly when the applied voltage increased from 5 mVrms to 100 mVrms. The change rate of capacitance at 50 mVrms is -29.1 ± 0.4 ‰/min, while 100 mVrms yields a change rate of -54.6 ± 2.1 ‰/min. The increase in capacitance change rate slows down when the voltage goes above 100 mVrms, which could be caused by possible adverse effect that electric field may have on the activities or adhesion of serum antibodies. Nevertheless, the increase of capacitance change rate with voltage amplitude serves to corroborate the contribution of ACEK effect in this capacitive assay. The results in Figure 6.6a also let us set 100 mVrms as the optimal operating voltage of serum antibody detection. Additionally, the control solution consistently exhibited low capacitance change rates throughout the voltage range, indicating that the high response from positive sample is not caused by electrochemical reactions or other impedimetric artifacts in the measurement.

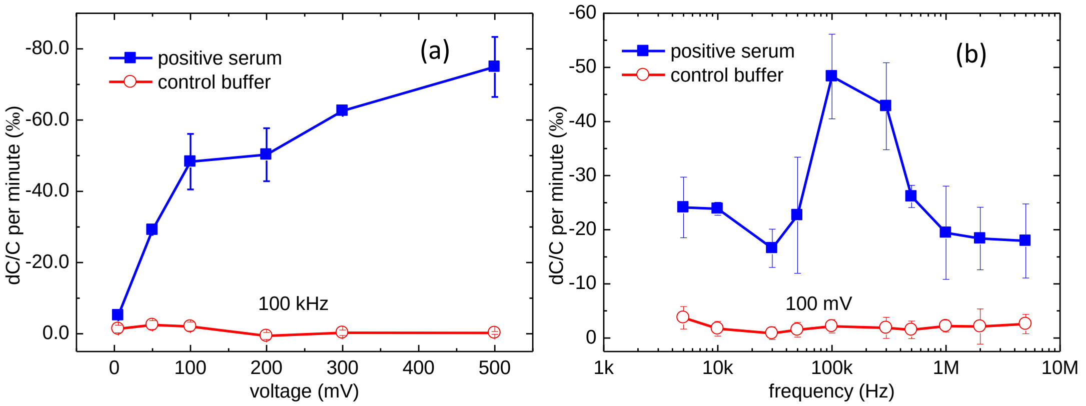

Figure 6.6 Capacitance change rates of JD positive serum sample and control buffer (0.1X PBS) when they are tested at (a) 100 kHz AC signals of various voltage amplitudes, (b) 100 mVrms AC signals at different frequencies. Each data point shows the average of three tests. Error bar indicates the standard deviation.

Secondly, as DEP force is frequency dependent, there should exist a specific frequency at which the target macromolecules will experience maximal attraction force to the electrodes (i.e. the strongest positive DEP). The accompanying ACET flows may add to the particle movement caused by DEP, but will not affect its frequency properties, since ACET effect is independent of AC frequency until a certain level [198, 199]. This time, binding experiments of JD positive antibodies are conducted at different frequencies at a fixed amplitude of 100 mVrms.

The capacitance change rates at different frequencies (ranging from 5 kHz to 5 MHz) are plotted in Figure 6.6b, which demonstrate a strong frequency dependency. The change rate is largest between 100 kHz and 300 kHz, and quickly dropped when AC frequency is deviated from this frequency range. The bell-shaped frequency dependence clearly indicates DEP characteristics. When AC frequency is outside the optimal range, the capacitance change rates are still much higher than those of control sample (in contrast to the results of 5 mVrms assay), which could be attributed to ACET microflows.

6.3.4 Detection results of serum samples

6.3.4.1 Johne's disease

As described before, a total of twenty JD serum samples are tested using SAW electrodes: ten positive samples and ten negative samples. An AC signal of 100 mVrms, 100 kHz is employed as the measuring signal for two minutes. The corresponding capacitance change rates are calculated and plotted in Figure 6.7, which demonstrating a clear differentiation between capacitance changes in JD-negative and JD-positive samples by using a cut-off value of -10.0 ‰/min.

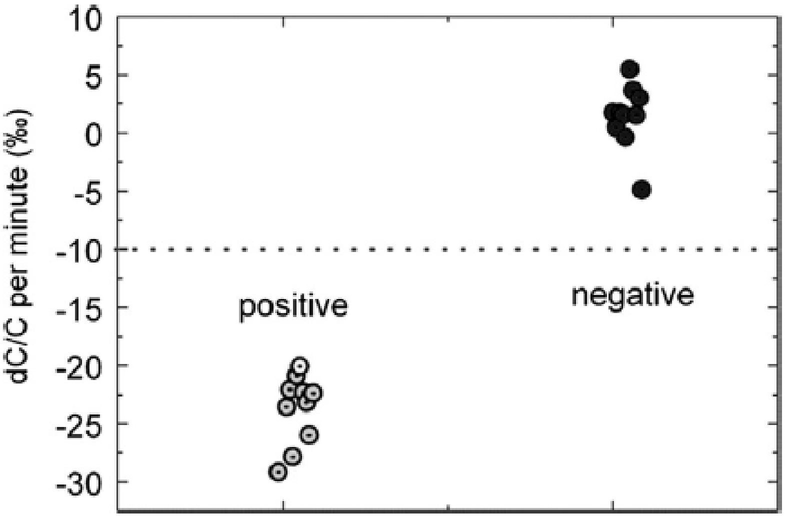

Figure 6.7 Detection results of Johne's disease serum samples.

Moreover, the repeatability test is also conducted by measuring one positive serum sample on five different sensor electrodes, with results shown in Figure 7.2. The calculated coefficient of variation (CV) [200] is only 12.7%, demonstrating decent repeatability.

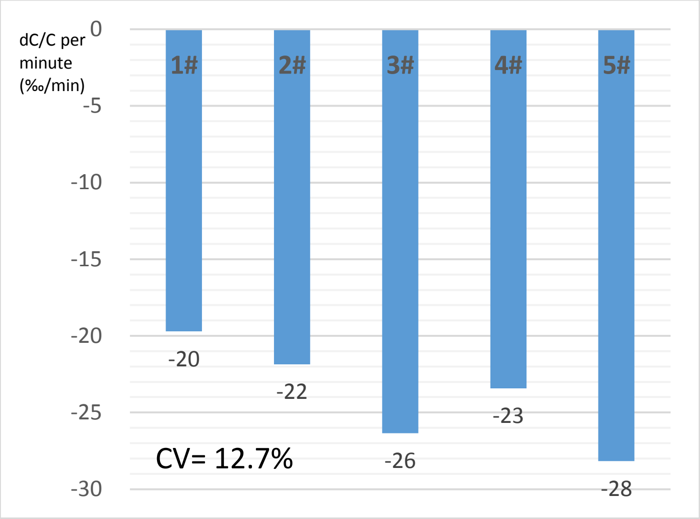

Figure 6.8 Repeatability test with JD positive sample. Same positive sample is tested five times on five different SAW electrodes.

6.3.4.2 Human and Bovine tuberculosis

11 Human TB serum samples (6 positive and 5 negative) and 10 Bovine TB serum samples (5 positive and five negative) are tested using SAW electrodes. The experimental procedure is described as follows: 10 μL of hTB/bTB specific antigens are coated on cleaned SAW electrodes for overnight (16hrs) under room temperature, then the functionalized electrodes are washed with 0.1xPBST for three times and blocked with 0.1x buffer B for 30 minutes. Both hTB and bTB serum samples are diluted in 0.1x PBS with a volume ratio of 1:20 prior to loading.

Before testing the serum batch, the frequency of the applied AC signal is optimized by testing a positive hTB serum sample with 100 mVrms AC signals at 10, 20, 50, 100, 200 kHz and 1 MHz on different electrodes Except for 100 kHz, responses from five of the AC frequencies average around ~10.0 ‰ change in C_{int}, while 100 kHz AC signal yields ~ 50.0 ‰ change. As a result, an AC signal of 100 mVrms at 100 kHz is applied to be the optimal test frequency for TB serum samples. Testing time is one minute for each sample.

The results of TB detection using capacitive sensing are shown and confirmed with the results of ELISA in Figure 6.9 and 6.10. 0.1x PBS is tested as the control sample.

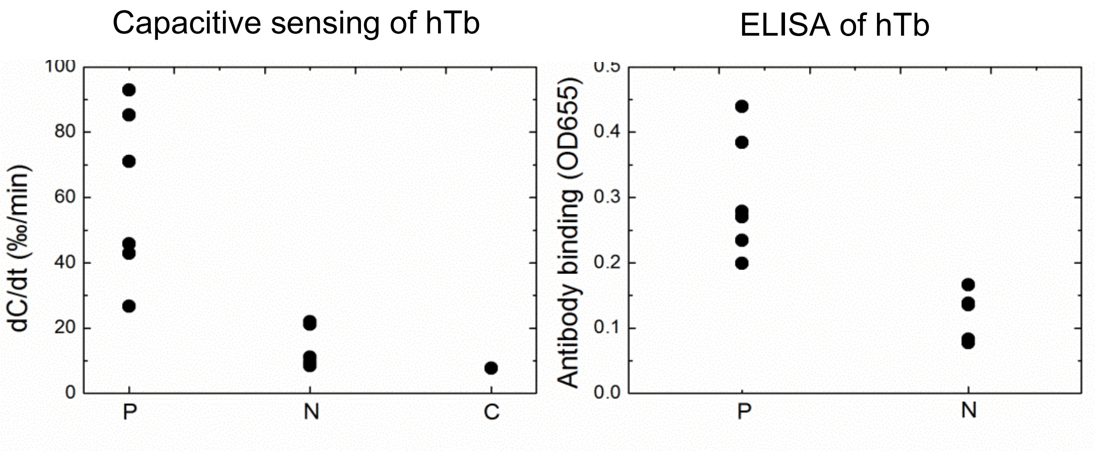

Figure 6.9 Capacitive sensing vs. ELISA of human TB (hTB) positive and negative serum samples. (P: positive samples, N: negative samples; C: control buffer)

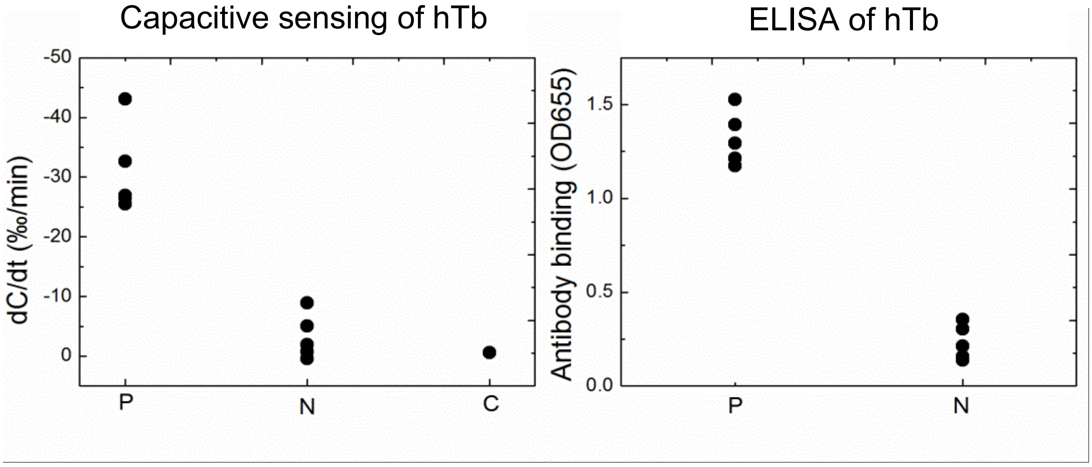

Figure 6.10 Capacitive sensing vs. ELISA of bovine TB (bTB) positive and negative serum samples from badgers. (P: positive samples, N: negative samples; C: control buffer)

As could be seen, disease-positive sera always exhibit large responses than disease-negative samples, which is consistent with the fact that disease-positive serum samples have higher concentrations of disease-specific antibody. Also, two types of control experiments are conducted. One, as shown in Figures 6.9 and 6.10, uses functionalized electrodes with serum-free buffer. Another control experiment (data not shown in the figure to avoid confusion) uses un-functionalized electrodes (blocked but without antigen) with positive serum samples. The control experiment shows little changes in C_{int}, which is -2.4 ± 1.1 ‰/min, demonstrating the specificity.

The fact that bovine TB shows negative changes in capacitance while human TB shows positive changes could be explained by referring to Chapter 3. Suppose bounded hTB antibodies have larger separation from each other than that of bound bTB antibodies, and then consequently hTB samples would lead to an increase of interfacial capacitance after binding, while bTB samples would lead to decreased interfacial capacitance after binding.

Again, to demonstrate the repeatability of the ACEK-based capacitive sensing method, one bTB-positive and one bTB-negative serum sample are tested on five different SAW electrodes for a total of ten chips. The test results and their respective CVs are shown in Table 6.4. The CV for bTB-positive serum is calculated to be 9.2%, showing good repeatability. The CV for bTB-negative serum is expected to be larger since the response of negative sample is relatively small.

Table 6.4 Repeatability test with bTB samples. Each sample is tested five times on five different chips.

Samples	**Capacitance change rate (‰/min)**						
	Chip 1	Chip 2	Chip 3	Chip 4	Chip 5	STD	CV
bTB-positive	-21.5	-29.5	-27.1	-25.9	-27.0	2.4	9.2%
bTB-negative	-2.4	-3.4	-2.0	-1.7	-3.1	0.6	23.3%

6.4 Influenza A virus Detection

Influenza (Flu) is a contagious respiratory infection caused by a variety of flu viruses [201]. There are three types of flu viruses: A, B and C [202]. Type A flu virus is the most commonly cause of large flu epidemics, it is capable of infecting both humans and animals. Compared with type A, type B can only affect humans and it is usually less common and severe. Type C can also cause flu symptoms but are much less severe compared with flu A and B. In this work, we focus on the detection of Influenza A virus using our capacitive affinity sensor.

6.4.1 Sample preparation

Influenza A antibody: mouse monoclonal Influenza A antibody (H1NI, isotype: IgG2a) is provided by Meridian Bioscience, Inc. In this work, antibody is diluted in 0.1x PBS.

Influenza A virus (clean standard): purified and inactivated Influenza A antigen strain (H3N2) cultured in embryonated chicken eggs are provided by Meridian Bioscience, Inc. In this work, virus samples (diluted in 0.1x PBST) of three concentrations are tested: 10, 100 and 1000 ng/mL. Tween 20 is added to help to release the available binding sites of the virus.

*Influenza A virus (nasal sw*ab): clinical nasal swab samples containing Influenza A viral particles are provided by Meridian Bioscience, Inc. In this work, clinical sawb samples are diluted in 0.1x PBST.

6.4.2 Specificity

Influenza A (Flu A) detection is performed using 2μm gold electrodes. The experimental procedure is described as follows: 10 μL of antibody at concentration of 200 ng/mL (diluted in 0.1x PBS) is first added on cleaned electrodes as probe molecule, and the electrodes are then kept in a humidor for six hours for surface functionalization under room temperature. After surface functionalization, the electrodes are washed with 0.1x PBST for three times and then blocked with 0.1x buffer B for 45 minutes. The electrodes are then connected to the impedance analyzer and Influenza A virus samples will be introduced to the surface. Samples are tested at concentrations from 10 ng/mL to 1000 ng/mL (diluted in 0.1x PBST). An AC signal of 10-100 mVrms at 100 kHz is then continuously applied for 30 seconds and the corresponding capacitance change versus time is recorded.

One of the biggest concerns in Flu A detection is whether the detected signal is from a specific biointeraction. In reality, most clinical samples are complex, which means both type A and B viruses can exist at the same time. As a result, there are chances that cross reactivity might take place and interfere with the detection. To verify the specificity of our capacitive affinity assay, four different scenarios are designed and tested, as shown in Figure 6.11:

1. True positive: Flu A antibody functionalized chips tested with Flu A virus.
2. Cross reactivity: Flu A antibody functionalized chips tested with Flu B virus.
3. True negative: Flu A antibody functionalized chips tested with buffer.
4. Non-specific: Unfunctionalized chips tested with Flu A virus.

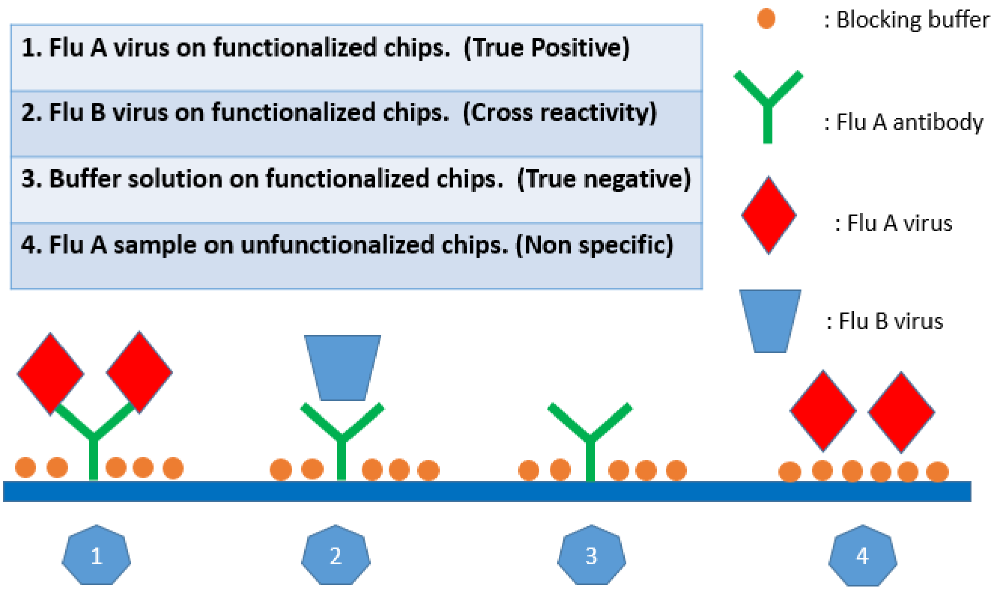
1. Flu A virus on functionalized chips. (True Positive)
2. Flu B virus on functionalized chips. (Cross reactivity)
3. Buffer solution on functionalized chips. (True negative)
4. Flu A sample on unfunctionalized chips. (Non specific)
: Blocking buffer
: Flu A antibody
: Flu A virus
: Flu B virus
1
2
3
4

Figure 6.11 Specificity test of Influenza A: four different scenarios.

Figure 6.12 shows the capacitance change rates of the four cases under two different voltage levels: 10 mVrms and 100 mVrms. The initial test plan is to apply 100 mVrms, yet it is found that the non-specific signal at 100 mVrms reaches $-0.49 \pm 0.16\ \%/\mathrm{min}$, which is very close to the specific binding signal of true positive ($-0.66 \pm 0.11\ \%/\mathrm{min}$). It indicates that the ACEK induced particle and fluid movement might be excessive. To prove our hypothesis, a much lower signal, 10 mVrms, is applied and the same test is performed again. As expected, non-specific signal at 10 mVrms is reduced to $-0.23 \pm 0.05\ \%/\mathrm{min}$, while specific binding signal remains at a relatively high level ($-0.48 \pm 0.10\ \%/\mathrm{min}$). In addition, it is exciting to see that cross reactivity signals stay at low level for both 10 mVrms ($-0.06 \pm 0.02\ \%/\mathrm{min}$) and 100 mVrms ($-0.23 \pm 0.07\ \%/\mathrm{min}$), proving the specificity of the ACEK-based capacitive affinity sensing.

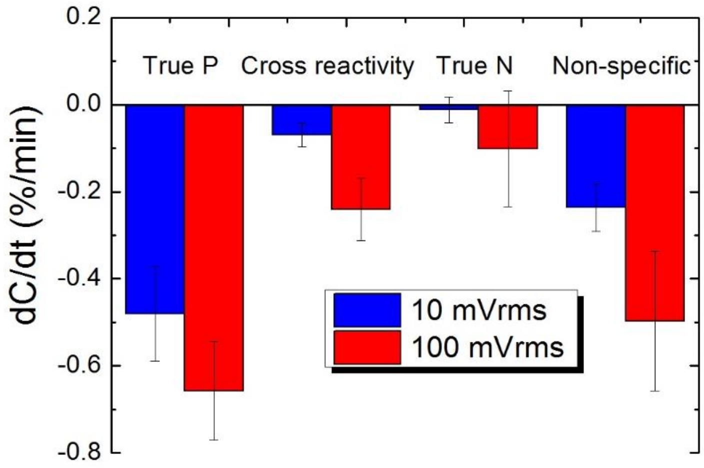

Figure 6.12 Capacitance change rates for the four scenarios under 10 and 100 mVrms. Each data point is the average of three repeated tests. Error bar indicates standard deviation.

6.4.3 Effect of linker molecules

So far, for the assays we have described (bovine IgG antibody, JD, TB and Influenza A), only passive adsorption has been applied as the surface functionalization method. In Chapter 5, we mentioned that using linker molecules could possibly facilitate surface functionalization by forming strong and uniform probe coating, hence the sensor is expected to show better sensitivity and stability.

In the detection of Influenza A, sensors functionalized with passive adsorption are found to show some instable results, especially for high concentration samples. Table 6.5 listed the capacitance change rates of 1000 ng/mL virus sample from five different sensors. As can be seen, for the same sample, the highest response reaches $-0.9\ \%/\mathrm{min}$, while the lowest response is only $-0.29\ \%/\mathrm{min}$. Moreover, CV is calculated to be 45%, which is obviously out of the usable range (normally <15% is required). Therefore, for the purpose of improving sensing stability and repeatability, the usage of linker is introduced for Influenza A detection.

Table 6.5 Repeatability test with flu A virus. 1000 ng/mL virus sample is tested five times on five different chips.

Samples	**Capacitance change rate (%/min)**						
	Chip 1	Chip 2	Chip 3	Chip 4	Chip 5	STD	CV
Flu A virus (1000 ng/mL)	-0.47	-0.97	-0.90	-0.42	-0.29	0.28	45%

As described before, thiol linker molecules have strong affinity towards gold electrodes. In this work, thiol linker (3-MPA) is applied on 2μm gold electrodes for surface functionalization following the procedure described in Chapter 5. After the formation of thiol SAM, antibody is added to the surface for two hours in a humidor under room temperature. Blocking and analyte detection procedures are the same as described in 6.4.2. An AC signal of 10 mVrms at 100 kHz is applied as the measuring signal for 30 seconds, with capacitance change results shown in Figure 6.13.

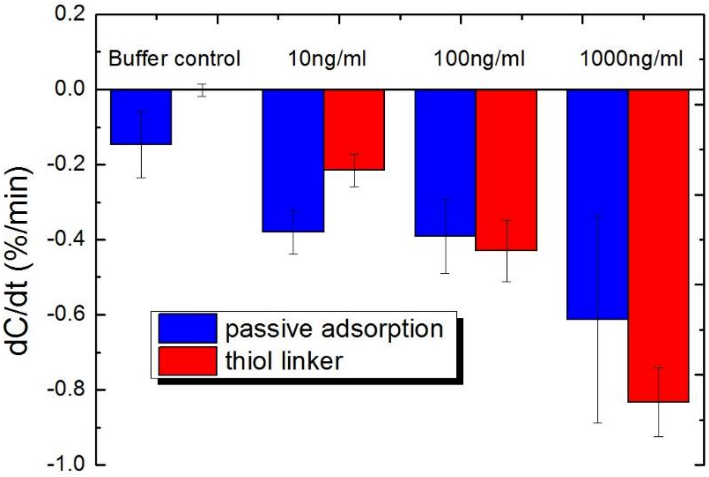

Figure 6.13 Flu A detection results: passive adsorption vs. thiol linker. Each data point is the average of five repeated tests. Error bar indicates standard deviation.

In Figure 6.13, it is clear that binding responses get much more stable with linker functionalized sensors: for example, at 1000 ng/mL, the capacitance change rate is $-0.61 \pm 0.27\ \%/\mathrm{min}$ for passive adsorption, which is improved to $-0.83 \pm 0.09\ \%/\mathrm{min}$ for linker functionalized sensors. It demonstrates higher responses while lower instability, which proves the effectiveness of using thiol linker molecules. Moreover, the binding sensitivity is also improved from $-0.21 \pm 0.15\ \%/\log(\mathrm{ng/mL})$ to $-0.48 \pm 0.10\ \%/\log(\mathrm{ng/mL})$ when thiol linker is applied for surface functionalization.

6.4.4 Blocking optimization

As mentioned in Chapter 5, the purpose of surface blocking is to cover the open spaces on the electrodes to minimize non-specific deposition of bioparticles. In the detection of Influenza A, various blocking methods are adopted. Based on the binding responses from flu A virus samples, their effects are briefly concluded in Table 6.6.

Table 6.6 Descriptions of various blocking methods and major conclusions.

Blocking reagent	Time	Temperature	Conclusions
0.1x buffer B	30 mins	RT	Commonly used blocking plan in affinity biosensing. Works fine with Influenza A detection.
0.1x buffer B	45 mins	RT	Slightly better at reducing non-specific responses.
0.1x buffer B	1 hr	RT	No clear difference compared with 45 mins blocking.
0.1x buffer B	1 hr	37℃	No clear difference compared with RT.
1x buffer B	30 mins	RT	Too strong, specific response is reduced a lot.
1x buffer B	1 hr	RT	Too strong, specific response is reduced a lot.
2 v/v% BSA	30 mins	RT	Too strong, specific response is reduced a lot.
0.2 v/v% BSA	30 mins	RT	Works fine with Influenza A detection, but not showing any better than 0.1x buffer B.

From Table 6.7, it is concluded that a 45 minutes blocking with 0.1x buffer B under room temperature yields the optimal binding response. It is therefore chosen to be the blocking method for influenza A detection.

6.4.5 Blind test of clinical swab samples

Twenty clinical swabs samples collected from different patients are provided by Meridian Bioscience Inc. The identities of the samples are confirmed by PCR (Cepheid Xpert [203]), yet they are not informed before being tested by the ACEK-based capacitive affinity sensor. Prior to detection, these swab samples are diluted 1:1000 v/v% in 0.1x PBST.

Table 6.7 listed and compared the results obtained by the capacitive affinity sensing method with the PCR confirmed results. Out of the twenty samples, only four of them are detected wrongly (in red) and one of them is called to be undetermined by both methods (in orange). The overall success rate reaches

79% (15/19), which is very promising.

Table 6.7 Blind test results of twenty clinical swab Influenza A samples.

Sample	dC/dt (%/min)	Capacitive sensing results	PCR results provide by Meridian Bioscience Inc.
No.1	1.57	N	N
No.2	-1.59	P	N
No.3	-2.14	P	P
No.4	0.43	N	P
No.5	-0.17	N	N
No.6	0.05	N	N
No.7	-1.83	P	P
No.8	3.78	N	N
No.9	-3.71	P	P
No.10	-0.50	?	P
No.11	0.76	N	N
No.12	-3.03	P	P
No.13	-1.39	P	N
No.14	0.53	N	N
No.15	-0.56	?	?
No.16	1.01	N	N
No.17	-0.86	P	P
No.18	-3.44	P	P
No.19	-0.96	P	P
No.20	-1.24	P	P

6.5 Small molecule detection

As the name implies, small molecule refers to biomolecules which sizes are on the order of nm (low molecular weight, < 900 Da). For example, the molecular weight of BPA is only 228 Da, while for anti-bovine IgG antibody, the molecular weight is 150 kDa. In this work, two types of small molecules with biological significances are tested in their spiked form: Bisphenol A and progesterone.

Bisphenol A (BPA) is an industrial chemical used as an intermediate to make polycarbonate plastic, epoxy resins and many other specialty products [204]. It can be found in many of daily used items including water bottles, food containers, and paper products for decades [205]. Yet recent studies have found the exposure of BPA could probably cause adverse health issues to humans [185, 206]. It is reported that BPA is an endocrine-disrupting chemical and its estrogenic activity could affect different organs [207]. Thus detection of BPA level within the environment as well as human serum is of crucial importance. Current BPA detection methods include high performance liquid chromatography (HPLC) [208, 209] and gas chromatography-mass spectrometry (GC-MS) [210, 211]. While good detection limits were reported, e.g. 0.04 ng/mL by HPLC, these methods require the use of sophisticated and costly instruments by skilled personnel, and yet the operation is complex and time-consuming. Therefore, a simple, affordable and label-free method to monitor BPA level in environmental samples is highly desired.

Progesterone is a hormone produced mainly in the ovaries. In pregnancy, after an ovum is released, progesterone helps make the uterus ready for implantation of a fertilized ovum and prepares the uterus for pregnancy and the breasts for milk production [212]. In dairy industry, pregnancy test is an important management measure to keep cattle producing milk with minimized open (non-lactating) period [213, 214]. Currently, pregnancy tests are conducted by either transrectal palpation or immunoassay in diagnostic laboratory. Previous studies indicated that palpation in early gestation increased risk of embryonic mortality [215]. Current format of immunoassay for progesterone is enzyme-linked immunosorbent assay (ELISA), which requires the use of laboratory equipment and several hours of labor. Comparing with the current format, ACEK-based capacitive affinity sensing is expected to obtain better sensitivity in shorter time, with less sensor preparation and sample processing.

6.5.1 Sample preparation

6.5.1.1 Bisphenol A

The preparation of BPA specific aptamer and spiked BPA sample is described as follows:

- *BPA specific aptamer:* The specific aptamer with 5’ thiol modifier C6 SH is synthesized by Sangon Biotech (Shanghai) Co., Ltd. The sequence of the aptamer (5’ to 3’) is 5’-CCG GTG GGT GGT CAG GTG GGA TAG CGT TCC GCG TAT GGC CCA GCG CAT CAC GGG TTC GCA CCA-3’. In this work, aptamer is diluted in 0.1x PBS.
- *Spiked BPA sample:* 4, 4’-Isopropylidenediphenol (BPA) is purchased from Fisher Scientific, Pittsburgh, PA. Dimethyl Sulfoxide (DMSO), ≥99.7% is also purchased from Fisher Scientific, which is used as the solvent for BPA. 0.1x PBS is used for the dilution of BPA.
- Triton X-100 stock solution is purchased from Alfa Aesar, Ward Hill, MA, which is used as the blocking buffer.

6.5.1.2 Progesterone

The preparation of anti-PG antibody and spiked PG sample is described as follows:

- *Anti-progesterone polyclonal antibody (Fisher Scientific, PA175366), Host Species:* Sheep Species Reactivity: Chemical Immunogen: Progesterone (11)-BSA 100 µL; Unlabeled 100 µL). In this work, purified anti-progesterone polyclonal antibody is diluted in 0.1x PBS.
- *Spiked progesterone:* Acros Organics (thru Thermo Fisher Scientific [Pittsburg, PA] #225650050), stock 10 mg/mL in DMSO. In this work, progesterone is diluted in 0.1x PBS.

6.5.2 Detection of BPA

The detection of BPA is performed using both SAW and gold electrodes, with procedures described as follows: cleaned electrodes are functionalized with thiol modified aptamer (0.1 μM, diluted in 0.1x PBS) for two hours in a humidor under room temperature, then the electrodes are washed with 0.1x PBST for three times and blocked with 0.1 v/v% Triton X-100 for 30 minutes. 0.1 v/v% Triton X-100 is prepared by adding 10 μL of Triton X-100 stock solution into 10 mL of purified water. BPA (11.3 mg) is dissolved into 5 mL DMSO to make 10 mM BPA solution, which is then serial diluted to reach concentrations from 1 fM to 1 pM using 0.1x PBS. The electrodes are then connected to the impedance analyzer and BPA samples will be introduced to the surface for testing.

For BPA testing, the test frequency is chosen to be 20 kHz instead of 100 kHz because the whole electrolyte/electrode system is more capacitively dominant around this specific frequency. Taking SAW electrode as an example, actual impedance measurement at 20 kHz showed a R_f of 1879 Ω and a C_{int} of 7.63 nF. Given the dimension of the electrodes, according to $R_f = \frac{l}{\sigma A}$, where $l = \pi l/2$ is the half circle over the electrode gap of 1.1 μm, and A is the electrode area, 628×150×0.7 μm^2 for the whole array; σ=0.15 S/m is the fluid conductivity. R_f is estimated to be 1747 Ω for the electrode array. Meanwhile, according to $C_{int} = \frac{\varepsilon A}{d}$, where ε is the permittivity of the fluid and biomolecule ($\varepsilon = \varepsilon_0 \varepsilon_r$, with ε_0 being the permittivity of free space and ε_r being the relative permittivity of fluid and biomolecule), A is the area (628×150×1.4 μm^2) and d is the thickness of the double layer plus the immobilized biomolecules (around 10 nm), C_{int} is estimated to be around 9.1 nF. Since both of the theoretical values are very close to the measured value, a simplified C_{int}-R_f serial connected equivalent circuit can adequately account for the impedance of the sensor cell, and the measured capacitance can be regarded as C_{int}.

6.5.2.1 Proof-of-concept

First of all, as a proof of concept, different concentrations of BPA samples are tested under 500 mVrms AC signal at 20 kHz for a total of 20 seconds using SAW electrodes. Figure 6.14 presents how normalized capacitance changes with time for various sample concentrations. The curve of buffer (black line with square) remained flat throughout the detection period, showing no occurrence of biointeraction. For BPA samples ranging from 1 to 1000 fM, the capacitance change rates become larger with increasing concentrations, manifesting the increasing level of specific BPA binding. Meanwhile, the curve of non-specific (100 fM BPA, without aptamer) goes down a little, indicating the existence of certain level of non-specific binding (red line with circle).

Also, according to Figure 6.14, there are signs of BPA depletion for lower concentrations after the first 10 seconds of binding, as the curves are gradually becoming flatter. To demonstrate the binding event with time more accurately, Table 6.8 lists the change rates at two different time periods: 0-10 seconds and 10-20 seconds. Except for 1000 fM, the change rate in the first 10-second period is always larger than that in the second 10-second period, as the depletion of target molecules starts to show as time goes by. In the first 10 seconds, the capacitance change rate of 10 fM BPA quickly reaches $-1.73\%/\mathrm{min}$, which is higher than both of the non-specific ($-1.23\ \%/\mathrm{min}$) and buffer control (-$0.02\ \%/\mathrm{min}$), demonstrating a successful detection.

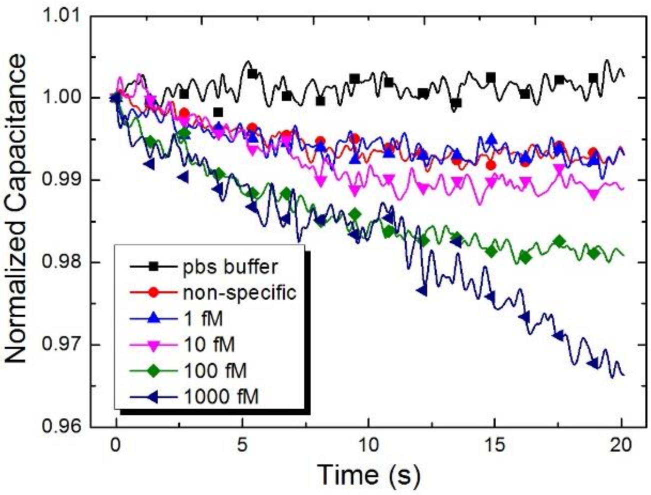

Figure 6.14 Characteristic changes of interfacial capacitance with time when different samples are tested. Binding reactions with 1, 10, 100 and 1000 fM BPA are shown here. Buffer (blank without BPA) and non-specific (1pM BPA sample tested on dummy electrodes) are shown as controls.

Table 6.8 Capacitance change rates within two different time periods.

dC/dt (%/min)	**0-10s**	**10-20s**
0.1x PBS	-0.02	0.23
Non-specific	-1.23	-0.1
1 fM (0.28 fg/mL)	-0.68	-0.34
10 fM (2.8 fg/mL)	-1.73	-0.08
100 fM (28 fg/mL)	-1.71	-1.1
1 pM (280 fg/mL)	-2.74	-1.12

6.5.2.2 Study of ACET effect

As discussed earlier, the size of small molecules are much tinier compared with antibodies. From Chapter 4, we see that the relative importance of DEP and ACET forces will shift in favor of ACET effect with smaller molecules, as DEP force is dependent on the particle volume while ACET force is not. As a result, DEP enrichment will be much weaker for BPA than for antibodies. So the use of ACET effect should be more important to small molecule detection. BPA samples from 1 to 100 fM are tested on both SAW and 5μm gold electrodes as a comparison. The applied electric field strength is very similar, which is 50 mV/μm on SAW electrodes and 46 mV/μm on 5μm electrodes.

Figure 6.15 shows the outputs from both SAW and 5μm gold electrodes. It can be seen that the rate of decrease in capacitance steadily gets larger with more concentrated samples on both electrodes. The responses from both electrodes exhibited a logarithmic dependence on BPA concentration ranging from 1 to 100 fM. As expected, much larger capacitance change is seen from 5μm gold electrodes, which is clearly the result of stronger ACET convection. While for SAW electrodes, although the electric field strength is slightly larger, the response is less obvious than that from 5μm gold electrodes. The detection sensitivity of 5μm gold electrodes is calculated to be $-0.40 \pm 0.08\ \%/\log(\mathrm{fM})$, much higher than that of SAW electrodes, which is only $-0.09 \pm 0.04\ \%/\log(\mathrm{fM})$.

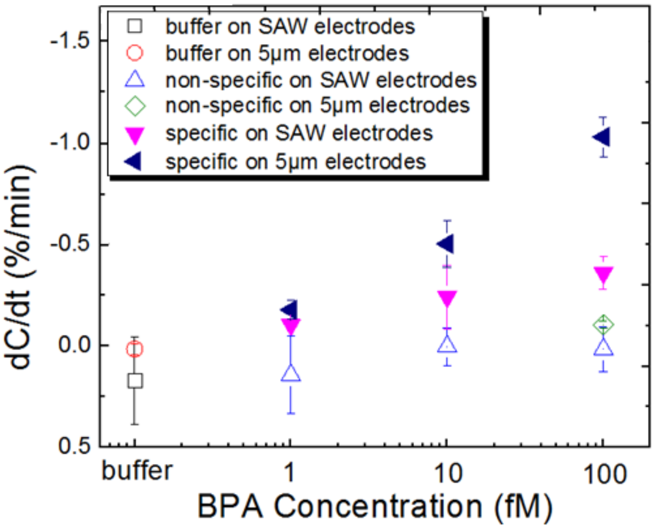

Figure 6.15 BPA detection results on both electrodes. Buffer tests are 0.1x PBS on functionalized electrodes; non-specific tests are 1-100 fM BPA on dummy electrodes; specific tests use 1-100 fM BPA samples on functionalized electrodes. Each data point is the average of three repeated tests and the error bar indicates standard deviation.

6.5.2.3 Determination of LOD

From Figure 6.15, we could also determine the limit of detection (LOD) of the two electrodes. Baseline responses are obtained by measuring buffer, which are $0.01 \pm 0.02\ \%/\mathrm{min}$ on 5μm gold electrodes and $0.16 \pm 0.15\ \%/\mathrm{min}$ on SAW electrodes. Besides, responses from non-specific binding are minimal on both electrodes. 100 fM BPA caused a change rate of $-0.10 \pm 0.02\ \%/\mathrm{min}$ for 5μm electrodes, and $0.01 \pm 0.11\ \%/\mathrm{min}$ for SAW electrodes, showing good specificity. In comparison, 5μm electrode produces a change rate of $-0.50 \pm 0.11\ \%/\mathrm{min}$ for 10 fM BPA, which can easily be distinguished from the baseline. SAW electrodes yield a change rate of $-0.36 \pm 0.07\ \%/\mathrm{min}$ for 100 fM BPA, which could be also be differentiated. Therefore, LOD is determined to be 10 fM for 5μm electrode and 100 fM for SAW electrodes.

6.5.3 Preliminary detection of PG

Similar to BPA, the detection of progesterone is also categorized as small molecule detection. Progesterone is very small in size and weight, with a molecular weight of only 315 Da. Some preliminary experiments are performed in this work using SAW electrodes.

The experimental procedure is described as follows: cleaned electrodes are functionalized with anti-PG polyclonal antibody (0.15 μM, diluted in 0.1x PBS) for two hours in a humidor under room temperature, then the electrodes are washed with 0.1x PBST for three times and blocked with 0.1x buffer B for 30 minutes. The electrodes are then connected to the impedance analyzer and PG samples will be loaded for test. PG sample is diluted in 0.1x PBS to get three different concentrations of progesterone: 0.5ng, 1ng and 5 ng/mL.

An AC signal of 100 mVrms at 100 kHz is applied continuously for one minute as the measuring signal. Preliminary results with passive adsorption as surface functionalization method do not show an adequate differentiation, thus in order to achieve better performance, we also introduce APTES-treated SAW electrodes to improve its sensitivity. The procedure of APTEPS treatment has been described in Chapter 5.

Figure 6.16 shows the preliminary results of spiked PG sample detection. Three different concentrations of PG are tested consecutively on the same chip, from low to high. 0 ng/mL means control buffer (0.1x PBS). As could be seen, binding begins to saturate at 5 ng/mL, since the available binding sites are limited, capacitance would not change much after the binding starts to saturate. Furthermore, as expected, chips treated with APTES showed higher capacitance change compared with bare chips. This could be explained by the fact that APTES increases the surface availability, i.e. more binding sites are provided. Although the limit of detection is not increased since the background also goes higher, the sensitivity is indeed increased with APTES-treated chips. For APTES-treated chips, sensitivity is about 0.6 %/ (ng/mL), while for bare chips, sensitivity is only around 0.2 %/ (ng/mL). The limit of detection is determined to be 1 ng/mL (3.2 nM) for spiked progesterone detection.

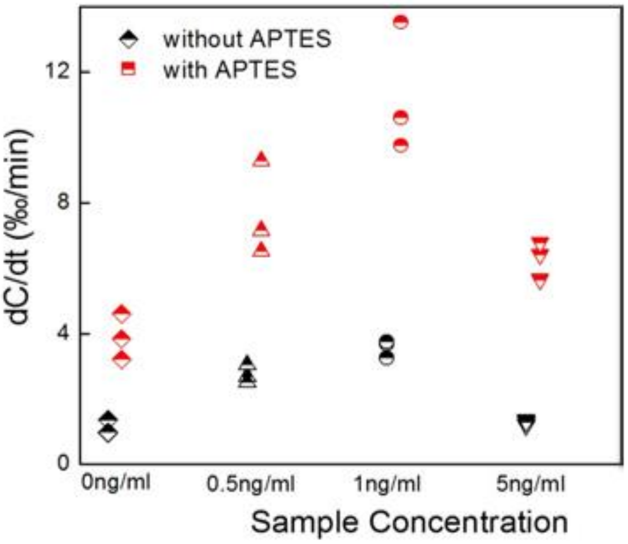

Figure 6.16 Detection results of progesterone binding. Different change rates indicate different binding levels. Each test is repeated three times. Error bar represents the standard deviation of three test results.

Chapter 7. Conclusions and Future Work

7.1 Summary

This work presents an ACEK-based capacitive affinity sensing method that holds high promise for POC disease diagnosis. The detection is realized through a capacitive sensing technique with a microelectrode array.

The capacitive affinity sensing technique has two major functions: realizing the study of nanoscale surface structure and deposition; and carrying out the detection of specific surface biomolecular interactions. In this work, the first function is used for surface quality controlling of sensor electrodes, while the second function is applied to detect specific biomolecular interaction, such as antigen-antibody binding.

The capacitive assay presented in this work can achieve ACEK enrichment of biomolecules and label-free detection of deposition on the microelectrode surface simultaneously. The experiments proved that DEP and ACET effect could speed up the biointeraction process to achieve rapid and sensitive detection. Compared with conventional methods, the detection time has been greatly reduced from hours to minutes.

We also carefully choose our electrode design and detection protocol, so that at the AC enrichment frequency, the detection cell can be represented with a simplified resistor-capacitor serial connection (fluid resistance in series with electrode/fluid interfacial capacitance). Because the effect of sample matrix mostly shows up in its resistive component (e.g. charge transfer resistance), the detection method and device combined is relatively unsusceptible to the interference from the background solution. As a result, this method needs little pretreatment of the sample (sample pre-treatment requires only volume dilution of serum samples with physiological buffer), and does not require a washing step after binding, which is a major advantage over traditional impedimetric biosensors.

In summary, the ACEK-based capacitive biosensor has a shorter assay time, reduced reagent and device cost, simpler device design and operation than conventional diagnostic system. The potential of this sensing technique for rapid disease detection might greatly facilitate the battle against the epidemic of infectious diseases in the future.

7.2 Future Work

7.2.1 Further improvement of feasibility

To build a fully qualified sensing technology for POC diagnosis in real world, the feasibility of the ACEK-based capacitive sensor needs further improvement. Compared to electrical signal readout, biological related issues pose more uncertainties to sensor performance. Surface functionalization is always the most crucial step in affinity biosensing. In this work, only the effect of 3-MPA is studied on gold electrodes. Further effort would be focused on the study of various thiol linker molecules, such as 11-mercaptoundecanioc acid (11-MUA). Compared with 3-MPA, 11-MUA has longer chains, which is expected to improve the stability of surface functionalization.

Moreover, the size of the probe molecules could also affect the detected signal. For example, in progesterone detection, the size of current probe antibody is much larger than the size of progesterone molecule. The huge size of probe brings down the detection sensitivity, as the change of capacitance due to progesterone binding is less notable. Therefore, finding more proper probe molecules in size for different analytes is one of the tasks of future work.

7.2.2 Multiplexed assay with high specificity

Multiplexed assay, as opposed to single detection, refers to the detection of multiple analyte samples simultaneously. It is very useful in real life diagnosis, as sometimes it is needed to deal with hundreds or thousands of samples within a short time period. To achieve multiplexed detection, IC integration is needed to combine several sensors to a single chip, while each sensor should have its own independent signal source to avoid interference.

7.2.3 Handheld device

The current measurement device is a clumsy benchtop instrument. A desired prototype for realizing POC diagnosis would be a light, portable and robust handheld device, as conceptually shown in Figure 7.1. Detection results could be easily displayed on the screen and can be transferred to a smart phone if available.

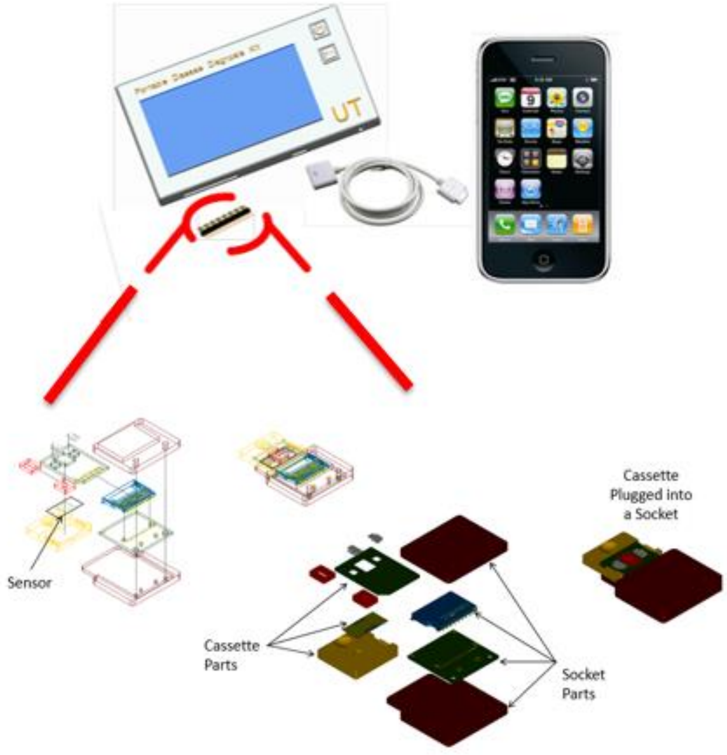
Portable Disease Diagnosis Kit
UT
Sensor
Cassette Plugged into a Socket
Cassette Parts
Socket Parts

Figure 7.1 Concept of a portable POC device.

LIST OF REFERENCES

1. Hays, J.N., The burdens of disease: epidemics and human response in western history. 2009: Rutgers University Press.
2. Keeler, E., et al., Reducing the global burden of tuberculosis: the contribution of improved diagnostics. Nature, 2006. 444: p. 49-57.
3. Wadhwa, A., et al., Overview of Johne's disease immunology. Veterinary World, 2013. 6(11): p. 901-904.
4. Halasa, T., et al., Economic effects of bovine mastitis and mastitis management: A review. Veterinary Quarterly, 2007. 29(1): p. 18-31.
5. Urdea, M., et al., Requirements for high impact diagnostics in the developing world. Nature, 2006. 444: p. 73-79.
6. Bryce, J., et al., WHO estimates of the causes of death in children. The Lancet, 2005. 365(9465): p. 1147-1152.
7. Van Lerberghe, W., et al., Make every mother and child count. 2005: World Health Organization.
8. O’Ryan, M., V. Prado, and L.K. Pickering. A millennium update on pediatric diarrheal illness in the developing world. in Seminars in pediatric infectious diseases. 2005. Elsevier.
9. Fewtrell, L., et al., Water, sanitation, and hygiene interventions to reduce diarrhoea in less developed countries: a systematic review and meta-analysis. The Lancet infectious diseases, 2005. 5(1): p. 42-52.
10. Lopez-Fraga, M., N. Wright, and A. Jimenez, RNA interference-based therapeutics: new strategies to fight infectious disease. Infectious Disorders-Drug Targets (Formerly Current Drug Targets-Infectious Disorders), 2008. 8(4): p. 262-273.
11. Zwane, A.P. and M. Kremer, What works in fighting diarrheal diseases in developing countries? A critical review. The World Bank Research Observer, 2007. 22(1): p. 1-24.
12. Spellberg, B., et al., The epidemic of antibiotic-resistant infections: a call to action for the medical community from the Infectious Diseases Society of America. Clinical Infectious Diseases, 2008. 46(2): p. 155-164.

13. Organization, W.H., Global Health Observatory:(GHO). 2013: World Health Organization.

14. Burgess, D.C.H., J. Wasserman, and C.A. Dahl, Global health diagnostics. Nature, 2006. 444: p. 1-2.

15. Yager, P., G.J. Domingo, and J. Gerdes, Point-of-care diagnostics for global health. Annu. Rev. Biomed. Eng., 2008. 10: p. 107-144.

16. Glaros, C. and D.I. Fotiadis, Wearable devices in healthcare, in Intelligent Paradigms for Healthcare Enterprises. 2005, Springer. p. 237-264.

17. Kost, G.J., Goals, guidelines and principles for point-of-care testing. Kost GJ (ed), 2002: p. 3-12.

18. Howick, J., et al., Current and future use of point-of-care tests in primary care: an international survey in Australia, Belgium, The Netherlands, the UK and the USA. BMJ open, 2014. 4(8): p. e005611.

19. Pejcic, B., R. De Marco, and G. Parkinson, The role of biosensors in the detection of emerging infectious diseases. Analyst, 2006. 131(10): p. 1079-1090.

20. Luppa, P.B., L.J. Sokoll, and D.W. Chan, Immunosensors—principles and applications to clinical chemistry. Clinica Chimica Acta, 2001. 314(1): p. 1-26.

21. Spichiger-Keller, U.E., Chemical sensors and biosensors for medical and biological applications. 2008: John Wiley & Sons.

22. Rivet, C., et al., Microfluidics for medical diagnostics and biosensors. Chemical Engineering Science, 2011. 66(7): p. 1490-1507.

23. Mello, L.D. and L.T. Kubota, Review of the use of biosensors as analytical tools in the food and drink industries. Food chemistry, 2002. 77(2): p. 237-256.

24. Waswa, J., J. Irudayaraj, and C. DebRoy, Direct detection of< i> E. Coli</i> O157: H7 in selected food systems by a surface plasmon resonance biosensor. LWT-Food Science and Technology, 2007. 40(2): p. 187-192.

25. Pedrosa, V.A., et al., Determination of parathion and carbaryl pesticides in water and food samples using a self assembled monolayer/acetylcholinesterase electrochemical biosensor. Sensors, 2008.

8(8): p. 4600-4610.

26. Chai, C., Label-free immunosensor for toxin detection in food matrix, 2008, Rutgers, The State University of New Jersey.

27. Batzias, F. and C.G. Siontorou, A novel system for environmental monitoring through a cooperative/synergistic scheme between bioindicators and biosensors. Journal of environmental management, 2007. 82(2): p. 221-239.

28. Rana, J., et al., Utility biosensors for applications in agriculture–A Review. Journal of American Science, 2010. 6(9): p. 353-375.

29. Rai, V., S. Acharya, and N. Dey, Implications of Nanobiosensors in Agriculture. Journal of Biomaterials and Nanobiotechnology, 2012. 3(2): p. 315-324.

30. Tothill, I.E., Biosensors developments and potential applications in the agricultural diagnosis sector. Computers and Electronics in Agriculture, 2001. 30(1): p. 205-218.

31. Janata, J., Principles of chemical sensors. 2010: Springer Science & Business Media.

32. Rogers, K.R., Principles of affinity-based biosensors. Molecular biotechnology, 2000. 14(2): p. 109-129.

33. Wang, J., Electrochemical glucose biosensors. Chemical reviews, 2008. 108(2): p. 814-825.

34. Chen, C., et al., Recent advances in electrochemical glucose biosensors: a review. Rsc Advances, 2013. 3(14): p. 4473-4491.

35. Daniels, J.S. and N. Pourmand, Label‐Free Impedance Biosensors: Opportunities and Challenges. Electroanalysis, 2007. 19(12): p. 1239-1257.

36. Li, J., et al., An electrochemical immunosensor for carcinoembryonic antigen enhanced by self-assembled nanogold coatings on magnetic particles. Analytica chimica acta, 2010. 665(1): p. 98-104.

37. Khan, W., M. Kapoor, and N. Kumar, Covalent attachment of proteins to functionalized polypyrrole-coated metallic surfaces for improved

biocompatibility. Acta Biomaterialia, 2007. 3(4): p. 541-549.

38. Hafaid, I., et al., Effect of electrical conditions on an impedimetric immunosensor based on a modified conducting polypyrrole. Sensors and Actuators B: Chemical, 2010. 144(1): p. 323-331.

39. Zou, Z., et al., Functionalized nano interdigitated electrodes arrays on polymer with integrated microfluidics for direct bio-affinity sensing using impedimetric measurement. Sensors and Actuators A: Physical, 2007. 136(2): p. 518-526.

40. Chaki, N.K. and K. Vijayamohanan, Self-assembled monolayers as a tunable platform for biosensor applications. Biosensors and Bioelectronics, 2002. 17(1): p. 1-12.

41. Vessman, J., et al., Selectivity in analytical chemistry (IUPAC Recommendations 2001). Pure and Applied Chemistry, 2001. 73(8): p. 1381-1386.

42. Thompson, I.M., et al., Prevalence of prostate cancer among men with a prostate-specific antigen level≤ 4.0 ng per milliliter. New England Journal of Medicine, 2004. 350(22): p. 2239-2246.

43. Määttänen, L., et al., Three-year results of the Finnish prostate cancer screening trial. Journal of the National Cancer Institute, 2001. 93(7): p. 552-553.

44. Guo, S. and S. Dong, Biomolecule-nanoparticle hybrids for electrochemical biosensors. TrAC Trends in Analytical Chemistry, 2009. 28(1): p. 96-109.

45. Song, S., et al., Aptamer-based biosensors. TrAC Trends in Analytical Chemistry, 2008. 27(2): p. 108-117.

46. Justino, C.I., T.A. Rocha-Santos, and A.C. Duarte, Review of analytical figures of merit of sensors and biosensors in clinical applications. TrAC Trends in Analytical Chemistry, 2010. 29(10): p. 1172-1183.

47. Luong, J.H., K.B. Male, and J.D. Glennon, Biosensor technology: technology push versus market pull. Biotechnology advances, 2008. 26(5): p. 492-500.

48. Pei, X., et al., Sandwich-type immunosensors and immunoassays

exploiting nanostructure labels: A review. Analytica chimica acta, 2013. 758: p. 1-18.

49. Mohammed, M.-I. and M.P. Desmulliez, Lab-on-a-chip based immunosensor principles and technologies for the detection of cardiac biomarkers: a review. Lab on a Chip, 2011. 11(4): p. 569-595.

50. Jiang, H., X. Weng, and D. Li, Microfluidic whole-blood immunoassays. Microfluidics and nanofluidics, 2011. 10(5): p. 941-964.

51. Ricci, F., et al., A review on novel developments and applications of immunosensors in food analysis. Analytica chimica acta, 2007. 605(2): p. 111-129.

52. Cloarec, J.-P., et al., A multidisciplinary approach for molecular diagnostics based on biosensors and microarrays. IRBM, 2008. 29(2): p. 105-127.

53. Rich, R.L. and D.G. Myszka, Survey of the year 2007 commercial optical biosensor literature. Journal of Molecular Recognition, 2008. 21(6): p. 355-400.

54. Rich, R.L. and D.G. Myszka, Survey of the 2009 commercial optical biosensor literature. Journal of Molecular Recognition, 2011. 24(6): p. 892-914.

55. Lakowicz, J.R., Principles of fluorescence spectroscopy. 2007: Springer.

56. Lequin, R.M., Enzyme immunoassay (EIA)/enzyme-linked immunosorbent assay (ELISA). Clinical Chemistry, 2005. 51(12): p. 2415-2418.

57. Duménigo, B., A. Espino, and C. Finlay, Detection of< i> Fasciola hepatica</i> antigen in cattle faeces by a monoclonal antibody-based sandwich immunoassay. Research in veterinary science, 1996. 60(3): p. 278-279.

58. Liu, X., et al., Development of an AC electrokinetics-based immunoassay system for on-site serodiagnosis of infectious diseases. Sensors and Actuators A: Physical, 2011. 171(2): p. 406-413.

59. Homola, J., S.S. Yee, and G. Gauglitz, Surface plasmon resonance sensors: review. Sensors and Actuators B: Chemical, 1999. 54(1): p. 3-15.

60. Dodeigne, C., L. Thunus, and R. Lejeune, Chemiluminescence as diagnostic tool. A review. Talanta, 2000. 51(3): p. 415-439.

61. Ma, F., et al., Ultrasensitive electrogenerated chemiluminescence

biosensor for the determination of mercury ion incorporating G4 PAMAM dendrimer and Hg (II)-specific oligonucleotide. Biosensors and Bioelectronics, 2012. 32(1): p. 37-42.

62. Yang, H., et al., Electrogenerated chemiluminescence biosensor incorporating ruthenium complex-labelled Concanavalin A as a probe for the detection of Escherichia coli. Biosensors and Bioelectronics, 2012. 35(1): p. 376-381.

63. Liu, F. and C. Zhang, A novel paper-based microfluidic enhanced chemiluminescence biosensor for facile, reliable and highly-sensitive gene detection of Listeria monocytogenes. Sensors and Actuators B: Chemical, 2015. 209: p. 399-406.

64. Vestergaard, M., K. Kerman, and E. Tamiya, An overview of label-free electrochemical protein sensors. Sensors, 2007. 7(12): p. 3442-3458.

65. Thévenot, D.R., et al., Electrochemical biosensors: recommended definitions and classification. Biosensors and Bioelectronics, 2001. 16(1): p. 121-131.

66. Wan, Y., et al., Development of electrochemical immunosensors towards point of care diagnostics. Biosensors and Bioelectronics, 2013. 47: p. 1-11.

67. Ronkainen, N.J., H.B. Halsall, and W.R. Heineman, Electrochemical biosensors. Chemical Society Reviews, 2010. 39(5): p. 1747-1763.

68. Iqbal, M.A., S. Gupta, and S. Hussaini, A Review on Electrochemical Biosensors: Principles and Applications. Advances in Bioresearch, 2012. 3(4).

69. Ghindilis, A.L., et al., Immunosensors: electrochemical sensing and other engineering approaches. Biosensors and Bioelectronics, 1998. 13(1): p. 113-131.

70. Wang, J., Electrochemical biosensors: towards point-of-care cancer diagnostics. Biosensors and Bioelectronics, 2006. 21(10): p. 1887-1892.

71. Zhou, M. and S. Dong, Bioelectrochemical interface engineering: toward the fabrication of electrochemical biosensors, biofuel cells, and self-powered logic biosensors. Accounts of chemical research, 2011. 44(11): p. 1232-1243.

72. Liu, F., et al., Fabrication of free-standing graphene composite films as electrochemical biosensors. Carbon, 2012. 50(1): p. 123-133.

73. Xu, Y. and E. Wang, Electrochemical biosensors based on magnetic micro/nano particles. Electrochimica Acta, 2012. 84: p. 62-73.

74. Belluzo, M.S., M.É. Ribone, and C.M. Lagier, Assembling amperometric biosensors for clinical diagnostics. Sensors, 2008. 8(3): p. 1366-1399.

75. Wang, L., et al., A novel amperometric biosensor for superoxide anion based on superoxide dismutase immobilized on gold nanoparticle-chitosan-ionic liquid biocomposite film. Analytica chimica acta, 2013. 758: p. 66-71.

76. Chauhan, N. and C.S. Pundir, An amperometric biosensor based on acetylcholinesterase immobilized onto iron oxide nanoparticles/multi-walled carbon nanotubes modified gold electrode for measurement of organophosphorus insecticides. Analytica chimica acta, 2011. 701(1): p. 66-74.

77. Catsimpoolas, N., Isoelectric focusing. 2012: Elsevier.

78. Purvis, D., et al., An ultrasensitive and stable potentiometric immunosensor. Biosensors and Bioelectronics, 2003. 18(11): p. 1385-1390.

79. Koncki, R., Recent developments in potentiometric biosensors for biomedical analysis. Analytica chimica acta, 2007. 599(1): p. 7-15.

80. Vieira, N., et al., Nanostructured polyaniline thin films as pH sensing membranes in FET-based devices. Sensors and Actuators B: Chemical, 2011. 160(1): p. 312-317.

81. Hafeman, D.G., J.W. Parce, and H.M. McConnell, Light-addressable potentiometric sensor for biochemical systems. Science, 1988. 240(4856): p. 1182-1185.

82. Prodromidis, M.I., Impedimetric immunosensors—A review. Electrochimica Acta, 2010. 55(14): p. 4227-4233.

83. Erlandsson, P.G. and N.D. Robinson, Electrolysis - reducing electrodes for electrokinetic devices. Electrophoresis, 2011. 32(6 - 7): p. 784-790.

84. Pruneanu, S., et al., Impedimetric measurements for monitoring avidin-biotin interaction on self-assembled monolayer. Particulate Science and

Technology, 2008. 26(2): p. 136-144.

85. Wang, Y., Z. Ye, and Y. Ying, New trends in impedimetric biosensors for the detection of foodborne pathogenic bacteria. Sensors, 2012. 12(3): p. 3449-3471.

86. Arya, S.K., et al., Recent advances in self-assembled monolayers based biomolecular electronic devices. Biosensors and Bioelectronics, 2009. 24(9): p. 2810-2817.

87. Mabrook, M., C. Pearson, and M. Petty, Inkjet-printed polypyrrole thin films for vapour sensing. Sensors and Actuators B: Chemical, 2006. 115(1): p. 547-551.

88. Rusmini, F., Z. Zhong, and J. Feijen, Protein immobilization strategies for protein biochips. Biomacromolecules, 2007. 8(6): p. 1775-1789.

89. Sassolas, A., L.J. Blum, and B.D. Leca-Bouvier, Immobilization strategies to develop enzymatic biosensors. Biotechnology advances, 2012. 30(3): p. 489-511.

90. Song, G., Equivalent circuit model for AC electrochemical impedance spectroscopy of concrete. Cement and Concrete Research, 2000. 30(11): p. 1723-1730.

91. Harrington, D.A. and P. Van den Driessche, Mechanism and equivalent circuits in electrochemical impedance spectroscopy. Electrochimica Acta, 2011. 56(23): p. 8005-8013.

92. Suleiman, A.A. and G.G. Guilbault, Recent developments in piezoelectric immunosensors. A review. Analyst, 1994. 119(11): p. 2279-2282.

93. Sauerbrey, G., Verwendung von Schwingquarzen zur Wägung dünner Schichten und zur Mikrowägung. Zeitschrift für Physik, 1959. 155(2): p. 206-222.

94. Kumar, A., Biosensors based on piezoelectric crystal detectors: theory and application. JOM-e, 2000. 52(10).

95. Chou, S.-F., et al., Determination of α-fetoprotein in human serum by a quartz crystal microbalance-based immunosensor. Clinical chemistry, 2002.

48(6): p. 913-918.

96. Su, X.-L. and Y. Li, A self-assembled monolayer-based piezoelectric immunosensor for rapid detection of< i> Escherichia coli</i> O157: H7. Biosensors and Bioelectronics, 2004. 19(6): p. 563-574.

97. Gijs, M.A., F. Lacharme, and U. Lehmann, Microfluidic applications of magnetic particles for biological analysis and catalysis. Chemical reviews, 2009. 110(3): p. 1518-1563.

98. Millen, R.L., et al., Giant magnetoresistive sensors and superparamagnetic nanoparticles: a chip-scale detection strategy for immunosorbent assays. Analytical chemistry, 2005. 77(20): p. 6581-6587.

99. Srinivasan, B., et al., A Detection System Based on Giant Magnetoresistive Sensors and High‐Moment Magnetic Nanoparticles Demonstrates Zeptomole Sensitivity: Potential for Personalized Medicine. Angewandte Chemie International Edition, 2009. 48(15): p. 2764-2767.

100. Nikitin, P.I., P.M. Vetoshko, and T.I. Ksenevich, New type of biosensor based on magnetic nanoparticle detection. Journal of Magnetism and Magnetic Materials, 2007. 311(1): p. 445-449.

101. Lin, Y.-Y., et al., Magnetic beads-based bioelectrochemical immunoassay of polycyclic aromatic hydrocarbons. Electrochemistry communications, 2007. 9(7): p. 1547-1552.

102. Pericleous, P., et al., Detection of colorectal circulating cancer cells with the use of a quantum dot labelled magnetic immunoassay method. Hellenic Journal of Surgery, 2013. 85(2): p. 127-134.

103. Manickam, A., Integrated Impedance Spectroscopy Biosensors. 2012: THE UNIVERSITY OF TEXAS AT AUSTIN.

104. Ingle Jr, J., Sensitivity and limit of detection in quantitative spectrometric methods. Journal of Chemical Education, 1974. 51(2): p. 100.

105. Mani, D., S.E. Abbatiello, and S.A. Carr, Statistical characterization of multiple-reaction monitoring mass spectrometry (MRM-MS) assays for quantitative proteomics. BMC bioinformatics, 2012. 13(Suppl 16): p. S9.

106. Wolfbeis, O.S., Fluorescence spectroscopy: new methods and applications. 1993: Springer.

107. Giuliano, K.A., et al., Fluorescent protein biosensors: measurement of molecular dynamics in living cells. Annual review of biophysics and biomolecular structure, 1995. 24(1): p. 405-434.

108. Kricka, L.J. and G.H. Thorpe, Chemiluminescent and bioluminescent methods in analytical chemistry. Analyst, 1983. 108(1292): p. 1274-1296.

109. Roda, A., et al., Bio-and chemiluminescence in bioanalysis. Fresenius' journal of analytical chemistry, 2000. 366(6-7): p. 752-759.

110. Wang, J., Electrochemical nucleic acid biosensors. Analytica chimica acta, 2002. 469(1): p. 63-71.

111. Veitch, N.C., Horseradish peroxidase: a modern view of a classic enzyme. Phytochemistry, 2004. 65(3): p. 249-259.

112. Chen, L., et al., A novel chemiluminescence immunoassay of staphylococcal enterotoxin B using HRP-functionalised mesoporous silica nanoparticle as label. Food Chemistry, 2012. 135(1): p. 208-212.

113. Cooper, M.A., Label-free screening of bio-molecular interactions. Analytical and bioanalytical chemistry, 2003. 377(5): p. 834-842.

114. Vollmer, F. and S. Arnold, Whispering-gallery-mode biosensing: label-free detection down to single molecules. Nature methods, 2008. 5(7): p. 591-596.

115. Wang, X.-D. and O.S. Wolfbeis, Fiber-optic chemical sensors and biosensors (2008–2012). Analytical chemistry, 2012. 85(2): p. 487-508.

116. Watts, H.J., D. Yeung, and H. Parkes, Real-time detection and quantification of DNA hybridization by an optical biosensor. Analytical chemistry, 1995. 67(23): p. 4283-4289.

117. Jönsson, U. Real-time biospecific interaction analysis. in Biosensors 92 Proceedings: The Second World Congress on Biosensors. 2014. Elsevier.

118. Plaxco, K.W. and H.T. Soh, Switch-based biosensors: a new approach towards real-time, in vivo molecular detection. Trends in biotechnology, 2011.

29(1): p. 1-5.

119. Zheng, G. and C.M. Lieber, Nanowire biosensors for label-free, real-time, ultrasensitive protein detection, in Nanoproteomics. 2011, Springer. p. 223-237.

120. Carrascosa, L.G., et al., Molecular inversion probe-based SPR biosensing for specific, label-free and real-time detection of regional DNA methylation. Chemical Communications, 2014. 50(27): p. 3585-3588.

121. Chang, B.-Y. and S.-M. Park, Electrochemical impedance spectroscopy. Annual Review of Analytical Chemistry, 2010. 3: p. 207-229.

122. Orazem, M.E. and B. Tribollet, Electrochemical impedance spectroscopy. Vol. 48. 2011: John Wiley & Sons.

123. Ohno, R., et al., Electrochemical impedance spectroscopy biosensor with interdigitated electrode for detection of human immunoglobulin A. Biosensors and Bioelectronics, 2013. 40(1): p. 422-426.

124. Macdonald, J.R. and E. Barsoukov, Impedance spectroscopy: theory, experiment, and applications. History, 2005. 1: p. 8.

125. Rickayzen, G., Electric Double Layer. Amorphous Solids and the Liquid State, 2013.

126. Morgan, H. and N.G. Green, AC electrokinetics: colloids and nanoparticles. 2003: Research Studies Press.

127. Bard, A.J. and L.R. Faulkner, Electrochemical methods: fundamentals and applications. Vol. 2. 1980: Wiley New York.

128. Erickson, R., Bode diagrams of transfer functions and impedances, pdf datoteka u prilogu.

129. Instruments, G., Basics of electrochemical impedance spectroscopy. G. Instruments, Complex impedance in Corrosion, 2007: p. 1-30.

130. Lisdat, F. and D. Schäfer, The use of electrochemical impedance spectroscopy for biosensing. Analytical and bioanalytical chemistry, 2008. 391(5): p. 1555-1567.

131. Hedström, M., I.Y. Galaev, and B. Mattiasson, Continuous

measurements of a binding reaction using a capacitive biosensor. Biosensors and Bioelectronics, 2005. 21(1): p. 41-48.

132. Ertürk, G., et al., Microcontact-BSA imprinted capacitive biosensor for real-time, sensitive and selective detection of BSA. Biotechnology Reports, 2014. 3: p. 65-72.

133. Tsouti, V., et al., Capacitive microsystems for biological sensing. Biosensors and Bioelectronics, 2011. 27(1): p. 1-11.

134. Kohonen, M.M., M.E. Karaman, and R.M. Pashley, Debye length in multivalent electrolyte solutions. Langmuir, 2000. 16(13): p. 5749-5753.

135. Simonson, T. and C.L. Brooks, Charge screening and the dielectric constant of proteins: insights from molecular dynamics. Journal of the American Chemical Society, 1996. 118(35): p. 8452-8458.

136. Reverberi, R. and L. Reverberi, Factors affecting the antigen-antibody reaction. Blood Transfusion, 2007. 5(4): p. 227.

137. Sheehan, P.E. and L.J. Whitman, Detection limits for nanoscale biosensors. Nano letters, 2005. 5(4): p. 803-807.

138. Qureshi, A., et al., Label-free RNA aptamer-based capacitive biosensor for the detection of C-reactive protein. Physical Chemistry Chemical Physics, 2010. 12(32): p. 9176-9182.

139. Smith, J.E., et al., Optimization of antibody-conjugated magnetic nanoparticles for target preconcentration and immunoassays. Analytical biochemistry, 2011. 410(1): p. 124-132.

140. Tennico, Y.H. and V.T. Remcho, In‐line extraction employing functionalized magnetic particles for capillary and microchip electrophoresis. Electrophoresis, 2010. 31(15): p. 2548-2557.

141. Fan, X. and I.M. White, Optofluidic microsystems for chemical and biological analysis. Nature photonics, 2011. 5(10): p. 591-597.

142. Velasco, V., A.H. Work, and S.J. Williams, Electrokinetic concentration and patterning of colloids with a scanning laser. Electrophoresis, 2012. 33(13): p. 1931-1937.

143. Wu, J., In Situ Nanoparticle Focusing Within Microfluidics. Microfluidic Devices in Nanotechnology: Fundamental Concepts, 2010: p. 295-316.

144. Wang, D., M. Sigurdson, and C.D. Meinhart, Experimental analysis of particle and fluid motion in ac electrokinetics. Experiments in fluids, 2005. 38(1): p. 1-10.

145. Ahualli, S., et al., AC electrokinetics of concentrated suspensions of soft particles. Langmuir, 2009. 25(4): p. 1986-1997.

146. Wu, J., Biased AC electro-osmosis for on-chip bioparticle processing. Nanotechnology, IEEE Transactions on, 2006. 5(2): p. 84-89.

147. Green, N.G., et al., Electric field induced fluid flow on microelectrodes: the effect of illumination. Journal of Physics D: Applied Physics, 2000. 33(2): p. L13.

148. Yang, K. and J. Wu, Numerical study of in situ preconcentration for rapid and sensitive nanoparticle detection. Biomicrofluidics, 2010. 4(3): p. 034106.

149. Li, S., et al., AC electrokinetics-enhanced capacitive immunosensor for point-of-care serodiagnosis of infectious diseases. Biosensors and Bioelectronics, 2014. 51: p. 437-443.

150. Li, S., et al., Dielectrophoretic responses of DNA and fluorophore in physiological solution by impedimetric characterization. Biosensors and Bioelectronics, 2013. 41: p. 649-655.

151. Wu, J., Interactions of electrical fields with fluids: laboratory-on-a-chip applications. Nanobiotechnology, IET, 2008. 2(1): p. 14-27.

152. Lenshof, A. and T. Laurell, Continuous separation of cells and particles in microfluidic systems. Chemical Society Reviews, 2010. 39(3): p. 1203-1217.

153. Castellanos, A., et al., Electrohydrodynamics and dielectrophoresis in microsystems: scaling laws. Journal of Physics D: Applied Physics, 2003. 36(20): p. 2584.

154. Sin, M.L., et al., Electrothermal fluid manipulation of high-conductivity samples for laboratory automation applications. Journal of the Association for Laboratory Automation, 2010. 15(6): p. 426-432.

155. Gao, J., et al., Hybrid electrokinetic manipulation in high-conductivity media. Lab on a Chip, 2011. 11(10): p. 1770-1775.

156. Wu, J., M. Lian, and K. Yang, Micropumping of biofluids by alternating current electrothermal effects. Applied physics letters, 2007. 90(23): p. 234103-234103-3.

157. Feldman, H.C., M. Sigurdson, and C.D. Meinhart, AC electrothermal enhancement of heterogeneous assays in microfluidics. Lab on a Chip, 2007. 7(11): p. 1553-1559.

158. Ramos, A., et al., Ac electrokinetics: a review of forces in microelectrode structures. Journal of Physics D: Applied Physics, 1998. 31(18): p. 2338.

159. Oh, J., et al., Comprehensive analysis of particle motion under non-uniform AC electric fields in a microchannel. Lab on a Chip, 2009. 9(1): p. 62-78.

160. Lian, M., N. Islam, and J. Wu, AC electrothermal manipulation of conductive fluids and particles for lab-chip applications. IET Nanobiotechnology, 2007. 1(3): p. 36-43.

161. Shearer, S.A. and J.R. Hudson, Fluid mechanics: Stokes' law and viscosity. Measurement Laboratory, 2008(3).

162. Brinkman, H., Brownian motion in a field of force and the diffusion theory of chemical reactions. Physica, 1956. 22(1): p. 29-34.

163. Voller, A., D.E. Bidwell, and A. Bartlett, The enzyme linked immunosorbent assay (ELISA). A guide with abstracts of microplate applications. 1979: Dynatech Europe, Borough House, Rue du Pre.

164. Arefin, M.S. and T.L. Porter, An ac electroosmosis device for the detection of bioparticles with piezoresistive microcantilever sensors. Journal of Applied Physics, 2012. 111(5): p. 054919.

165. Hart, R., et al., Improved protein detection on an AC electrokinetic quartz crystal microbalance (EKQCM). Biosensors and Bioelectronics, 2011. 26(8): p. 3391-3397.

166. Wu, J., et al., Long-range AC electroosmotic trapping and detection of bioparticles. Industrial & engineering chemistry research, 2005. 44(8): p. 2815-2822.

167. Wu, J., Y. Ben, and H.-C. Chang, Particle detection by electrical impedance spectroscopy with asymmetric-polarization AC electroosmotic trapping. Microfluidics and Nanofluidics, 2005. 1(2): p. 161-167.

168. Ho, Y.-T., et al. AC electrokinetics assisted impedance biosensors for rapid bacteria detection. in Biomedical Circuits and Systems Conference (BioCAS), 2012 IEEE. 2012. IEEE.

169. Stanke, S., F. Bier, and R. Hölzel, Fluid streaming above interdigitated electrodes in dielectrophoresis experiments. Electrophoresis, 2011. 32(18): p. 2448-2455.

170. Li, H. and R. Bashir, Dielectrophoretic separation and manipulation of live and heat-treated cells of Listeria on microfabricated devices with interdigitated electrodes. Sensors and Actuators B: Chemical, 2002. 86(2): p. 215-221.

171. Eda, S., et al., A highly sensitive and subspecies-specific surface antigen enzyme-linked immunosorbent assay for diagnosis of Johne's disease. Clinical and vaccine immunology, 2006. 13(8): p. 837-844.

172. Ulman, A., Formation and structure of self-assembled monolayers. Chemical reviews, 1996. 96(4): p. 1533-1554.

173. Wink, T., et al., Self-assembled monolayers for biosensors. Analyst, 1997. 122(4): p. 43R-50R.

174. Dong, S. and J. Li, Self-assembled monolayers of thiols on gold electrodes for bioelectrochemistry and biosensors. Bioelectrochemistry and bioenergetics, 1997. 42(1): p. 7-13.

175. Chai, C.-H., Label-free immunosensor for toxin detection in food matrix, 2008, Rutgers University-Graduate School-New Brunswick.

176. Dąbrowski, A., Adsorption—from theory to practice. Advances in colloid and interface science, 2001. 93(1): p. 135-224.

177. Plueddemann, E.P., Silane coupling agents. 1982: Springer Science & Business Media.

178. Maddox, P. and D. Jenkins, 3-Aminopropyltriethoxysilane (APES): a new advance in section adhesion. Journal of clinical pathology, 1987. 40(10): p. 1256.

179. Chai, C. and P. Takhistov, Label-free toxin detection by means of time-resolved electrochemical impedance spectroscopy. Sensors, 2010. 10(1): p. 655-669.

180. Patel, N., et al., Immobilization of protein molecules onto homogeneous and mixed carboxylate-terminated self-assembled monolayers. Langmuir, 1997. 13(24): p. 6485-6490.

181. Savitzky, A. and M.J. Golay, Smoothing and differentiation of data by simplified least squares procedures. Analytical chemistry, 1964. 36(8): p. 1627-1639.

182. Hurley, I.P., et al., Measurement of bovine IgG by indirect competitive ELISA as a means of detecting milk adulteration. Journal of dairy science, 2004. 87(3): p. 543-549.

183. Wadhwa, A., et al., Overview of Johne's disease immunology. Veterinary World, 2013. 6(11): p. 901-904.

184. Alexander, D.J., An overview of the epidemiology of avian influenza. Vaccine, 2007. 25(30): p. 5637-5644.

185. Liao, C. and K. Kannan, Widespread occurrence of bisphenol A in paper and paper products: implications for human exposure. Environmental science & technology, 2011. 45(21): p. 9372-9379.

186. Cui, H., et al. Rapid detection of progesterone by commercially available microelectrode chips. in SENSORS, 2013 IEEE. 2013. IEEE.

187. Hadley, G., Basic Histology. Journal of Anatomy, 2007. 211(3): p. 412-412.

188. Nagelkerke, N.J., A note on a general definition of the coefficient of determination. Biometrika, 1991. 78(3): p. 691-692.

189. Loire, S., et al., A theoretical and experimental study of ac electrothermal flows. Journal of Physics D: Applied Physics, 2012. 45(18): p. 185301.

190. Martin, E.A., Concise medical dictionary. 2010: Oxford University Press.

191. Wadhwa, A., G.J. Hickling, and S. Eda, Opportunities for improved serodiagnosis of human tuberculosis, bovine tuberculosis, and paratuberculosis. Veterinary medicine international, 2012. 2012.

192. Nordlund, K., et al., Associations between subclinical paratuberculosis and milk production, milk components, and somatic cell counts in dairy herds. Journal of the American Veterinary Medical Association, 1996. 208(11): p. 1872-1876.

193. O'Reilly, L.M. and C. Daborn, The epidemiology of Mycobacterium bovis infections in animals and man: a review. Tubercle and Lung Disease, 1995. 76: p. 1-46.

194. Manning, E.J., Paratuberculosis in captive and free-ranging wildlife. Veterinary Clinics of North America: Food Animal Practice, 2011. 27(3): p. 621-630.

195. Small, P.M. and M. Pai, Tuberculosis diagnosis—time for a game change. New England Journal of Medicine, 2010. 363(11): p. 1070-1071.

196. Rie, A.V., et al., Xpert® MTB/RIF for point-of-care diagnosis of TB in high-HIV burden, resource-limited countries: hype or hope? 2010.

197. Salem, M., et al., Mycobacterium avium subspecies paratuberculosis: an insidious problem for the ruminant industry. Tropical animal health and production, 2013. 45(2): p. 351-366.

198. Green, N.G., et al., Electrothermally induced fluid flow on microelectrodes. Journal of Electrostatics, 2001. 53(2): p. 71-87.

199. Hong, F., J. Cao, and P. Cheng, A parametric study of AC electrothermal flow in microchannels with asymmetrical interdigitated electrodes. International Communications in Heat and Mass Transfer, 2011. 38(3): p. 275-279.

200. Abdi, H., Coefficient of variation. Encyclopedia of research design, 2010: p. 169-171.

201. Organization, W.H., Influenza (Seasonal) Fact Sheet No. 211, March 2014, 2014.

202. Kawaoka, Y., Influenza virology: current topics. 2006: Caister Academic Press.

203. Popowitch, E.B., E. Rogers, and M.B. Miller, Retrospective and prospective verification of the Cepheid Xpert influenza virus assay. Journal of clinical microbiology, 2011. 49(9): p. 3368-3369.

204. Staples, C.A., et al., A review of the environmental fate, effects, and exposures of bisphenol A. Chemosphere, 1998. 36(10): p. 2149-2173.

205. Vandenberg, L.N., et al., Human exposure to bisphenol A (BPA). Reproductive Toxicology, 2007. 24(2): p. 139-177.

206. Le, H.H., et al., Bisphenol A is released from polycarbonate drinking bottles and mimics the neurotoxic actions of estrogen in developing cerebellar neurons. Toxicology letters, 2008. 176(2): p. 149-156.

207. Vandenberg, L.N., et al., Bisphenol-A and the great divide: a review of controversies in the field of endocrine disruption. Endocrine reviews, 2009. 30(1): p. 75-95.

208. Sun, Y., et al., Determination of bisphenol A in human breast milk by HPLC with column‐switching and fluorescence detection. Biomedical Chromatography, 2004. 18(8): p. 501-507.

209. Braunrath, R., et al., Determination of bisphenol A in canned foods by immunoaffinity chromatography, HPLC, and fluorescence detection. Journal of agricultural and food chemistry, 2005. 53(23): p. 8911-8917.

210. Zafra, A., et al., Gas chromatographic–mass spectrometric method for the determination of bisphenol A and its chlorinated derivatives in urban wastewater. Water research, 2003. 37(4): p. 735-742.

211. Gatidou, G., et al., Simultaneous determination of the endocrine disrupting compounds nonylphenol, nonylphenol ethoxylates, triclosan and

bisphenol A in wastewater and sewage sludge by gas chromatography–mass spectrometry. Journal of Chromatography A, 2007. 1138(1): p. 32-41.

212. King, T.L. and M.C. Brucker, Pharmacology for women's health. 2010: Jones & Bartlett Publishers.

213. Bisinotto, R. Effects of progesterone supplementation on reproductive responses in dairy cows subjected to timed AI programs: a meta-analysis. in 2014 ADSA-ASAS-CSAS Joint Annual Meeting. 2014. Asas.

214. Bulman, D.C. and G. Lamming, Milk progesterone levels in relation to conception, repeat breeding and factors influencing acyclicity in dairy cows. Journal of Reproduction and Fertility, 1978. 54(2): p. 447-458.

215. Speroff, L. and M.A. Fritz, Clinical gynecologic endocrinology and infertility. 2005: lippincott Williams & wilkins.

VITA

Haochen Cui was born in Shijiazhuang, P.R.China. He received his B.S. degree in Microelectronics from Changchun Institute of Optics and Fine Mechanics, China in 2010. He is currently a Ph.D. student of Electrical Engineering at the University of Tennessee, Knoxville. His research interests include design and development of bioelectronics based immunosensor for rapid disease detection, microfluidics, microelectronics fabrication and electronic device modeling.

Email id: hcui2@vols.utk.edu